Application of the Jaynes-Cummings Model in Quantum Information Processing

Phumzile Madonsela

WITS
UNIVERSITY

School of Physics

University of the Witwatersrand

A dissertation submitted to the Faculty of Science, University of the Witwatersrand, Johannesburg, in fulfilment of the requirements for the degree of Master of Science.

Johannesburg, 2020

Declaration

I declare that this dissertation is my own, unaided work. It is being submitted for the Degree of Master of Science at the University of the Witwatersrand, Johannesburg. It has not been submitted before for any degree or examination at any other University.

P. Madonula

(Signature of candidate)

30th day of October 20 20 at Johannesburg

Abstract

The advent of quantum computation and information science has seen the re-emergence of squeezed states of light being of critical importance in the field of quantum metrology. The generation of the squeezed states of light in circuit QED has proven to achieve quantum measurement in a faster way than conventional optical methods. The Jaynes-Cummings physics is used to study the degree of squeezing generated in a dissipative atom-cavity system by computing the master equation of the interacting atom-cavity quantum system. The collapse-revival oscillations of the dynamical process in the Markovian and non-Markovian regime are observed to be dependent on the coupling strength g of the two-level atom-cavity quantum system including those of the Bohr frequency.

By transforming the original Rabi Hamiltonian to a dispersive Hamiltonian, significant squeezing can be observed through sudden qubit flips via the squeezing protocol scheme presented. The degree of squeezing is calculated after N cycles of the protocol are carried out at certain frequency jumps. A comparison of the degree of squeezing generated by the dispersive model and the Rabi model carried out by the frequency-shift protocol proves that the degree of squeezing in the Rabi model is higher.

We implement the generation of light squeezing in a quantum circuit environment by first developing a hybrid quantum system consisting of superconducting flux qubits and an ensemble of nitrogen-vacancy centers (NVE). Within such an architecture one of the most important thing to measure is the entanglement between the flux qubits and NV ensemble. This we will measure using a metric called concurrence C. An ideal quantum circuit should be able to effectively store quantum memory and have long coherence times through spin ensembles. We measure bipartite, residual and dissipative entanglement dynamics using concurrence.

We conclude the thesis by introducing a novel technique to genearate squeezed states of an NVE within a hybrid quantum system by making use of the superconducting qubit which couples the resonator to the NVE so that we can generate single-mode squeezed states of an NVE from the entangled states of the bosonic mode with the NVE.

To my late grandmother Sesi Julia Madonsela

Acknowledgements

I would like to thank my supervisor Prof Somnath Bhattacharyya for offering me this project in the new emerging field of sciences together with his support and guidance. I sincerely thank Prof Yorick Hardy from the School of Mathematics at Wits university for his clear and concise explanation of the field of quantum information and quantum computing, going over the theory and mathematics behind the subject and answering my endless questions. Dr Martin Muller for offering his time to teach me the basics of the computational programming that was needed for performing simulations in this project.

I extend my gratitude to the members of the Nano-Scale Transport Physics Laboratory in particular Christopher Coleman who did a great job in explaining the experimental concepts that were needed to successfully tackle the project deliverables, Siphephile Ncube who has been supportive of the work I do and Farai Mazhandu who I have been working closely with on a similar project.

I wish to thank the DST-NRF Centre of Excellence in Strong Materials (CoE-SM) for financial support. Opinions expressed and conclusions arrived at in this thesis are those of the author and are not necessarily to be attributed to the CoE-SM.

I am grateful of the support from my mother, aunt and Elvis Banele Seshoene during this time of study and completion of this dissertation.

Contents

List of Figures

Chapter 1

Introduction

In the year 1982, Richard Feynman posed a question of what kind of computer will be able to simulate the behaviour of quantum systems since classical computers are meant to compute classical mechanics [1, 2]. This led to the birth of quantum simulation. Figure 1.1 shows a schematic representation of the mapping of a quantum system to its quantum simulator. The quantum system is initially in the state $|\phi(0)\rangle$ and this corresponds to the state $|\psi(0)\rangle$ on the simulator. The prepared state $|\psi(0)\rangle$ evolves through the unitary operator $\hat{U}' = e^{-i\hat{H}t}$ to the state $|\psi(t)\rangle$ that can be measured. Unlike the simulated system, the simulator can be controlled through the preparation of the initial state $|\psi(0)\rangle$, engineering of the evolution operator $\hat{U}'$ and measurement of $|\psi(t)\rangle$.

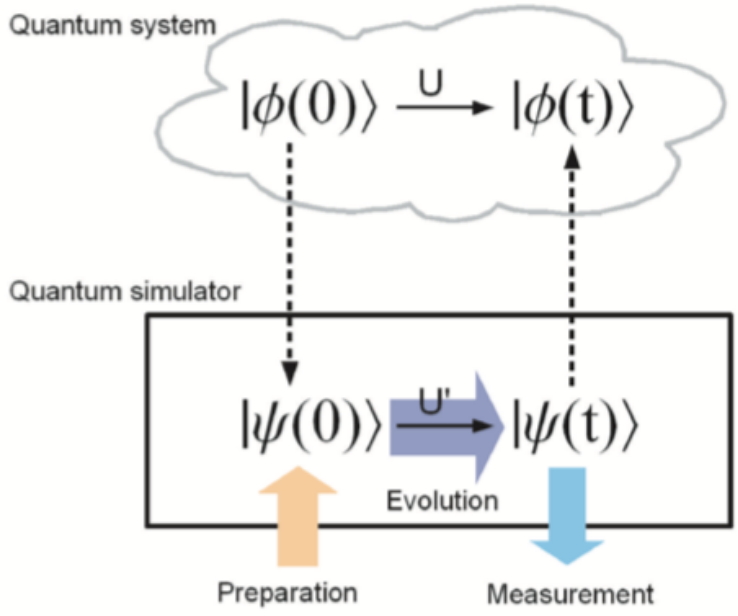

Figure 1.1: **A mapping of an evolution of a quantum system and its corresponding quantum simulator** [3].

What should a universal quantum simulator be made of?

The simulator should be able to emulate a quantum system and perform quantum computation.It should be able to simulate single particle states with the occupation of each state being either 0 or 1 and mapping it to a quantum bit (qubit) [4]. A qubit is analogous to a computer's bit that stores information. Similarly a qubit stores and processes quantum information. The physical implementation includes that of trapped ions, photons in optical cavities (QED) and nuclei spins [5, 6]. The first experimental work performed by Li et al. in [7] and Peng et al. in [8] used Nuclear Magnetic Resonance (NMR) to implement a quantum algorithm. Simulations of quantum information processes using electron spins in quantum dots [9] has proved to be successful because of the scalability of qubits using quantum dot arrays [10].

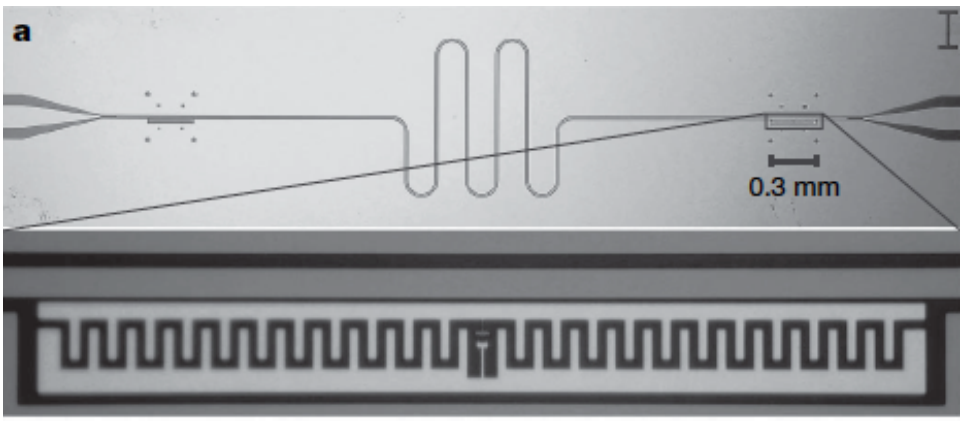

(a) Optical image showing the superconducting resonator and transmon qubit with the magnified view of the qubit at the bottom [11].

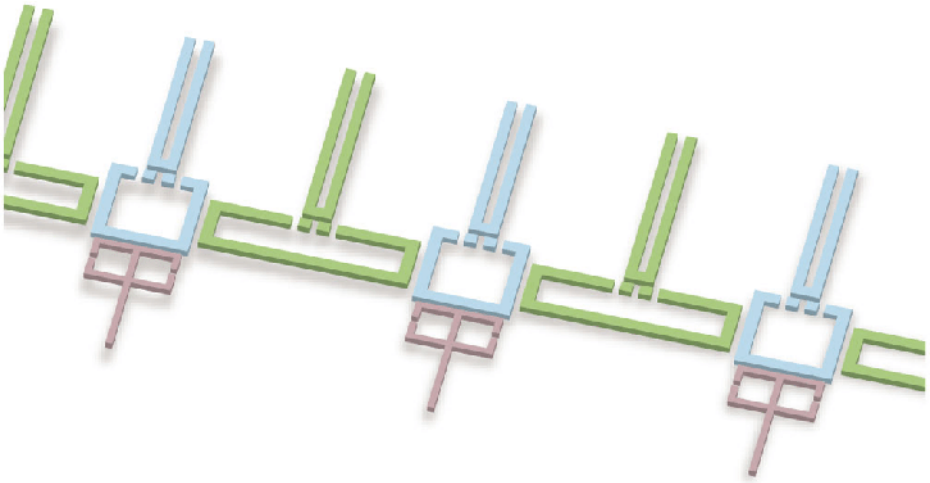

(b) An array of superconducting flux qubits shown in blue color coupled to other qubits through green circuits and brown readout circuits [12].

Figure 1.2: **Superconducting circuits**

New technology that uses coherent nano-scale systems allows for the development of superconducting circuits [13, 14]. Superconducting circuits consists of elements that have superconducting properties [15] such as flux qubits and resonators as shown in Figure 1.2a,1.2b. These have an advantage of simulating quantum systems better than other methods presented above. The circuit geometry can be constructed to meet tailored specifications characteristic to the circuit. In Chapter 6 we study and measure the entanglement of a hybrid quantum system.
Within a quantum circuit, operations on qubits are done by elements called quantum gates. These are analogous to classical logical gates of computers. Figure 1.3 shows a quantum state $|\psi_T(n-1\rangle)$ of one electron occupying n orbitals and is used to generate vacuum states. The quantum gates involved are the X gate commonly known as bit-flip mapping $|0\rangle$ to $|1\rangle$ and $|1\rangle$ to $|0\rangle$, cNOT where one or more qubits acts as control and then three unitary operators $Q(n-2,1)$, $\tilde{H}$, $\tilde{H}'$.

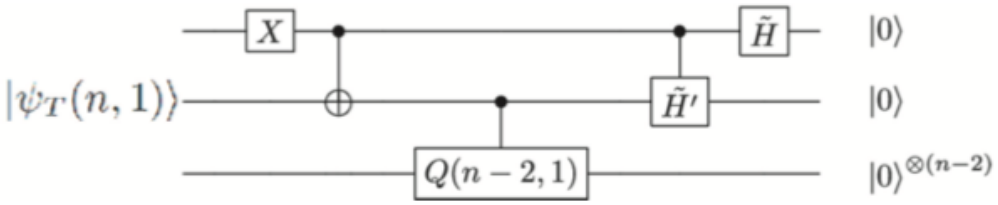

Figure 1.3: **Quantum Circuit** consisting of quantum gates that transform the $|\psi_T(n,1)\rangle$ into vacuum states [16].

The scalability of quantum circuits to having more than 200 qubits has been fabricated in a single chip from the work of Houck et al. in [17]. The scalability of circuits has been of particular interest to the field of condensed matter, in particular that of lattice structures and models such as Jaynes-Cummings lattice [18] (Figure 1.4) and the Anderson-Kondo model [19]. Experimental simulations of the quantum Hall effect has been demonstrated in Ref.[20] using superconducting qubits.

Nitrogen-vacancy centers in diamond have received great attention [3, 21–23] as they prove to be a promising platform for implementing quantum information processing because of the electron vacancy center that acts as a quantum memory or storage. In Chapter 6 we study a quantum system consisting of NV center ensemble.

In this thesis we critically study the use of squeezed states of light [24] in quantum information processes such as quantum computing, quantum metrology and quantum entanglement.Over the years squeezed states have been theoretically treated in the field of optics [25]. Pure quantum states are squeezed states developed in a quantum model framework that effectively generates and achieves squeezing of light. We work within the Jaynes-Cummings model [26], an approximation to the Rabi model. The first use of the model was in the study of spontaneous emission [27] and how to achieve superradiant light emission known as Dicke superradiance. One of the things that quantum systems suffer from is the perfect isolation of the system from the rest of the environment. The work done by Zou et al. in [28] on generating the squeezed states in an open quantum system took an approach of using the

time-convolutionless master equation to generate squeezed states of light. We follow their approach in this thesis and perform a different measurement by utilizing and varying the limit of the degree of squeezing in which we are certain to improve the degree of squeezing achieved.

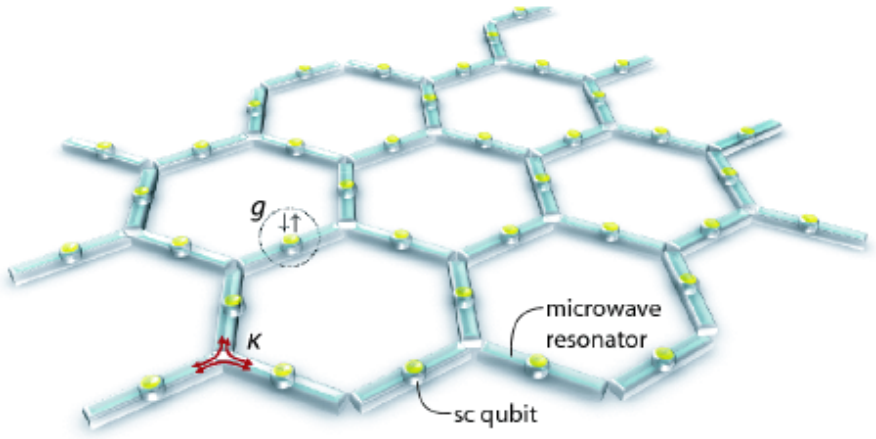

Figure 1.4: **Jaynes-Cummings** photon lattice consisting of superconducting qubits coupled to microwave resonators [18].

Following the study and work of Joshi et al. in [29] we provide an alternative method to the generation of squeezed states inspired by the experimental work in the dispersive readout of qubits [30] and performing a transformation on the Jaynes-Cummings model to effectively extract apparent features of the dispersive regime. A very common experimental measure used to quantify the degree of squeezing is in the unit of decibels (dB) (details in Chapter 5). We note that the protocol used is limited to the decoherence and noise errors that result from photon loss due to cavity imperfections. Nonetheless the degree of squeezing generated proved to be better compared to other experimental methods such as nonlinear parametric amplifiers.

Having generated squeezing of light in two different ways, we move towards combining different quantum systems in a single geometry known as a quantum circuit. We study such a circuit in order to compute entanglement measurements of interest (details in Chapter 6). The purpose of the investigation stems from the study done by Liao et al. in [31] using the Jaynes-Cummings model and calculated the concurrences of the system as a quantifiable measure of entanglement that is commonly used. We apply the same measure in our circuit and determine concurrences of different systems. We apply an alternative calculation to the one used in the original work by using single entropy of the system other than concurrence as mentioned in the conclusion of the chapter. We further explore how to realize squeezed states in the above quantum system by coupling a transmission line resonator (TLR) to the NVE and induce a collective excitation in an NVE resulting in entangled squeezed states of the bosonic mode and the NVE.

This thesis is organized as follows: Composed of five chapters with the first two being the introductory chapters and the remaining three chapters containing main results of the study.

In **Chapter 2**, we introduce the Jaynes-Cummings Model by deriving the model Hamiltonian and analyze model features including the experimental observation of some of the model features.

In **Chapter 3** we extend the Jaynes-Cummings model to include the dissipative features, this is done by introducing the mathematics involved in deriving the dissipative Jaynes-Cummings model including the description of the density matrices, the derivation of the quantum master equation which is used in the main results of the subsequent chapters. We then conclude the chapter with an example that shows the dynamics of the master equation for an atom-cavity system with one excitation of the field.

In **Chapter 4** we introduce the non-Markovian master equation which is used to generate the squeezed states in the dissipative model. We review the squeezing properties of the light field and plot the squeezing factor of dissipative Jaynes-Cummings model. We further discuss the results of the study and their potential impact in various fields.

Chapter 5 introduces an alternative technique that ensures we achieve greater amounts of squeezing. We work with the approximated Rabi model and derive the dispersive regime of it before we develop the protocol to generate the squeezed states through qubit flipping and frequency jumps. We discuss the results of the chapter and conclude by noting implications of the work.

Finally in **Chapter 6** we look at the hybrid quantum circuit and systems that consists of superconducting flux qubits coupled to an NV center ensemble. We perform a calculation that will give the overall density matrix of the physical system and then the concurrence measure in the first section. We also look at the impact of dissipation on the bipartite and residual entanglement concluding with the shortfalls of the study under the discussion section. In the second section we introduce a novel way generate single-mode squeezed states of NVEs within a similar type of hybrid system, we construct an effective Hamiltonian that describes the interacting system and observe the system's total variance under dissipation.

The overall summary and conclusions of the thesis are detailed in the last chapter.

Chapter 2

Jaynes-Cummings Model

The Jaynes-Cummings Model was originally developed in the field of quantum optics by Edwin Jaynes and Fred Cummings [32] in 1963 on the investigation of spontaneous emission of electromagnetic radiation interacting with a two-level atomic system, with the first experimental demonstration in 1984 by Rempe et al. in [33]. The model that described the interaction of a cavity field with the atom was a semi-classical Rabi model in which the electromagnetic field frequency was at the atom's resonant frequency. A quantum model needed to be developed to fully understand phenomena such as the spontaneous emission. In 1936, Rabi came with a quantum model that discussed the effects of a magnetic field on an atom's nuclear spin. It was not exactly solvable [34] in which Jaynes and Cummings added an approximation known as rotating wave approximation (RWA) that excludes counter-rotating terms in the Rabi Hamiltonian and results in the Hamiltonian given in Eq. (2.34). In this chapter we derive the Jaynes-Cummings model, discuss and analyze the features of model that include the dressed states of the model, the Jaynes-Cummings Ladder, the Rabi oscillations and lastly the collapse-revival phenomena.

2.1 Derivation of Jaynes-Cummings Model

2.1.1 Quantization of Electromagnetic field

In order to quantize the single-mode free electromagnetic field, we consider in Figure 2.1 a 1-dimensional cavity along the z-axis with perfectly conducting walls located at z = 0 and z = L with the electric field polarized in the x-direction i.e $\mathbf{E}(r,t) = E_x(z,t)\hat{\mathbf{x}}$.

From Maxwell's equations in free space

$$\nabla \cdot \mathbf{E} = 0, \tag{2.1}$$

$$\nabla \times \mathbf{E} = -\frac{\partial \mathbf{B}}{\partial t}, \tag{2.2}$$

$$\nabla \cdot \mathbf{B} = 0, \tag{2.3}$$

$$\nabla \times \mathbf{B} = \mu_0 \epsilon_0 \frac{\partial \mathbf{E}}{\partial t}, \tag{2.4}$$

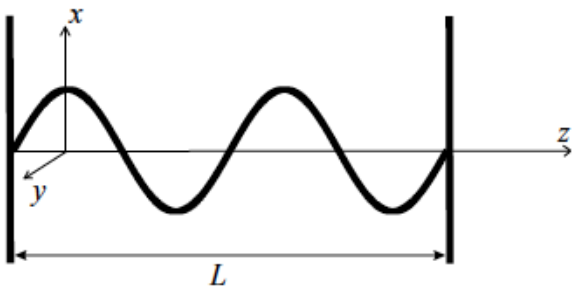

Figure 2.1: **Cavity with perfectly conducting walls** at $z = 0$ to $z = L$ [35].

we can then derive the wave equation by taking the time derivative of Eq. (2.4)

$$\frac{\partial}{\partial t}\nabla \times \mathbf{B} = \mu_0\epsilon_0\frac{\partial^2 \mathbf{E}}{\partial t^2}, \tag{2.5}$$

$$\implies \nabla \times -\frac{\partial \mathbf{B}}{\partial t} = \mu_0\epsilon_0\frac{\partial^2 \mathbf{E}}{\partial t^2}, \tag{2.6}$$

$$\implies -\nabla \times (\nabla \times \mathbf{E}) = \mu_0\epsilon_0\frac{\partial^2 \mathbf{E}}{\partial t^2}. \tag{2.7}$$

Then using the vector identity $\nabla \times (\nabla \times \mathbf{A}) = \nabla(\nabla \cdot \mathbf{A}) - \boldsymbol{\nabla^2 \mathbf{A}}$ we have

$$\nabla^2 \mathbf{E} = \frac{1}{c^2}\frac{\partial^2 \mathbf{E}}{\partial t^2}, \tag{2.8}$$

which is the standard wave equation with $c^2 = \frac{1}{\sqrt{\mu_0\epsilon_0}}$.

With the electric field polarized in x-direction the wave equation then becomes

$$\frac{\partial^2 E_x}{\partial z^2} = \frac{1}{c^2}\frac{\partial^2 E_x}{\partial^2 t}. \tag{2.9}$$

Solving this differential equation using separation of variables with $E_x(z,t) = P(z)T(t)$ we obtain the following solution

$$E_x(z,t) = \sqrt{\frac{2\omega^2}{\epsilon_0 V}}q(t)sin(kz). \tag{2.10}$$

From Maxwell's equation Eq. (2.4)

$$\nabla \times \mathbf{B} = \mu_0\epsilon_0\frac{\partial \mathbf{E}}{\partial t},$$

the magnetic field is

$$\begin{aligned} B_y(z,t) &= -\mu_0\epsilon_0\int\frac{\partial E_x}{\partial t}dz \\ &= \frac{\mu_0\epsilon_0}{k}\sqrt{\frac{2\omega^2}{\epsilon_0 V}}\dot{q}(t)cos(kz), \end{aligned} \tag{2.11}$$

where V is the effective volume of the cavity, q is a time-dependent amplitude with units of length, and $k = \frac{m\pi}{L}$ for $m > 0$.
The energy of the electromagnetic field is given by

$$\begin{aligned} H &= \frac{1}{2}\int dV\big(\epsilon_0\mathbf{E}^2 + \frac{1}{\mu_0}\mathbf{B}^2\big) \\ &= \frac{1}{2}\int dV\big(\epsilon_0 E_x^2(z,t) + \frac{1}{\mu_0}B_y^2(z,t)\big) \\ &= \frac{1}{2}[\dot{q}^2(t) + \omega^2 q^2(t)], \end{aligned} \tag{2.12}$$

where the volume integral is over the z domain. The Hamiltonian in Eq. (2.12) is similar to that of a harmonic oscillator with unit mass. To quantize the field we promote the Hamiltonian into an operator and rewrite $\dot{q} \equiv p$ giving us

$$\hat{H} = \frac{1}{2}[\hat{p}^2(t) + \omega^2\hat{q}(t)]. \tag{2.13}$$

Introducing the creation and annihilation operators in terms of $\hat{p}$ and $\hat{q}$

$$\hat{a}^\dagger(t) = \frac{1}{\sqrt{2\hbar\omega}}[\omega\hat{q}(t) - i\hat{p}(t)]. \tag{2.14}$$

$$\hat{a}(t) = \frac{1}{\sqrt{2\hbar\omega}}[\omega\hat{q}(t) + i\hat{p}(t)]. \tag{2.15}$$

We have $\hat{E}_x(z,t)$ and $\hat{B}_y(z,t)$ become

$$\hat{E}_x(z,t) = E_0[\hat{a}(t) + \hat{a}^\dagger(t)]sin(kz). \tag{2.16}$$

$$\hat{B}_y(z,t) = E_0[\hat{a}(t) - \hat{a}^\dagger(t)]cos(kz), \tag{2.17}$$

where $E_0 = \sqrt{\frac{\hbar\omega_c}{\epsilon_0 V}}$.
Using the commutation relation $[\hat{q},\hat{p}] = i\hbar$, the Hamiltonian of the field becomes

$$\begin{aligned} \hat{H}_{field} &= \hbar\omega\left[\hat{a}(t)\hat{a}^\dagger(t) + \frac{1}{2}\right] \\ &\approx \hbar\omega\hat{a}^\dagger(t)\hat{a}(t) \\ &= \hbar\omega\hat{a}^\dagger\hat{a}. \end{aligned} \tag{2.18}$$

The time dependence in Eq. (2.18) is dropped since $\hat{H}_{field}$ is time independent as total energy in closed system.

2.1.2 Hamiltonian of the two-level atom

The two-level system consists of a ground state $|g\rangle$ and the excited state $|e\rangle$ with energy $E = \hbar\omega_0$ as shown in Figure 2.2.

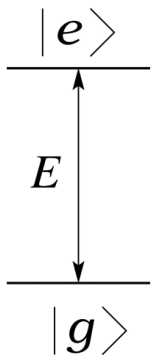

Figure 2.2: **Two-level system energy structure**.

The Hamiltonian is given by

$$\hat{H}_{atom} = \hbar\omega_0 \left|e\right\rangle \left\langle e\right| + 0 \left|g\right\rangle \left\langle g\right|, \tag{2.19}$$

with

$$|g\rangle = \begin{pmatrix} 0 \\ 1 \end{pmatrix}, |e\rangle = \begin{pmatrix} 1 \\ 0 \end{pmatrix}. \tag{2.20}$$

Thus,

$$\begin{aligned} \hat{H}_{atom} &= \hbar\omega_0 \begin{pmatrix} 1 \\ 0 \end{pmatrix} \begin{pmatrix} 1 & 0 \end{pmatrix} + 0 \begin{pmatrix} 0 \\ 1 \end{pmatrix} \begin{pmatrix} 0 & 1 \end{pmatrix} \\ &= \begin{pmatrix} \hbar\omega_0 & 0 \\ 0 & 0 \end{pmatrix} \\ &= \frac{1}{2} \begin{pmatrix} \hbar\omega_0 & 0 \\ 0 & \hbar\omega \end{pmatrix} + \frac{1}{2} \begin{pmatrix} \hbar\omega_0 & 0 \\ 0 & -\hbar\omega \end{pmatrix} \\ &= \frac{1}{2}(0 + \hbar\omega_0)\hat{\mathbf{1}} + \frac{1}{2}(\hbar\omega_0)\hat{\sigma}_z. \end{aligned} \tag{2.21}$$

The Hamiltonian of the two-level atom is

$$\hat{H}_{atom} = \hbar\omega_0\hat{\sigma}_z. \tag{2.22}$$

2.1.3 Interaction Hamiltonian

The interaction Hamiltonian is given by

$$\begin{aligned}\hat{H} &= -\hat{\boldsymbol{\mu}} \cdot \hat{\mathbf{E}} \\ &= -\hat{\mu} \cdot E_0(\hat{a} + \hat{a}^\dagger) sin(kz)\hat{\mathbf{x}} \\ &= \beta\hat{\mu}(\hat{a} + \hat{a}^\dagger),\end{aligned} \tag{2.23}$$

with $\beta = -\frac{\hbar\omega}{\epsilon_0 V} sin(kz)$.

We expand the dipole moment operator in terms of the basis states $\{|g\rangle, |e\rangle\}$

$$\hat{\mu} = \mu |g\rangle \langle e| + \mu^* |e\rangle \langle g| . \tag{2.24}$$

Recalling the Pauli spin matrices

$$\hat{\sigma}_x = \begin{pmatrix} 0 & 1 \\ 1 & 0 \end{pmatrix}, \qquad \hat{\sigma}_y = \begin{pmatrix} 0 & -i \\ i & 0 \end{pmatrix}, \qquad \hat{\sigma}_z = \begin{pmatrix} 1 & 0 \\ 0 & -1 \end{pmatrix}. \tag{2.25}$$

And their combinations

$$\hat{\sigma}^+ = \frac{1}{2}(\hat{\sigma}_x + i\hat{\sigma}_y) = \begin{pmatrix} 0 & 1 \\ 0 & 0 \end{pmatrix}, \qquad \hat{\sigma}^- = \frac{1}{2}(\hat{\sigma}_x - i\hat{\sigma}_y) = \begin{pmatrix} 0 & 0 \\ 1 & 0 \end{pmatrix}. \tag{2.26}$$

We have,

$$|e\rangle \langle g| = \begin{pmatrix} 0 & 1 \\ 0 & 0 \end{pmatrix} = \hat{\sigma}^+, \tag{2.27}$$

$$|g\rangle \langle e| = \begin{pmatrix} 0 & 0 \\ 1 & 0 \end{pmatrix} = \hat{\sigma}^-. \tag{2.28}$$

Then Eq. (2.24) becomes

$$\begin{aligned}\hat{\mu} &= \mu\hat{\sigma}^- + \mu\hat{\sigma}^+ \\ &= \mu(\hat{\sigma}^- + \hat{\sigma}^+),\end{aligned} \tag{2.29}$$

in which we assumed that μ is real thus making the interaction Hamiltonian to be

$$\hat{H}_{interaction} = \hbar g(\hat{\sigma}^- + \hat{\sigma}^+)(\hat{a} + \hat{a}^\dagger), \tag{2.30}$$

where $g = -\frac{\mu}{\hbar}\sqrt{\frac{\hbar\omega}{\epsilon_0 V}} sin(kz)$.

Under the interaction picture the operators can be written as

$$\hat{a}(t) = \hat{a}(0)e^{-i\omega t}, \qquad \hat{a}^\dagger(t) = \hat{a}^\dagger(0)e^{-i\omega t}, \qquad \hat{\sigma}^\pm = \hat{\sigma}^\pm(0)e^{\pm i\omega_0 t}. \tag{2.31}$$

Eq. (2.30) then becomes

$$\begin{aligned}\hat{H}_{interaction} &= \hbar g\Big(\hat{\sigma}^{-}\hat{a} + \hat{\sigma}^{-}\hat{a}^{\dagger} + \hat{\sigma}^{+}\hat{a} + \hat{\sigma}^{+}\hat{a}^{\dagger}\Big) \\ &= \hbar g\Big(\hat{\sigma}^{-}\hat{a}e^{-i(\omega_0+\omega)t} + \hat{\sigma}^{-}\hat{a}^{\dagger}e^{-i(\omega_0-\omega)t} \\ &+ \hat{\sigma}^{+}\hat{a}e^{i(\omega_0-\omega)t} + \hat{\sigma}^{+}\hat{a}^{\dagger}e^{i(\omega_0+\omega)t}\Big).\end{aligned} \tag{2.32}$$

Before we can further simply $\hat{H}_{interaction}$ in Eq. (2.32) we first define the concept of rotating wave approximation. The rotating wave approximation is an approximation to find an approximate solution to the Schrödinger equation with the rapidly oscillating terms in $\hat{H}_{interaction}$, $e^{\pm i(\omega_0+\omega)t}$ being neglected. The approximation is valid when the field frequency is near resonance with the atomic transition frequency.

Invoking the rotating wave approximation, we see that $\omega_0 - \omega \ll \omega_0 + \omega$ with the exponentials rapidly oscillating. These oscillations will average to zero and thus,

$$\hat{H}_{interaction} = \hbar g\big(\hat{\sigma}^{+}\hat{a} + \hat{\sigma}^{-}\hat{a}^{\dagger}\big). \tag{2.33}$$

The Jaynes-Cummings Hamiltonian is then,

$$H_{JC} = \omega\hat{a}^{\dagger}\hat{a} + \frac{1}{2}\omega_0\hat{\sigma_z} + g(\hat{a}^{\dagger}\hat{\sigma}^{-} + \hat{a}\hat{\sigma^{+}}), (\hbar = 1). \tag{2.34}$$

2.2 Features of the Jaynes-Cummings Model

Now that we have fully derived the Jaynes-Cummings Hamiltonian (Eq. (2.34)), we can now analyze the features given by the model. In order to analyze the properties of the JC Hamiltonian we further simplify the Hamiltonian by introducing the number operator $\hat{N} = \hat{a}^{\dagger}\hat{a} + \hat{\sigma}^{+}\hat{\sigma}^{-}$. The Jaynes-Cummings Hamiltonian in the rotating wave approximation

$$H_{JC} = \omega\hat{a}^{\dagger}\hat{a} + \omega_0\hat{\sigma}^{+}\hat{\sigma}^{-} + g(\hat{a}\hat{\sigma}^{+} + \hat{a}^{\dagger}\hat{\sigma}^{-}), \tag{2.35}$$

is transformed into a simpler Hamiltonian by introducing the number operator $\hat{N}$ and the detuning parameter $\Delta = \omega_0 - \omega$ between the field frequency and atomic transition frequency. The Hamiltonian now reads

$$H_{JC} = \omega\hat{N} + \Delta\hat{\sigma}^{+}\hat{\sigma}- + g(\hat{a}\hat{\sigma}^{+} + \hat{a}^{\dagger}\hat{\sigma}^{-}). \tag{2.36}$$

We can now explore the properties of the above Hamiltonian for example, its eigenstates and eigenvalues, but first, we investigate the commutation relation between the number operator $\hat{N}$ and the Hamiltonian H_{JC} given by

$$[\hat{N}, \hat{H}_{JC}] = \omega[\hat{N}, \hat{N}] + \Delta[\hat{N}, \hat{\sigma}^{+}\hat{\sigma}^{-}] + g([\hat{N}, \hat{a}\hat{\sigma}^{+}] + [\hat{N}, \hat{a}^{\dagger}\hat{\sigma}^{-}]), \tag{2.37}$$

with $[\hat{N}, \hat{N}] = 0$

$$[\hat{a}^\dagger, \hat{\sigma}^-] = [\hat{a}, \hat{\sigma}^-] = [\hat{a}^\dagger, \hat{\sigma}^+] = [\hat{a}, \hat{\sigma}] = 0. \tag{2.38}$$

Since all operators act in their respective subspaces the commutator between operators acting in different subspaces becomes zero (See Appendix A). This implies that

$$[\hat{N}, \hat{\sigma}^+\hat{\sigma}^-] = [\hat{N}, \hat{a}^\dagger\hat{a}] = 0. \tag{2.39}$$

From the commutation relations in Appendix A we find that

$$[\hat{N}, \hat{a}\hat{\sigma}^+] = [\hat{N}, \hat{a}^\dagger\hat{\sigma}^+] = 0. \tag{2.40}$$

Thus

$$[\hat{N}, \hat{H}_{JC}] = 0. \tag{2.41}$$

The number operator commutes with the Jaynes-Cummings Hamiltonian. The result of this commutation is a conserved quantity of the number operator called the polariton, which is a coupled excitation of photonic and atomic system. Both operators $\hat{N}$ and $\hat{H}_{JC}$ share common eigenstates between subspaces as such we propose the basis $|\psi_{1n}\rangle = |n, g\rangle$ and $|\psi_{2n}\rangle = |n-1, e\rangle$. Then the Hamiltonian can be diagonalized as

$$\hat{H}^{(n)} = \langle i| \hat{H}_{JC} |j\rangle , \tag{2.42}$$

where in matrix form

$$\begin{aligned} \hat{H}^{(n)} &= \begin{pmatrix} \langle\psi_{1n}| \hat{H}_{JC} |\psi_{1n}\rangle & \langle\psi_{1n}| \hat{H}_{JC} |\psi_{2n}\rangle \\ \langle\psi_{2n}| \hat{H}_{JC} |\psi_{1n}\rangle & \langle\psi_{2n}| \hat{H}_{JC} |\psi_{2n}\rangle \end{pmatrix} \\ &= \begin{pmatrix} \langle n, g| \hat{H}_{JC} |n, g\rangle & \langle n, g| \hat{H}_{JC} |n-1, e\rangle \\ \langle n-1, e| \hat{H}_{JC} |n, g\rangle & \langle n-1, e| \hat{H}_{JC} |n-1, e\rangle \end{pmatrix}. \end{aligned} \tag{2.43}$$

Using the ladder operators and spin operators acting on the eigenstates we find the following eigenstates

$$\begin{aligned} \hat{a}^\dagger\hat{a} |n, g\rangle &= n |n, g\rangle , & \hat{a}^\dagger\hat{a} |n-1, e\rangle &= (n-1) |n-1, e\rangle , \\ \hat{\sigma}^+\hat{\sigma}^- |n, g\rangle &= 0, & \hat{\sigma}^+\hat{\sigma}^- |n-1, e\rangle &= |n-1, e\rangle , \\ \hat{a}\hat{\sigma}^+ |n, g\rangle &= \sqrt{n} |n-1, e\rangle , & \hat{a}\hat{\sigma}^+ |n-1, e\rangle &= 0, \\ \hat{a}^\dagger\hat{\sigma}^- |n, g\rangle &= 0, & \hat{a}^\dagger\hat{\sigma}^- |n-1, e\rangle &= \sqrt{n} |n, g\rangle . \end{aligned} \tag{2.44}$$

The Hamiltonian in the bare basis is written as

$$\hat{H}^{(n)} = \begin{pmatrix} \omega n & g\sqrt{n} \\ g\sqrt{n} & \omega n + \Delta \end{pmatrix}. \tag{2.45}$$

We can now find the eigenstructure of the system Hamiltonian $H^{(n)}$ by evaluating the characteristic polynomial $H^{(n)}$ which is given by

$$\begin{aligned} p(E_n) &= det\Big(H^n - E_n I\Big) \\ &= det\left(\begin{pmatrix} \omega n & g\sqrt{n} \\ g\sqrt{n} & \omega n + \Delta \end{pmatrix} - \begin{pmatrix} E_n & 0 \\ 0 & E_n \end{pmatrix} \right) \\ &= \Big(\omega n - E_n\Big)\Big(\omega n + \Delta - E_n\Big) - g^2 n. \end{aligned} \tag{2.46}$$

The eigenvalues E_n are roots of the characteristic polynomial i.e

$$p(E_n) = 0, \tag{2.47}$$

which gives the eigenvalues as

$$E_{n\pm} = \omega n + \frac{1}{2}(\Delta \pm R_n), \tag{2.48}$$

where

$$R_n = \sqrt{\Delta^2 + 4g^2 n}, n > 1, \tag{2.49}$$

is the generalized Rabi frequency.

The eigenstates are calculated by solving the following eigenvalue equation

$$\begin{pmatrix} \omega n & g\sqrt{n} \\ g\sqrt{n} & \omega n + \Delta \end{pmatrix} \begin{pmatrix} \nu_1^{\pm} \\ \nu_2^{\pm} \end{pmatrix} = E_{n\pm} \begin{pmatrix} \nu_1^{\pm} \\ \nu_2^{\pm} \end{pmatrix}. \tag{2.50}$$

The coefficients of the eigenstates satisfy the relation

$$(\nu_1^{\pm})^2 + (\nu_2^{\pm})^2 = 1. \tag{2.51}$$

The dependence of the coefficients on each other means we can use one of the equations in Eq. (2.50)

$$\omega \nu_1^+ + g\sqrt{n}\nu_2^+ = E_{n+}\nu_1^+. \tag{2.52}$$

Using Eq. (2.51)

$$\begin{aligned} (\omega n - E_{n+})\nu_1^+ + g\sqrt{n}\sqrt{1 - (\nu_1^+)^2} = 0 \\ \frac{1}{2}(\Delta + R_n)\nu_1^+ = g\sqrt{n}\sqrt{1 - (\nu_1^+)^2} \\ (\Delta + R_n)^2(\nu_1^+)^2 = 4g^2 n[1 - (\nu_1^+)^2], \end{aligned} \tag{2.53}$$

results in

$$\nu_1^+ = \frac{2g\sqrt{n}}{\sqrt{(\Delta + R_n)^2 + 4g^2 n}}, \tag{2.54}$$

$$\nu_2^+ = \frac{\Delta + R_n}{\sqrt{(\Delta + R_n)^2 + 4g^2 n}}. \tag{2.55}$$

Using the parametrization

$$\sin\theta_n := \nu_1^+, \cos\theta_n := \nu_2^+, \tag{2.56}$$

and the trigonometric identity

$$\begin{aligned} \cos(2\theta_n) = \cos{\theta_n}^2 - \sin{\theta_n}^2 &= \frac{(\Delta + R_n)^2 - 4g^2 n}{(\Delta + R_n)^2 + 4g^2 n} \\ &= \frac{2\Delta(\Delta + R_n)}{\Delta^2 + 2\Delta R_n + R_n^2 + R_n^2 - \Delta^2} = \frac{\Delta}{R_n}. \end{aligned} \tag{2.57}$$

And similarly for the sine:

$$\begin{aligned} \sin(2\theta_n) = 2\sin\theta_n\cos\theta_n &= \frac{4g\sqrt{n}(\Delta + Rn)}{(\Delta + R_n)^2 + 4g^2 n} \\ &= \frac{4g\sqrt{n}(\Delta + Rn)}{\Delta^2 + 2\Delta R_n + R_n^2 + 4g^2 n} \\ &= \frac{2g\sqrt{n}}{R_n}. \end{aligned} \tag{2.58}$$

Dividing Eq. (2.58) by Eq. (2.57) we find

$$\tan(2\theta_n) = \frac{2g\sqrt{n}}{\Delta}. \tag{2.59}$$

For the other amplitudes we find the coefficients to be

$$\nu_1^- = \frac{2g\sqrt{n}}{\sqrt{(\Delta - R_n)^2 + 4g^2 n}}. \tag{2.60}$$

$$\nu_2^- = \frac{\Delta - R_n}{\sqrt{(\Delta - R_n)^2 + 4g^2 n}}. \tag{2.61}$$

Thus,

$$(\nu_1^-)^2 = \frac{4g^2 n}{(\Delta - R_n)^2 + 4g^2 n} = \frac{(\Delta + R_n)^2}{4g^2 n + (\Delta + R_n)^2}. \tag{2.62}$$

$$(\nu_2^-)^2 = \frac{(\Delta - R_n)^2}{(\Delta - R_n)^2 + 4g^2 n} = \frac{4g^2 n}{4g^2 n + (\Delta + R_n)^2}. \tag{2.63}$$

We find that

$$(\nu_1^-)^2 = (\nu_2^+)^2. \tag{2.64}$$

$$(\nu_2^-)^2 = (\nu_1^+)^2. \tag{2.65}$$

Thus we find the corresponding eigenstates to be

$$|n,+\rangle = \sin\theta_n \,|n,g\rangle + \cos\theta_n \,|n-1,e\rangle\,. \tag{2.66}$$

$$|n,-\rangle = \cos\theta_n \,|n,g\rangle - \sin\theta_n \,|n-1,e\rangle\,, \tag{2.67}$$

with

$$\theta_n = \frac{1}{2}\arctan\left(\frac{2g\sqrt{n}}{\Delta}\right). \tag{2.68}$$

Figure 2.3 shows the polariton branches of the model with the frequency scaling in a nonlinear scale of $2\sqrt{n}g$ which comes with the splitting of the energy levels in the strongly coupled case (dressed states) as shown in the energy level structure in Figure 2.4.

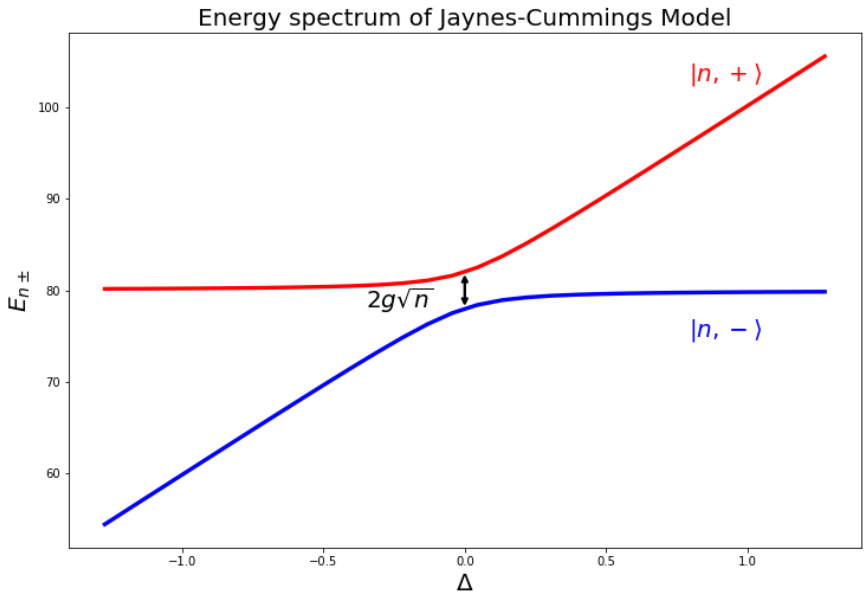

Figure 2.3: **Energy eigenvalues** of the Jaynes-Cummings model with states being split by $2g$ rad/s.

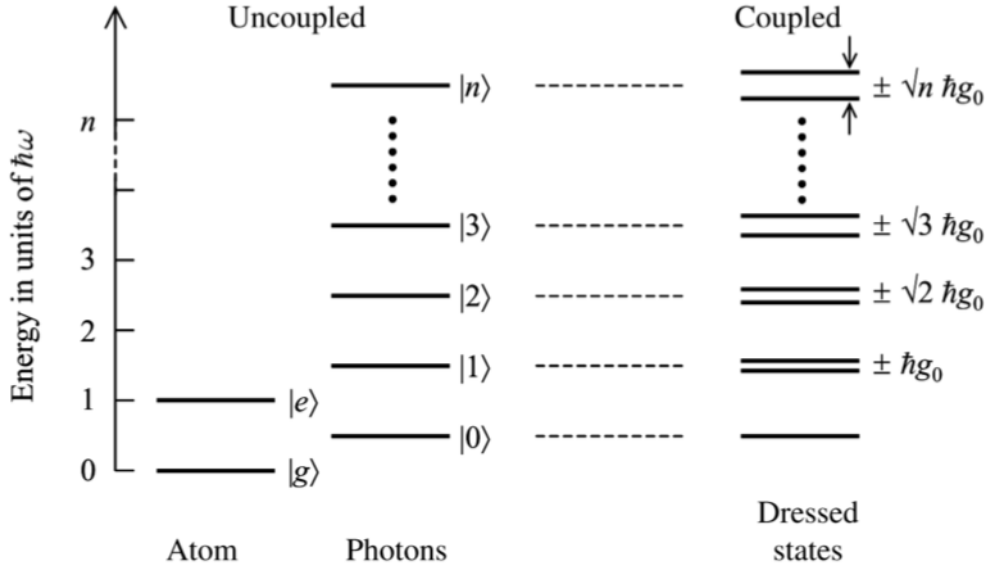

Figure 2.4: **Energy level Structure** of the Jaynes-Cummings model. Energy levels of the atom and photon/field are equally spaced as opposed to those of the atom-cavity system in which there is degeneracy in the levels.

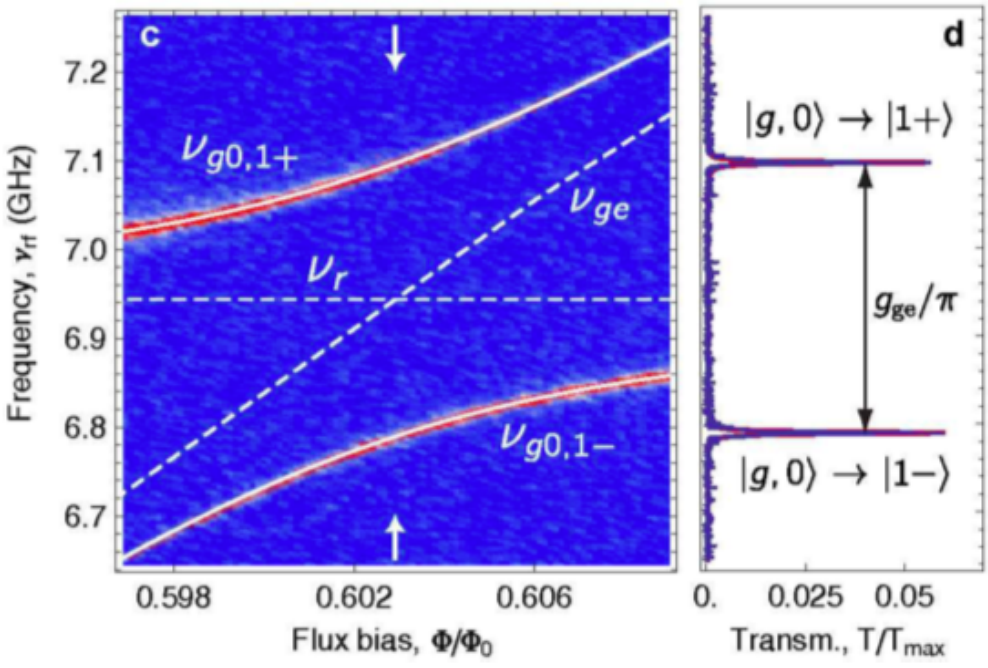

Figure 2.5: **Vacuum Rabi Splitting** of the energy levels of transmon qubit coupled to a coplanar waveguide with the states being split by $g/\pi s^{-1}$ [11].

Figure 2.5 shows the experimental observation of the vacuum Rabi mode splitting for transmon superconducting qubit coupled to a superconducting coplanar waveguide. Measurements of the transmission spectrum of the cavity, transition frequency of the qubit and the magnetic flux bias of the qubit. Observed in (c) is the groundstate

splitting of the energy levels to two polariton branches or the lowest doublet $|1,\pm\rangle$ with the corresponding peak separation.

Figure 2.6 shows the dressed states energy levels of the experiment on the transmon qubit. The energy levels were reconstructed from the probe measurements conducted in Figure 2.5. It is evident from the figure that the $\sqrt{n}$ nonlinearity of the energy levels is observed for single and two photons in the cavity.

Figure 2.7 shows the collapse-revival oscillations for an atom in a superposition and the field in a coherent state given by

$$|\psi(0)\rangle_{atom} = \frac{1}{\sqrt{2}}(|g\rangle + |e\rangle), \qquad |\psi(0)\rangle_{field} = \sum_{n=0}^{\infty} C_n |n\rangle . \tag{2.69}$$

$$\tag{2.70}$$

The initial atom-field is given by

$$|\psi(0)\rangle = |\psi(0)\rangle_{atom} \otimes |\psi(0)\rangle_{field} . \tag{2.71}$$

Solving the Schrödinger equation we obtain the state

$$|\Psi(t)\rangle = \sum_{n=0}^{\infty} C_n \Big\{ \cos gt\sqrt{n+1}\, |e\rangle\, |n\rangle - i \sin gt\sqrt{n+1}\, |g\rangle\, |n+1\rangle \Big\}. \tag{2.72}$$

The transition probabilities are given by

$$P_e(t) = |\langle e|\Psi(t)\rangle|^2 = \sum_{n=0}^{\infty} e^{-N} \frac{N^n}{n!} \cos^2(gt\sqrt{n+1}). \tag{2.73}$$

$$P_g(t) = |\langle g|\Psi(t)\rangle|^2 = \sum_{n=0}^{\infty} e^{-N} \frac{N^n}{n!} \sin^2(gt\sqrt{n+1}). \tag{2.74}$$

The atomic inversion is,

$$\begin{aligned} W(t) &= P_e(t) - P_g(t) \\ &= e^{-N} \sum_{n=0}^{\infty} \frac{N^n}{n!} \cos(2gt\sqrt{n+1}), \end{aligned} \tag{2.75}$$

where n = average photon number.

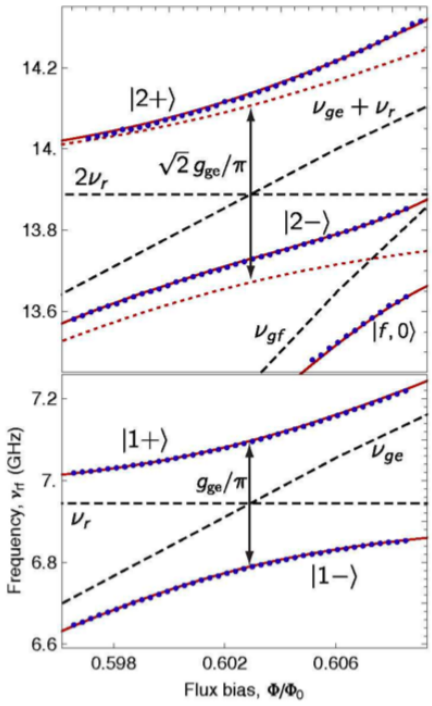

Figure 2.6: **Experimental Dressed states** of the transmon qubit coupled to a coplanar waveguide resonator [11].

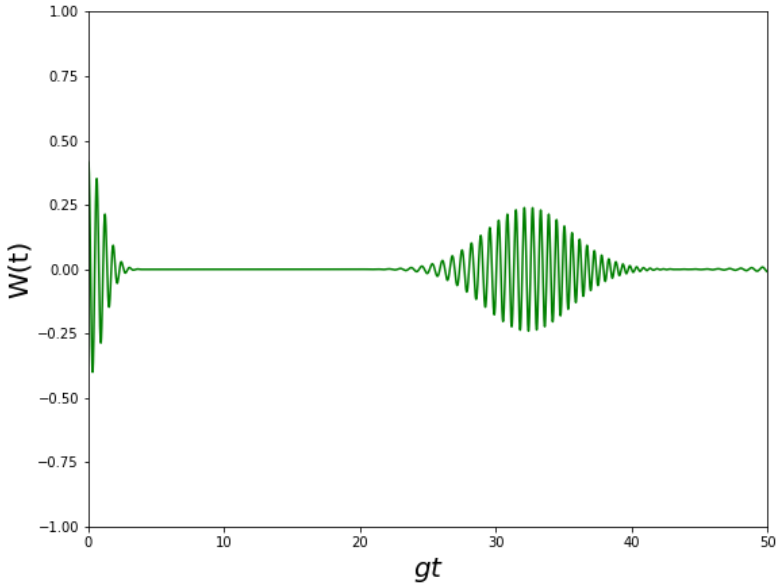

Figure 2.7: **Collapse-revival oscillations** of the quantized radiation field interacting with the two-level atom.

Chapter 3

Dissipative Jaynes-Cummings Model

In Chapter 2 we introduced the Jaynes-Cummings model that describes the dynamics of a two-level atom interacting with a quantized radiation field in which we assumed the system to be closed and not interacting with the rest of the environment. Quantum systems are never isolated, as such they lead to decoherence of the system affecting the ability to make accurate measurements of a quantum system. We need a complete description of the dynamics of open systems that take into account the full environmental interaction. To do this we consider the use of the master equation of the density operator of the system [36] for Markovian and non-Markovian dynamics. The dynamics are difficult to analyze and solve analytically hence the reason most dissipative cavity QED experiments are analyzed by performing numerical simulations [37]. In this chapter we review the formalism used to describe the dissipative processes from the density operator to the derivation of the quantum master equation and application of the of it to the one excitation problem. These will lay foundation for the applications of the model in processes of quantum information that we will study in subsequent chapters of this thesis.

The governing Hamiltonian for the interaction of a two-level atom (qubit) with a cavity coupled to a bosonic bath is given by

$$H = H_S + H_E + H_I. \tag{3.1}$$

where

$$H_S = \omega \hat{a}^\dagger \hat{a} + \frac{1}{2}\omega_0 \hat{\sigma}_z + g(\hat{a}^\dagger \hat{\sigma}^- + \hat{a}\hat{\sigma}^+). \tag{3.2}$$

$$H_E = \sum_k \omega_k \hat{b}_k^\dagger \hat{b}_k. \tag{3.3}$$

$$H_I = (\hat{a}^\dagger + \hat{a}) \sum_k g_k (\hat{b}_k^\dagger + \hat{b}_k), \tag{3.4}$$

and
$\hat{b}_k^\dagger \hat{b}_k$ being the creation and annihilation operators associated with the environment with following commutation relations

$$[\hat{b}_i, \hat{b}_j^\dagger] \equiv \hat{b}_i \hat{b}_j^\dagger - \hat{b}_j^\dagger \hat{b}_i = \delta_{ij}. \tag{3.5}$$

$$[\hat{b}_i^\dagger, \hat{b}_j^\dagger] = [\hat{b}_i, \hat{b}_j] = 0. \tag{3.6}$$

Before studying the dynamics of the model we need to describe a formalism that will enable us to fully understand the total system and extract information from it and that is through the density matrix.

3.1 Density Matrices

The density matrix or density operator for a pure state $|\psi\rangle$ is given by

$$\rho = |\psi\rangle \langle\psi| . \tag{3.7}$$

and has the following properties:

$$\rho^2 = \rho \qquad projection. \tag{3.8}$$
$$\rho \geq 0 \qquad positivity. \tag{3.9}$$
$$\rho = \rho^\dagger \qquad hermiticity. \tag{3.10}$$
$$Tr\rho = 1 \qquad normalization. \tag{3.11}$$

For an ensemble of mixed states (collection of systems that are not in the same state) the density operator takes the form

$$\rho = \sum_i p_i |\psi_i\rangle \langle\psi_i| , \tag{3.12}$$

with

$$p_i = \langle\psi_i| \rho |\psi_i\rangle , \tag{3.13}$$

being the probability to find an individual system of the ensemble. The density operator can be written in matrix form (density matrix) with the diagonal matrix elements representing population states and off-diagonal entries the coherences. These terms are sensitive to the relative phases of mixed states.

$$\begin{pmatrix} \rho_{11} & \rho_{12} \\ \rho_{21} & \rho_{22} \end{pmatrix} \Longleftarrow \rho = \sum p_i |\psi_i\rangle \langle\psi_i| \Longrightarrow \rho_{nm} = \begin{pmatrix} n = m(population) \\ n \neq m(coherences) \end{pmatrix}. \tag{3.14}$$

To find the equation of motion of the density matrix ρ we differentiate Eq. (3.12) with respect to time

$$\begin{aligned} \frac{d}{dt}\rho &= \frac{d}{dt}\sum_i p_i |\psi_i\rangle \langle\psi_i| \\ &= \sum_i p_i \Big[\Big(\frac{d}{dt} |\psi_i\rangle \Big) \langle\psi_i| + |\psi_i\rangle \Big(\frac{d}{dt} \langle\psi_i| \Big) \Big]. \end{aligned} \tag{3.15}$$

And using the time-dependent Schrödinger equation

$$i\hbar \frac{\partial}{\partial t} |\psi_i\rangle = \hat{H} |\psi_i\rangle . \tag{3.16}$$

we have that Eq. (3.15) becomes

$$\frac{d}{dt}\rho = -\sum_i p_i \frac{i}{\hbar}\big(\hat{H}\,|\psi_i\rangle\,\langle\psi_i| - |\psi_i\rangle\,\langle\psi_i|\,\hat{H}\big), \tag{3.17}$$

where $\frac{d}{dt}\,|\psi_i\rangle = -\frac{i}{\hbar}\hat{H}\,|\psi_i\rangle$ with $\hbar = 1$ Thus,

$$\frac{d}{dt}\rho = -i[\hat{H}, \rho], \tag{3.18}$$

the density matrix ρ, obeys the von Neumann equation.

3.2 Derivation of the Quantum Master Equation

Open quantum systems are stochastic in nature, in other words their dynamical evolution is probabilistic as the predictions of quantum mechanics are probabilistic. In such a case, the Schrödinger equation of motion can no longer be used to study the dynamics of open quantum systems. A master equation describes the non-unitary dynamics between the system interacting with its environment. Both the system denoted S and the environment denoted E are different quantum system with $S+E$ being a closed system [38]. The density matrix describes a probability distribution of quantum states $|\psi_i\rangle$ which is used to obtain the reduced density matrix of the system were the environment degrees of freedom have been traced out.
The first point of our derivation involves rewriting the total Hamiltonian in the Heisenberg interaction picture.

Transforming the Hamiltonian in Eq. (3.1) into the interaction picture we have

$$\tilde{H}_I(t) = e^{i(H_S+H_E)t} H_I e^{-i(H_S+H_E)t}. \tag{3.19}$$

Within the interaction picture the density operator evolves according to

$$\frac{\partial}{\partial t}\tilde{\rho}(t) = -i[\tilde{H}_I(t), \tilde{\rho}(t)]. \tag{3.20}$$

The solution of Eq. (3.20) takes the form

$$\tilde{\rho}(t) = -i\int_0^t [\tilde{H}_I(s), \tilde{\rho}(s)]ds + \rho(0). \tag{3.21}$$

Substituting back to Eq. (3.20) gives

$$\frac{\partial}{\partial t}\tilde{\rho}(t) = -\int_0^t [\tilde{H}_I(t), [\tilde{H}_I(s), \tilde{\rho}(s)]]ds - i[\tilde{H}_I(t), \rho(0)]. \tag{3.22}$$

We then trace over the environment to get the reduced density operator which describes the dynamics of the system

$$\frac{\partial}{\partial t}\tilde{\rho}_S(t) = -\int_0^t Tr_E\Big([\tilde{H}_I(t), [\tilde{H}_I(s), \tilde{\rho}(s)]]\Big)ds - iTr_E\Big([\tilde{H}_I(t), \rho(0)]\Big). \tag{3.23}$$

In the second step of the derivation, we make the following assumptions [39]:

Separability At the initial time t=0 the total density matrix can be written as a tensor product of the system and environment. At this time we assuming there is no correlation between the system and the environment.

$$\rho(0) = \rho_S(0) \otimes \rho_E(0). \tag{3.24}$$

We make the assumption that $Tr_E[\tilde{H}_I(t), \rho(0)] = 0$ with Eq. (3.23) becoming

$$\frac{\partial}{\partial t}\tilde{\rho}_S(t) = -\int_0^t Tr_E\Big([\tilde{H}_I(t), [\tilde{H}_I(s), \tilde{\rho}(s)]]\Big)ds. \tag{3.25}$$

Performing the **Born approximation** which assumes that the coupling between the system and the environment is weak, the environment is much larger than the system such that the environmental state does not change remarkably as its interaction with the system. The Born approximation further assumes that the total density matrix $\rho(t)$ is separable and approximated by

$$\tilde{\rho}(t) = \tilde{\rho}_S(t) \otimes \rho_E. \tag{3.26}$$

Eq. (3.25) is now given by

$$\frac{\partial}{\partial t}\rho_S(t) = -\int_0^t Tr_E\Big([\tilde{H}_I(t), [\tilde{H}_I(s), \tilde{\rho}_S(t) \otimes \rho_E]]\Big)ds. \tag{3.27}$$

At this stage the master equation is still difficult to solve and thus we make another approximation. In the **Markov approximation** we assume that the bath is memoryless and replace the lower limit of the integral by -∞ and s$\rightarrow t - \tau$ then

$$\frac{\partial}{\partial t}\tilde{\rho}_S(t) = -\int_0^\infty Tr_E\Big([\tilde{H}_I(t), [\tilde{H}_I(t-\tau), \tilde{\rho}_S(t) \otimes \rho_E]]\Big)d\tau. \tag{3.28}$$

To perform the **Rotating-Wave approximation** we redefine the interaction Hamiltonian in terms of the system and environment operators

$$H_I = A \otimes E, \tag{3.29}$$

where A and E are the operators acting on the system and environment. We then decompose H_I into eigenoperators of the system Hamiltonian H_S by the defining the following expansions of the operators

$$A = \sum_{\tilde{\omega}} A(\tilde{\omega}), \tag{3.30}$$

where

$$A(\tilde{\omega}) = \sum_{\epsilon' - \epsilon = \tilde{\omega}} \prod(\epsilon) A \prod(\epsilon'), \tag{3.31}$$

where $\prod(\epsilon)$ is the projection onto the eigenspace corresponding to the eigenvalue ϵ of the operator H_S and the sum is taken over the Bohr frequencies with respect to H_S. The following commutation relations hold

$$[H_S, A(\tilde{\omega})] = -\tilde{\omega}A(\tilde{\omega}). \tag{3.32}$$

$$[H_S, A^\dagger(\tilde{\omega})] = \tilde{\omega}A^\dagger(\tilde{\omega}). \tag{3.33}$$

The corresponding interaction picture for the operators is given by

$$e^{iH_St}A(\tilde{\omega})e^{-iH_St} = e^{-i\tilde{\omega}t}A(\tilde{\omega}). \tag{3.34}$$

$$e^{iH_St}A^\dagger(\tilde{\omega})e^{-iH_St} = e^{+i\tilde{\omega}t}A^\dagger(\tilde{\omega}). \tag{3.35}$$

Summing over all energy differences in Eq. (3.31) the new interaction Hamiltonian is written as

$$H_I(t) = \sum_{\tilde{\omega}} e^{i\tilde{\omega}t}A(\tilde{\omega}) \otimes E(t). \tag{3.36}$$

We then expand the commutators [38] in Eq. (3.28) to get

$$\begin{aligned}\frac{\partial}{\partial t}\tilde{\rho}_S(t) = -\int_0^\infty & tr_E\tilde{H}_I(t)\tilde{H}_I(t-\tau)\tilde{\rho}_S(t)\otimes\rho_E \\ & - \tilde{H}_I(t)\tilde{\rho}_S(t)\otimes\rho_E H_I(t-s) \\ & - H_I(t-s)\rho_S(t)\otimes\rho_E\tilde{H}_I(t) \\ & + \tilde{\rho}_S(t)\otimes\rho_E\tilde{H}_I(t-\tau)\tilde{H}_I(t)\}d\tau.\end{aligned} \tag{3.37}$$

Substituting Eq. (3.36) into the master equation Eq. (3.37) and defining the Fourier transformed environment correlation function as

$$\gamma(\tilde{\omega}) = \int_{-\infty}^{+\infty} d\xi e^{i\tilde{\omega}\xi}\left\langle E^\dagger(\xi)E(0)\right\rangle, \tag{3.38}$$

and transforming back to Schrödinger picture we have the master equation as

$$\begin{aligned}\dot{\rho}(t) = -i[H_S,\rho] &+ \sum_{\tilde{\omega}>0}\gamma(\tilde{\omega})\big[A(\tilde{\omega})\rho(t)A^\dagger(\tilde{\omega}) - \frac{1}{2}\big\{A^\dagger(\tilde{\omega})A(\tilde{\omega}),\rho(t)\big\}\big] \\ &+ \sum_{\tilde{\omega}>0}\gamma(-\tilde{\omega})\big[A^\dagger(\tilde{\omega})\rho(t)A(\tilde{\omega}) - \frac{1}{2}\big\{A(\tilde{\omega})A^\dagger(\tilde{\omega}),\rho(t)\big\}\big].\end{aligned} \tag{3.39}$$

For the Jaynes-Cummings system,the operator $A = (\hat{a} + \hat{a}^\dagger)$ defined in Eq. (3.30) and Eq. (3.31) is given by

$$A(\tilde{\omega}) = |E_{N,m}\rangle\langle E_{N,m}|\,(\hat{a}+\hat{a}^\dagger)\,|E_{N',l}\rangle\langle E_{N',l}|, \tag{3.40}$$

where $\tilde{\omega}$ is the energy difference of combined atom and cavity system, $|E_{N,\pm}\rangle = \frac{1}{\sqrt{2}}(|N,g\rangle \pm |N-1,e\rangle)$ with l,m taking values ± 1.

Using the definition of the ladder operators

$$\hat{a}^\dagger \left|n\right\rangle = \sqrt{n+1}\left|n+1\right\rangle . \tag{3.41}$$

$$\hat{a} \left|n\right\rangle = \sqrt{n}\left|n-1\right\rangle . \tag{3.42}$$

The operator $A(\tilde{\omega})$ becomes

$$A(\tilde{\omega}) = \frac{1}{2}\delta_{N,N'-1}\big(\sqrt{N+1} + lm\sqrt{N}\big)\left|E_{N,m}\right\rangle\left\langle E_{N+1,l}\right| , \tag{3.43}$$

for $N \geq 1$, where $\delta_{N,N'-1}$ is the Kronecker function defined

$$\delta_{N,N'-1} = \begin{cases} 0 & N \neq N'-1 \\ 1 & (N = N'-1); l = m \end{cases} . \tag{3.44}$$

From Eq. (3.39) the Markovian master equation for the Jaynes-Cummings Model interacting with a bath is

$$\begin{aligned}
\dot{\rho}(t) = -i[H_{JC},\rho] &+ \sum_{l=\pm 1} \frac{\gamma(E_{1,l}-E_0)}{2}\big(\left|E_0\right\rangle\left\langle E_1,l\right|\rho\left|E_1,l\right\rangle\left\langle E_0\right| - \frac{1}{2}\big\{\left|E_{1,l}\right\rangle\left\langle E_{1,l}\right|,\rho\big\}\big) \\
&+ \sum_{l,m=\pm}\sum_{N=1}^{\infty} \frac{\gamma(E_{N+1,l}-E_{N,m})}{4}\big(\sqrt{N+1}+lm\sqrt{N}\big)^2\big(\left|E_{N,m}\right\rangle\left\langle E_{N+1},l\right|\rho\left|E_{N+1},l\right\rangle\left\langle E_{N,m}\right| \\
&- \frac{1}{2}\big\{\left|E_{N+1,l}\right\rangle\left\langle E_{N+1,l}\right|,\rho\big\}\big) + \sum_{l=\pm 1} \frac{\gamma(E_0-E_{1,l})}{2}\big(\left|E_{1,l}\right\rangle\left\langle E_0\right|\rho\left|E_0\right\rangle\left\langle E_{1,l}\right| - \frac{1}{2}\big\{\left|E_0\right\rangle\left\langle E_0\right|,\rho\big\}\big) \\
&+ \sum_{l,m=\pm}\sum_{N=1}^{\infty} \frac{\gamma(E_{N+1,l}-E_{N,m})}{4}\big(\sqrt{N+1}+lm\sqrt{N}\big)^2\big(\left|E_{N,m}\right\rangle\left\langle E_{N+1,l}\right|\rho\left|E_{N+1},l\right\rangle\left\langle E_{N,m}\right| \\
&- \frac{1}{2}\big\{\left|E_{N,m}\right\rangle\left\langle E_{N,m}\right|,\rho\big\}\big).
\end{aligned} \tag{3.45}$$

For systems with enviroments satisfying the conditions (string of approximations) made above, the Markovian master equation governs the time-evolution of the system density matrix, giving an ensemble average of the system dynamics.

3.3 Dynamics of the master equation with one initial excitation

The initial state of the atom-cavity system is $|0e\rangle$. For a closed system there is a continuous exchange of energy between the atom and the cavity which is characterized by Rabi oscillations shown in Figure 3.1. Allowing the atom-cavity system to interact with the environment the atom and cavity occupation probabilities decrease as a result of dissipation (Figure 3.2).

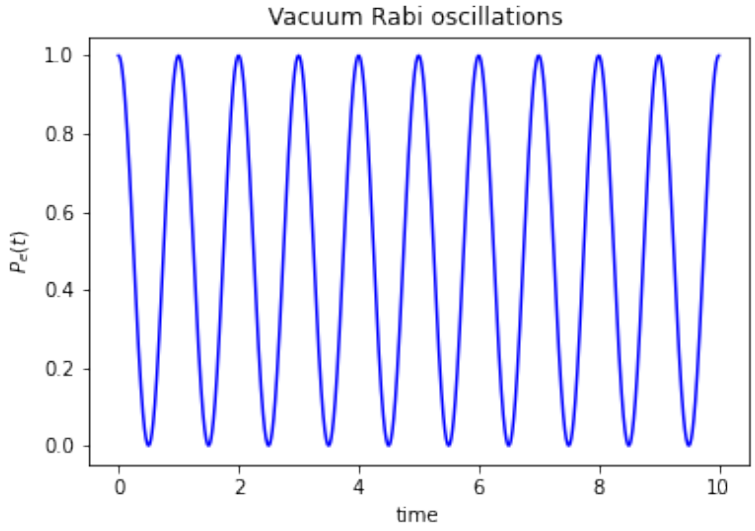

Figure 3.1: **Vacuum Rabi oscillations** at a coupling strength of $g = 1.15$.

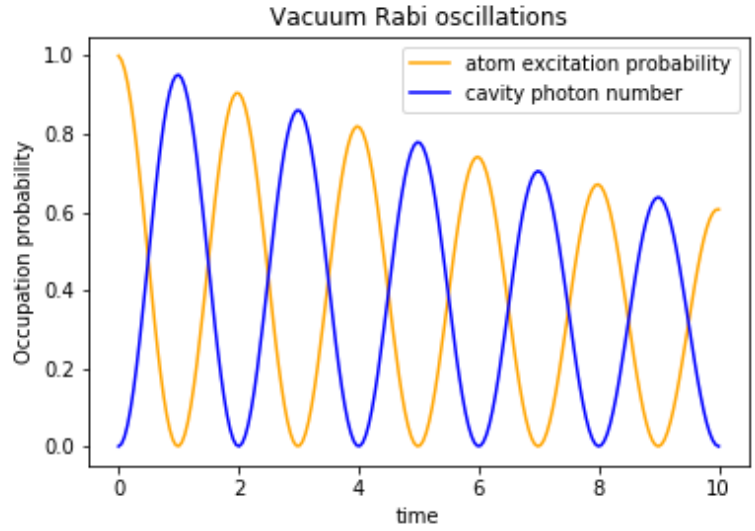

Figure 3.2: **Occupation probabilities** of the atom and cavity photon as a result of the dissipation.

For the initial state at zero temperature the excitation number of the atom-cavity system cannot increase. Neglecting the terms in Eq. (3.45) that have no contribution to the evolution state of the system, Eq.(3.45) reduces to the following master equation

$$\begin{aligned}\dot{\rho}(t) = &-i[H_{JC},\rho] + \gamma(\omega_0+g)\Big(\frac{1}{2}\left|E_0\right\rangle\left\langle E_{1,+}\right|\rho\left|E_{1,+}\right\rangle\left\langle E_0\right| \\ &- \frac{1}{4}\{\left|E_{1,+}\right\rangle\left\langle E_{1,+}\right|,\rho\}\Big) \\ &+ \gamma(\omega_0-g)\Big(\frac{1}{2}\left|E_0\right\rangle\left\langle E_{1,-}\right|\rho\left|E_{1,-}\right\rangle\left\langle E_0\right| \\ &- \frac{1}{4}\{\left|E_{1,1}\right\rangle\left\langle E_{1,-}\right|,\rho\}\Big).\end{aligned} \tag{3.46}$$

The dynamics of the ground state population $P_{0,g}(t)$ at the decay rate $\gamma = g/5$ (g is coupling strength) are shown in Figure 3.3. The populations are given by (See Appendix B)

$$\begin{aligned}P_{0,g}(t) = \left\langle 0g\right|\rho(t)\left|0g\right\rangle &= 1 - \frac{16g^2}{16g^2-\gamma^2}e^{-\frac{\gamma}{2}t} \\ &+ \frac{\gamma^2+\sqrt{\gamma^2-16g^2}}{2(16g^2-\gamma^2)}e^{\frac{-\gamma+\sqrt{\gamma^2-16g^2}}{2}t} \\ &+ \frac{\gamma^2-\gamma\sqrt{\gamma^2-16g^2}}{2(16g^2-\gamma^2)}e^{\frac{-\gamma-\sqrt{\gamma^2-16g^2}}{2}t}.\end{aligned} \tag{3.47}$$

Due to cavity losses, the ground state population of the atom-cavity system increases in time at an exponential rate. The state $|0e\rangle$ indirectly decays to the state $|1g\rangle$. The oscillatory behaviour of $P_{0,g}$ signifies the Rabi oscillations that induce the system decay when the state $|0e\rangle$ to coupled to the state $|1g\rangle$. The coupling between the states $|1g\rangle$ and $|0e\rangle$ is weak (Rotating Wave Approximation (RWA)) as such, the decay rate $\gamma(\omega_0+g) = \gamma(\omega_0-g)$ is the same for the two states inducing a non-oscillatory behaviour in the evolution of the population of $|0g\rangle$ as shown in the longer time behaviour on the insert in Figure 3.3. Different system dynamics arise when a measuring the atomic ground state population for example, the population

$$P_g(t) = \left\langle 0g\right|\rho(t)\left|0g\right\rangle + \left\langle 1g\right|\rho(t)\left|1g\right\rangle, \tag{3.48}$$

in which using Eq. (3.46) one finds (See Appendix B)

$$P_g(t) = 1 - \frac{8g^2}{16g^2-\gamma^2}e^{-\frac{\gamma}{2}t} + \frac{2\gamma^2+2\gamma\sqrt{\gamma^2-16g^2}-16g^2}{4(16g^2-\gamma^2)}e^{\frac{-\gamma+\sqrt{\gamma^2-16g^2}}{2}t} \tag{3.49}$$

$$+ \frac{2\gamma^2-2\gamma\sqrt{\gamma^2-16g^2}-16g^2}{4(16g^2-\gamma^2)}e^{\frac{-\gamma+\sqrt{\gamma^2-16g^2}}{2}t}. \tag{3.50}$$

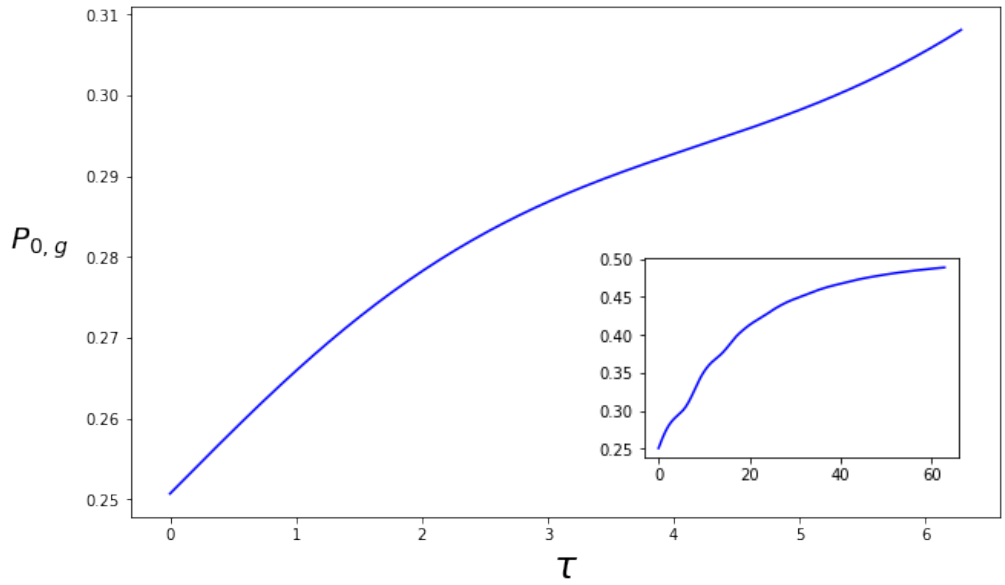

Figure 3.3: **Population of ground state** $P_{0,g}$ as a function of $\tau = 2gt$ for the system starting at an initial state $|0e\rangle$ with $\gamma/2g = 0.1$.

The below Figure 3.4 shows the evolution of the atomic ground state population $P_g(t)$, decaying presence of Rabi oscillations are observed with more of an oscillatory behaviour.

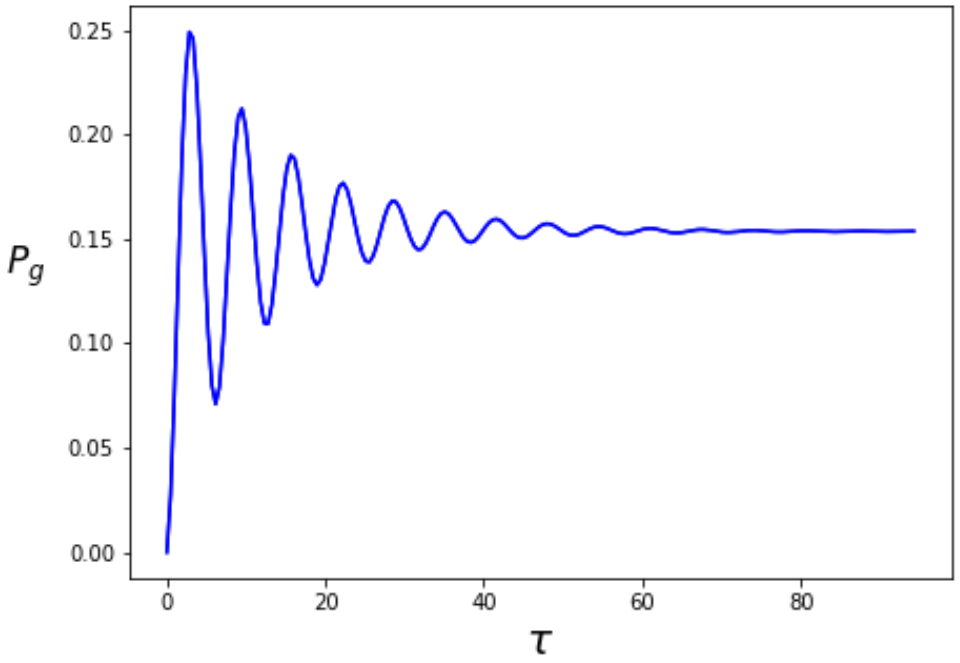

Figure 3.4: **Population of ground state** $P_g(t)$ as a function of $\tau = 2gt$.

Chapter 4

Generation of squeezed light in a dissipative Jaynes-Cummings Model

In chapter 2 and 3 we introduced the Jaynes-Cummings Model a quantum model that describes atom and light interaction in a cavity. In order to investigate open quantum systems it was imperative to derive an equation that fully describes the dynamics of open quantum systems i.e Quantum Master Equation by taking into account the imperfect isolation of such systems from the rest of the environment. We applied the equation to understand the dynamics at one initial excitation. In this chapter we consider the application of the dissipative Jaynes-Cummings model to generate squeezed states of light which are central to quantum information processes. Squeezed states of light are purely quantum states that have been widely investigated and observed first in the field of quantum optics [40] with the revolutionary experiment of atomic vapour Sodium atoms and recently in the field of cavity QED [28] which has shown that squeezing can be generated from atomic transitions in a two -level system (qubit). The Heisenberg uncertainty relation states that the minimum uncertainty for pairs of noncommuting operators i.e x, p must satisfy $(\Delta x)^2(\Delta p)^2 > \hbar^2/2$. For states exhibiting squeezing the variance of one operator is reduced below the standard quantum limit (SQL) at the expense of the other operator that does not commute with x such as p [28, 41–43]. This means that squeezed states have less quantum fluctuations or quantum noise as such they of interest to the fields of quantum information processing [44], quantum computing [45] and for performing precision measurement in quantum metrology [46]. Figure 4.1a,b show some of the properties of squeezed states. We will employ the non-Markovian master equation in the dissipative Jaynes-Cummings model to investigate the generation of squeezed states and analyze the influence of the initial atomic state, the atom-cavity coupling strengths, the non-Markovian effects on the squeezing of the light field as well as the collapse-revival phenomenon.

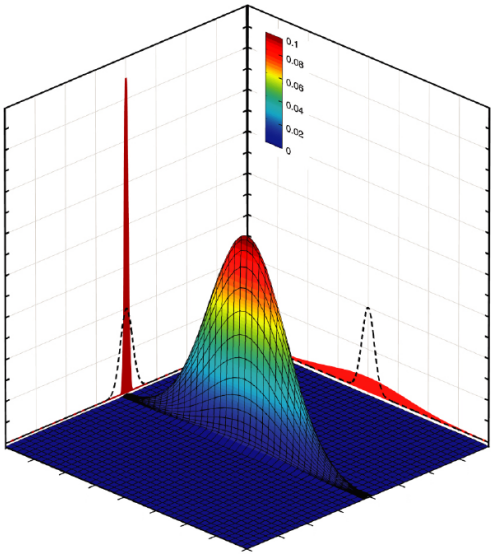

(a) **Wigner function** of squeezed vacuum state [47].

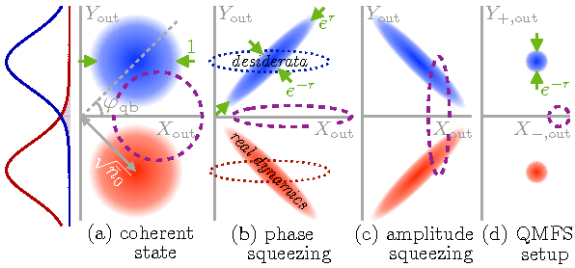

(b) **Phase space representation** of squeezed states [48].

Figure 4.1: **Properties** of squeezed states

4.1 Non-Markovian Master Equation

We consider the non-Markovian dynamics of the atom-cavity system at one-initial excitation and in the dressed-state basis $\{|E_0\rangle, |E_{1,-}\rangle, |E_{1,+}\rangle\}$. From Eq. (3.46) the non-Markoviann master equation [39] is given by

$$\begin{aligned}\dot{\rho}(t) = &-i[H_{JC}, \rho(t)] + \gamma(\omega_0 + g, t)\Big(\frac{1}{2}|E_0\rangle\langle E_{1,+}|\rho(t)|E_{1,+}\rangle\langle E_0| \\ &- \frac{1}{4}\{|E_{1,+}\rangle\langle E_{1,+}|, \rho(t)\}\Big) \\ &+ \gamma(\omega_0 - g, t)\Big(\frac{1}{2}|E_0\rangle\langle E_{1,-}|\rho(t)|E_{1,-}\rangle\langle E_0| \\ &- \frac{1}{4}\{|E_{1,1}\rangle\langle E_{1,-}|, \rho(t)\}\Big),\end{aligned} \tag{4.1}$$

with the time-dependent decay rates for $|E_{1,-}\rangle$ and $|E_{1,+}\rangle$ being $\gamma(\omega_0 + g, t)$ and $\gamma(\omega_0 - g, t)$ respectively.

The dressed state basis are the eigenstates of H_{JC} where $|E_0\rangle = |0g\rangle$, $|E_{1,-}\rangle = \frac{1}{\sqrt{2}}(|1g\rangle - |0e\rangle)$, $|E_{1,+}\rangle = \frac{1}{\sqrt{2}}(|1g\rangle + |0e\rangle)$ with decay rate of $\gamma(\omega_0 \pm g, t)$ for $|E_{1,\pm}\rangle$.

We model the environment by the Lorentzian spectral density [49]

$$J(\omega) = \frac{1}{2\pi} \frac{\gamma_0 \lambda^2}{(\omega_1 - \omega)^2 + \lambda^2}, \tag{4.2}$$

where:
λ = spectral width of the coupling.
$\gamma_0 = \frac{1}{\tau_R}$ is related to the time scale on which the system changes (relaxation time).

When the spectrum is peaked on the frequency of the state $|E_{1-}\rangle$ where $(\omega_1 = \omega_0 - g)$ the decay rates reduce to

$$\gamma(\omega_0 - g, t) = \gamma_0(1 - e^{-\lambda t}),$$

and

$$\gamma(\omega_0 + g, t) = \frac{\gamma_0 \lambda^2}{4g^2 + \lambda^2} \Big\{ 1 + [\frac{2g}{\lambda} \sin 2gt - \cos 2gt] e^{-\lambda t} \Big\}.$$

The initial density matrix for the system

$$\begin{aligned} \rho(0) = {} & \rho_{11}(0) \left|E_0\right\rangle \left\langle E_0\right| + \rho_{12}(0) \left|E_0\right\rangle \left\langle E_{1+}\right| + \rho_{13}(0) \left|E_0\right\rangle \left\langle E_{1-}\right| \\ & + \rho_{21}(0) \left|E_{1+}\right\rangle \left\langle E_0\right| + \rho_{22}(0) \left|E_{1+}\right\rangle \left\langle E_{1+}\right| + \rho_{23}(0) \left|E_{1+}\right\rangle \left\langle E_{1-}\right| \\ & + \rho_{31}(0) \left|E_{1-}\right\rangle \left\langle E_0\right| + \rho_{32}(0) \left|E_{1-}\right\rangle \left\langle E_{1+}\right| + \rho_{33}(0) \left|E_{1-}\right\rangle \left\langle E_{1-}\right|. \end{aligned} \tag{4.3}$$

Using the damping basis method (Appendix B) we can evaluate the density matrix at time t

$$\begin{aligned} \rho(t) = {} & e^{-h_2} \left|E_0\right\rangle \left\langle E_0\right| + e^{-2igt} e^{-\frac{1}{2}(h_2 + h_1)} \left|E_0\right\rangle \left\langle E_{1+}\right| + e^{-i(\omega_0 + g)t} e^{-\frac{1}{2}h_2} \left|E_0\right\rangle \left\langle E_{1-}\right| \\ & + e^{-h_1} \left|E_{1+}\right\rangle \left\langle E_{1+}\right| + e^{-i(\omega_0 - g)t} e^{-\frac{1}{2}h_1} \left|E_{1+}\right\rangle \left\langle E_{1-}\right| \\ & + 3 - e^{-h_2} - e^{-h_1} \left|E_{1-}\right\rangle \left\langle E_{1-}\right|, \end{aligned} \tag{4.4}$$

where

$$h_1 = \frac{1}{2} \int_0^t \gamma(\omega_0 - g, t') dt' = \frac{1}{2} \Big(\gamma_0 t + \frac{\gamma_0}{\lambda} (e^{-\lambda t} - 1) \Big), \tag{4.5}$$

and

$$\begin{aligned} h_2 = \frac{1}{2} \int_0^t \gamma(\omega_0 + g, t') dt' = \frac{1}{2} \frac{\gamma_0 \lambda^2}{4g^2 + \lambda^2} \Bigg[t - \frac{4g e^{-\lambda t} sin(2gt)}{4g^2 + \lambda^2} \\ + \frac{(\lambda^2 - 4g^2)(e^{-\lambda t} \cos 2gt - 1)}{\lambda(4g^2 + \lambda^2)} \Bigg]. \end{aligned} \tag{4.6}$$

4.2 Squeezing Properties of the light field

Squeezing properties of light are studied by analyzing the quadrature components of the light field. The quadrature operators are related to the field amplitudes with a phase difference of $\frac{\pi}{2}$ to each quadrature operator [50],

$$X_1 = \frac{1}{2}(\hat{a} + \hat{a}^\dagger), \qquad X_2 = \frac{1}{2i}(\hat{a} - \hat{a}^\dagger), \tag{4.7}$$

with their variances given by

$$(\Delta X_1)^2 = \left\langle X_1^2 \right\rangle - \langle X_1 \rangle^2, \qquad (\Delta X_2)^2 = \left\langle X_2^2 \right\rangle - \langle X_2 \rangle^2. \tag{4.8}$$

For the uncertainty principle to hold the variance of the quadrature operators must obey the following relation

$$(\Delta X_1)^2 \cdot (\Delta X_2)^2 \geq \frac{1}{16}. \tag{4.9}$$

The quadrature operator is said to be squeezed if X_i satisfies the condition

$$(\Delta X_i)^2 < \frac{1}{4}, \qquad (i = 1, 2), \tag{4.10}$$

or in terms of the squeezing factor S_i

$$S_i = (\Delta X_i)^2 - \frac{1}{4} < 0. \tag{4.11}$$

Rewriting Eq. (4.4) in terms of the light field and atomic operators we find

$$\begin{aligned}
\rho(t) = {} & e^{-h_2} |0\rangle \langle 0| \otimes |g\rangle \langle g| + e^{-2igt} e^{-\frac{1}{2}(h_2+h_1)} (|0\rangle \langle 1| \otimes |g\rangle \langle g| + |0\rangle \langle 0| \otimes |g\rangle \langle e|) \\
& + e^{-i(\omega_0+g)t} e^{-\frac{1}{2}h_2} (|0\rangle \langle 1| \otimes |g\rangle \langle g| - |0\rangle \langle 0| \otimes |g\rangle \langle g|) \\
& + e^{-h_1} (|1\rangle \langle 1| \otimes |g\rangle \langle g| + |1\rangle \langle 0| \otimes |g\rangle \langle e| + |0\rangle \langle 1| \otimes |e\rangle \langle g| + |0\rangle \langle 0| \otimes |e\rangle \langle e|) \\
& + e^{-i(\omega_0-g)t} e^{-\frac{1}{2}h_1} (|1\rangle \langle 1| \otimes |g\rangle \langle g| - |1\rangle \langle 0| \otimes |g\rangle \langle e| + |0\rangle \langle 1| \otimes |e\rangle \langle g| \\
& - |0\rangle \langle 0| \otimes |e\rangle \langle e|) + 3 - e^{-h_2} - e^{-h_1} (|1\rangle \langle 1| \otimes |g\rangle \langle g| - |1\rangle \langle 0| \otimes |g\rangle \langle e| \\
& - |0\rangle \langle 1| \otimes |e\rangle \langle g| - |0\rangle \langle 0| \otimes |e\rangle \langle e|).
\end{aligned} \tag{4.12}$$

Figure 4.2 depicts how the expectation values and variances of the quadrature operators X_1 and X_2 evolve in time when initially in different kinds of squeezed states.

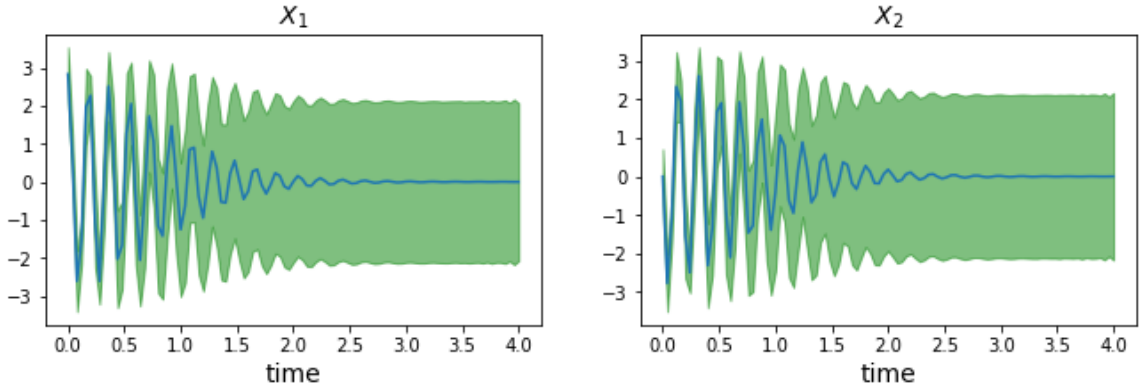

Figure 4.2: **Expectation values of X_1 and X_2** with an envelope that describes the operators variance for the initial state $|\psi(0)\rangle = (\cos\frac{\theta}{2}|e\rangle + e^{i\phi}\sin\frac{\theta}{2}|g\rangle)_A|0\rangle_f$ where A indicates the atom, f describes the cavity field, $\theta = \frac{2\pi}{2}$ is an amplitude parameter and $\phi = 0$ is the phase parameter.

Tracing out the atom to get the reduced density matrix for the field $\rho_f(t)$ we have,

$$\begin{aligned}\rho_f(t) = Tr_A\rho(t) &= e^{-h_2}|0\rangle\langle 0| + e^{-2igt}e^{-\frac{1}{2}(h_2+h_1)}|0\rangle\langle 1| - e^{-i(\omega_0+g)t}e^{-\frac{1}{2}h_2}(|0\rangle\langle 1| - |0\rangle\langle 0|)\\ &+ e^{-h_1}\big(|1\rangle\langle 1| + |0\rangle\langle 0|\big) + e^{-i(\omega_0-g)t}e^{-\frac{1}{2}h_1}\big(|1\rangle\langle 1| - |0\rangle\langle 0|\big)\\ &+ 3 - e^{-h_2} - e^{-h_1}\big(|1\rangle\langle 1| - |0\rangle\langle 0|\big)\\ &= \begin{pmatrix} e^{-h_2} - e^{-i(\omega_0+g)t}e^{-\frac{1}{2}h_2} + e^{-h_1} - e^{-i(\omega_0-g)t}e^{-\frac{1}{2}h_1} - \rho_{33}(t) & 0\\ e^{-2igt}e^{-\frac{1}{2}(h_2+h_1)} + e^{-i(\omega_0+g)t}e^{-\frac{1}{2}h_2} & e^{-h_1} + e^{-i(\omega_0-g)t}e^{-\frac{1}{2}h_1} + \rho_{33}(t)\end{pmatrix},\end{aligned} \tag{4.13}$$

where $\rho_{33}(t) = 3 - e^{-h_2} - e^{-h_1}$.

We can now get the quadrature operators to analyze the squeezing factor. The expectation value of the X_1 and X_2 quadrature operators are given by

$$\langle X_1\rangle = Tr(X_1\rho_f(t)), \qquad \langle X_1^2\rangle = Tr(X_1^2\rho_f(t)). \tag{4.14}$$

$$\langle X_2\rangle = Tr(X_2\rho_f(t)), \qquad \langle X_2^2\rangle = Tr(X_2^2\rho_f(t)). \tag{4.15}$$

We analyze numerically the squeezing properties of the light field by inserting Eq. (4.14) or Eq. (4.15) into Eq. (4.11).

We consider an initial atom-cavity state

$$|\psi(0)\rangle = \left(\cos\left(\frac{\theta}{2}\right) |e\rangle + e^{i\phi} \sin\left(\frac{\theta}{2}\right) |g\rangle \right)_A |0\rangle_f , \tag{4.16}$$

where θ, ϕ denote the amplitude and phase parameters.

Normal squeezing can occur in presence of small dissipation in an atom-cavity system (Figure 4.3). Initially, we observe slow oscillations of S_1 for the state $|\psi(0)\rangle$ due to the dependence of the squeezing on the atom-cavity coupling g, this property will be discussed in detail in the Discussion section. In the results section we describe squeezing in a regime of strong atom-cavity coupling and dissipation rate.

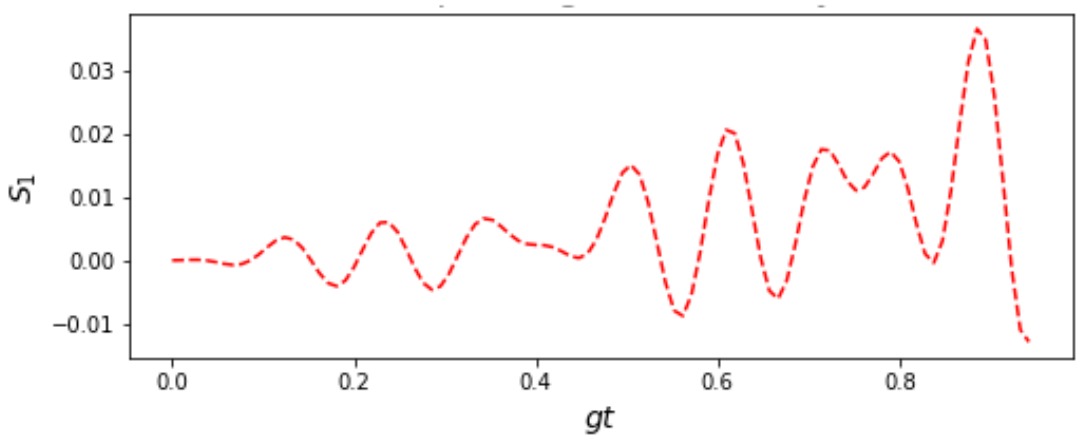

Figure 4.3: **Normal Squeezing** of the state $|\psi(0)\rangle$.

4.3 Results and Discussion

In this section of results we analyze the following effects on the squeezing of the light field: the initial atom-cavity state, the atom-cavity coupling, the non-Markovian effects and the atomic frequency.

In Figure 4.4a, the squeezing factor S_1 is shown as a function of ϕ and t for the Markovian regime where the spectral width of the coupling $\lambda = 5\gamma_0$. A Markovian regime is one were the relaxation time of the system is greater than the reservoir correlation time. This is for $\lambda > 2\gamma_0$ in Eq. (4.2). If $\lambda < 2\gamma_0$ the reservoir correlation time is greater than the relaxation time and thus the often the dynamical evolution of the system is non-Markovian.

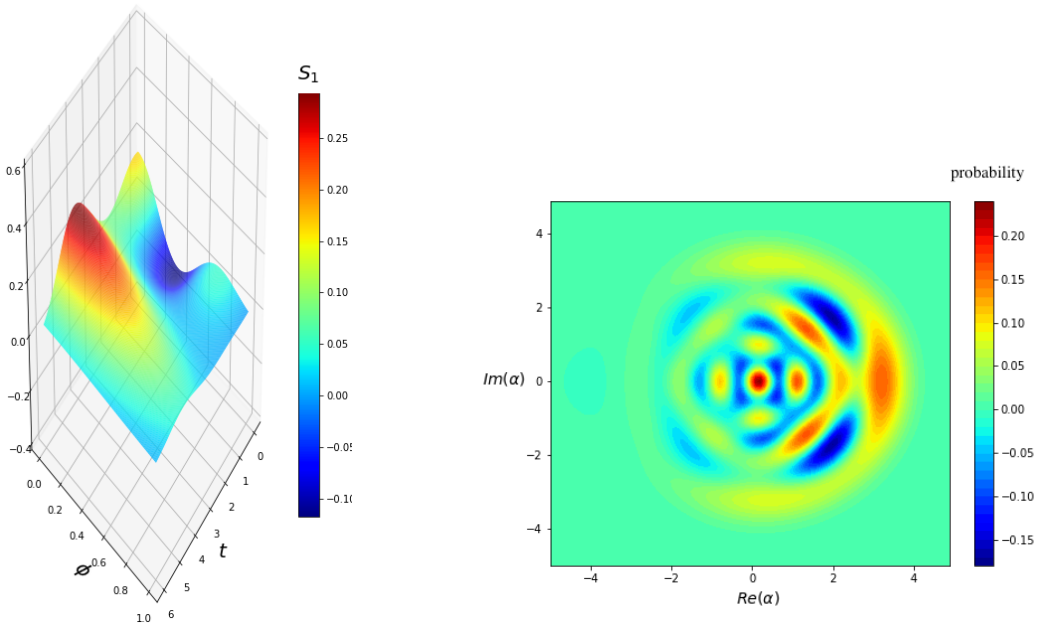

(a) Squeezing factor S_1 as a function of ϕ and t when $\theta = \frac{2\pi}{3}$.

(b) Wigner function of the initial state $|\psi(0)\rangle$ S_1 for $\phi = 0$ and $\theta = \frac{2\pi}{3}$.

Figure 4.4: **Dynamics of the initial atomic state** on the squeezing factor S_1 in the Markovian regime ($\lambda = 5\gamma_0$).

At certain values of the phase parameter ϕ we can observe that S_1 values vary from zero and then oscillate with time. As time increases we can observe greater amounts of squeezing that is due to the atomic transitions since initially there is no squeezing. Figure 4.4b shows a 2-dimensional representation of the Wigner function of the state $|\psi(0)\rangle$.

In Figure 4.5 we show the influence of the atom-cavity coupling g on the squeezing of the light field in the Markovian regime ($\lambda = 5\gamma_0$)(solid blue line). It can been seen that S_1 is clearly dependent on the atom-cavity coupling. Figure 4.5a,b displays the fast oscillations of S_1 as t increases due to the dissipative cavity interaction with the atom. The collapse-revival S_1 oscillations of the model are clearly observant for $\gamma_0 t \in [0, 8]$ and for periods π/g. Furthermore these collapse-revival oscillations are joined by the decay and re-population of the excited atom this is shown by the dotted-dashed red line with the dashed green line showing the modulation of the S_1 oscillations. The light field achieves its maximal squeezing (greatest degree of squeezing) when the population of the excited atom P_e reduces to zero. In this manner, S_1 oscillations collapse to the value zero when the population of the excited atom ascends from this value. The collapse-revival oscillations of S_1 will vanish due to the dissipative coupling with the Markovian environment. A comparison between Figure 4.5a and 4.5b, we can realize that their squeezing dynamics is comparable for a distinct g.
The distinction is in the collapse-revival recurrence of S_1 oscillations for the maximal squeezing acquired.The frequency of the collapse-revival oscillations of S_1 in the

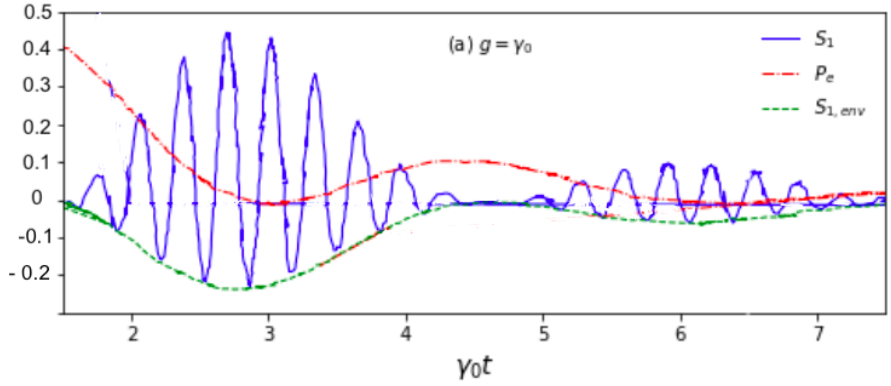

(a)

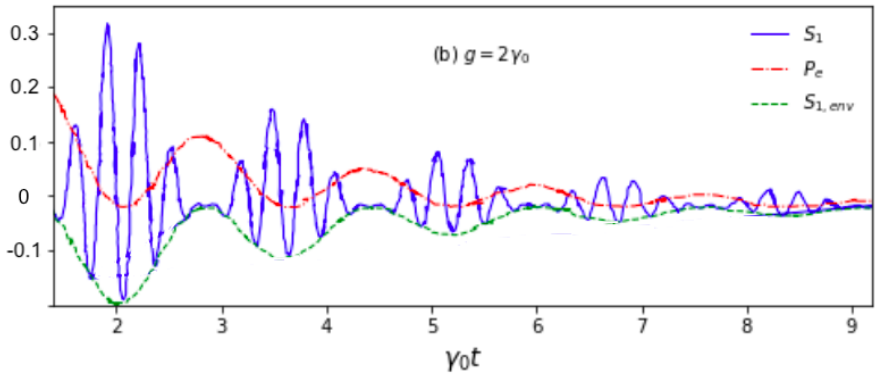

(b)

Figure 4.5: **The effect of the atom-cavity coupling** g on the squeezing factor S_1(solid blue line) and on the population of the excited atom(dotted-dashed red line) as function of γ_0 in the Markovian regime ($\lambda = 5\gamma_0$) for (a) $g = \gamma_0$, (b) $g = 2\gamma_0$. Additional parameters $\theta = \frac{2\pi}{3}, \phi = 0, \omega_0 = 10\gamma_0$.

latter case is half as in the former. It is clearly obvious that the maximum squeezing acquired is smaller than the previous. Henceforth, by weakening the atom-cavity coupling g we can increase the frequency of the collapse-revival oscillations of S_1.

Physically this means squeezing light can be produced when the atom de-excites to the ground state, the interaction between the atom and its cavity allows for photons to be exchanged between the atom and its cavity making the collapse-revival oscillations of S_1 to occur in a short period. Contrast to the coupling with the environment, the photon number decreases resulting in the collapse-revival oscillations of S_1 vanishing for a longer-time period as depicted by Figure 4.5a and 4.5b.

In Figure 4.6 we show the dynamics of the squeezing factor S_1 for generation in the non-Markovian regime $\lambda < 2\gamma_0$. For an equivalent atom-cavity coupling $g = \gamma_0$ the collapse-revival oscillations of S_1 are the same regardless of the regime of interest. The non-Markovian effects on S_1 are epitomized in the maximal value of

the squeezing. In Figure 4.6a where $\lambda = 3\gamma_0$ the cavity dissipation is pronounced as such, the revival oscillations of S_1 tend to zero. In Figure 4.6b where $\lambda = 0.3\gamma_0$ (non-Markovian effects) squeezing increases to $S_1 = -0.2$ from the minimal point at $\gamma_0 t = \pi/2$ it then collapses to the minimal point at $\gamma_0 t = \pi$ and revived to $S_1 = -0.04$ at $\gamma_0 t = 3\pi/2$. This demonstrates that the maximal degree of squeezing in the non-Markovian regime is greater than the Markovian regime as shown in Figure 4.6c when $\lambda = 0.03\gamma_0$ where maximum squeezing is reached at $S_1 = 0.21$ for a short period of time. The collapse-revival oscillations are remarkable in the non-Markovian regime. A special characteristic of the non-Markovian regime is the feedback effect where the number of photons returned to the cavity from the environment increase. At longer time periods the S_1 oscillation decay to the minimal point of squeezing in the Markovian and non-Markovian regimes. Therefore, the stronger the non-Markovian effects are the greater revived are the S_1-oscillations after decreasing to the minimal point.

In Figure 4.7 we show the effect of the resonant frequency ω_0 on the squeezing factor S_1. A dependence of the S_1-oscillation on the atomic frequency can be clearly observed from Figures 4.7a and 4.7b. As the magnitude of the frequency doubles so does the squeezing and the collapse-revival oscillations of S_1. Maximal squeezing is achieved in Figure 4.7b, in terms of the description of a resonant cavity the more intense are the Rabi oscillations.

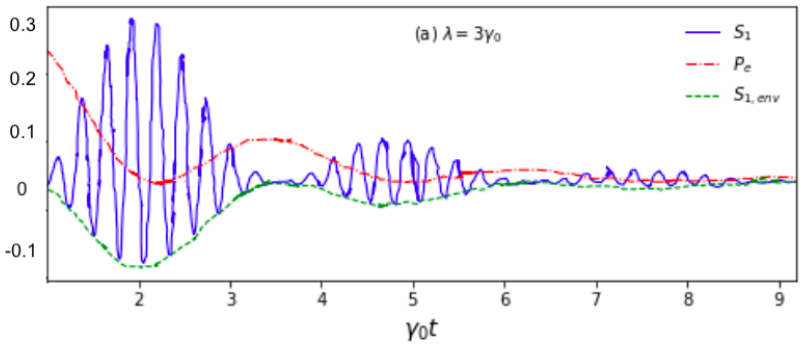

(a)

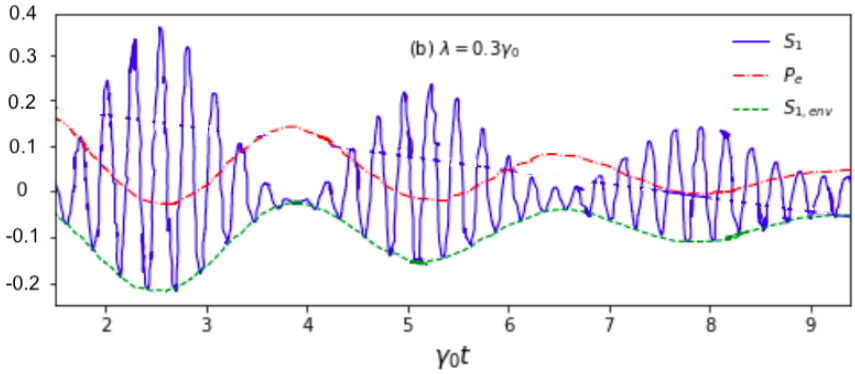

(b)

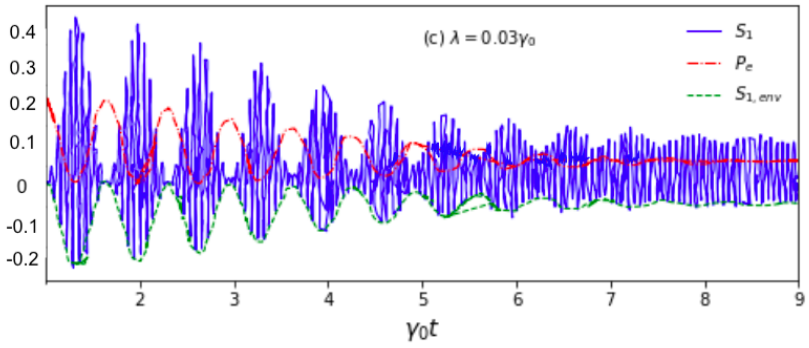

(c)

Figure 4.6: (a) **The influence of the non-Markovian effects** on the squeezing factor S_1(solid blue line) and on the population of the excited atom(dotted-dashed red line) at $\lambda = 3\gamma_0$. (b) At $\lambda = 0.3\gamma_0$ and (c) at $\lambda = 0.03\gamma_0$.

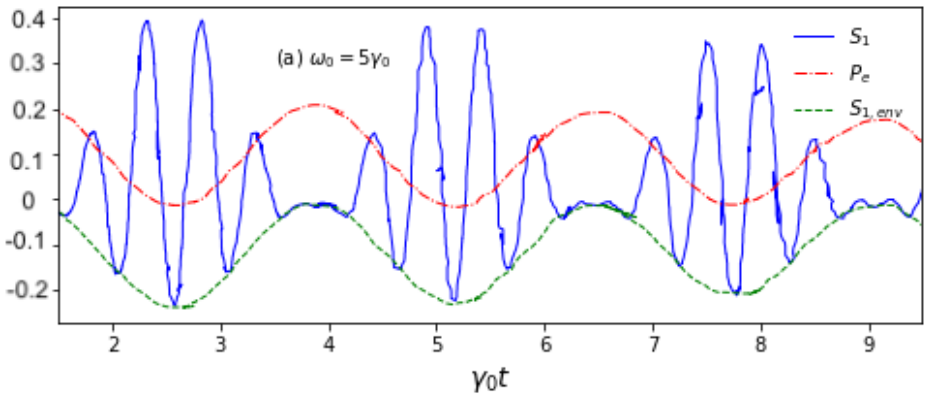

(a)

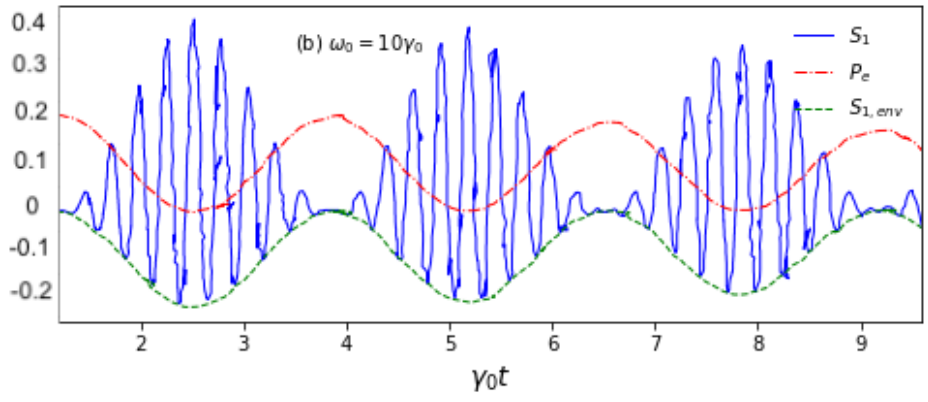

(b)

Figure 4.7: (a) **The effect of the resonant frequency** ω_0 on the squeezing factor S_1 (solid blue line) and on the population of the excited atom (dotted-dashed red line) in the non-Markovian regime ($\lambda = 0.01\gamma_0$).

4.4 Conclusion

By applying the non-Markovian master equation to analyze squeezing properties of an atom-cavity system interacting with the bosonic environment as a bath many aspects of the dissipative Jaynes-Cummings model and the original Jaynes-Cummings model were recovered from the Rabi oscillations to the collapse-revival phenomena oscillations. This was done to capture the decoherence effects that cannot be avoided when doing measuring for such systems. We have shown that squeezing of the light field can be generated when the atom transits from an excited state to a ground state this was shown by the influence of the initial atomic state $|\psi(0)\rangle$ (Eq. (4.16)) on the squeezing factor S_1. We noted that the frequency of the collapse-revival S_1 oscillations initially increased and then decreased at longer times t showing the depends of squeezing on the atom-cavity coupling g. Maximal squeezing occurs for

a smaller atom-cavity strength coupling. Significant squeezing and collapse-revival phenomena was observed in the non-Markovian regime where $\lambda < 2\gamma_0$. From the results it can be concluded that the smaller the λ the greater the S_1 oscillations. Comparison of the Markovian and non-Markovian effects show that the collapse revival frequency oscillations of S_1 do occur in both regimes. We also showed that the atomic resonant frequency influences the squeezing factor S_1 and the collapse revival oscillations. The greater the frequency the more the collapse-revival oscillations of S_1. These findings are of interest to the experimental work in cavity QED for the generation of squeezed states for quantum communication and information processing. A shift from the optical technique to generate such states to superconducting nanoscale is what motivated the study. Although the degree of squeezing was maximal in certain regimes of the model for example, the non-Markovian regime degree of squeezing can be achieved by using the strongly coupled regime of the Jaynes-Cummings which explore in the next chapter.

Chapter 5

Generation of squeezed states in dispersive regime of quantum Rabi Model

In chapter 4 we introduced a way to generate squeezed states of light from atomic transitions when an atom transits to the ground state from an excited state. The approach that was followed was based on the quantum master equation in a dissipative Jaynes-Cummings model. We showed that significant amount of squeezing of the light field was generated in the non-Markovanian limit of the system. In this chapter we introduce a different protocol to generate squeezed states beyond RWA in the dispersive limit of the quantum Rabi model proposed by Joshi et al. in [29], where by applying frequency changes using the control state of the qubit and the dispersive energy shift the quantum noise of the states is significantly increased. Instead of the using the solvable Jaynes-Cummings we revert to the original quantum Rabi model containing "counter-rotating" light field and atomic terms as this introduces interesting physics in the strong coupling regime. The dispersive regime is where the detuning parameter (Δ) between the the qubit and cavity is greater than the coupling g between them ($\Delta \gg g$), a non-resonant interaction of the Jaynes-Cummings model. In experimental settings the detuning is used to control the frequency pulses that go in the qubit and resonator as well as the readout states of the qubit. One particular characteristic of the dispersive limit is the cavity frequency shift [51] that is introduced as we shall see this is because of the transformation applied to the model Hamiltonian and disperive approximation in the coupling strength. We consider the original quantum Rabi Hamiltonian as opposed to the Jaynes-Cummings to derive the effective dispersive Hamiltonian that is used to bring the squeezing property of the Hamiltonian. A comparison between the groundstates of the Rabi Hamiltonian and dispersive Hamiltonian is investigated to see how they influence the degree of squeezing.

5.1 Dispersive Rabi Hamiltonian

In the dispersive limit the qubit and the resonator are considered to be far detuned such that $g \ll |\omega_0 - \omega|$ [51, 52]. The beyond RWA theory involves keeping the counter-rotating terms when simplifying the Rabi Hamiltonian H_{Rabi},

$$H_{Rabi} = \omega \hat{a}^\dagger \hat{a} + \frac{\omega_0}{2}\sigma_z + g(\hat{a}^\dagger + \hat{a})(\hat{\sigma}^+ + \hat{\sigma}^-). \tag{5.1}$$

We decompose H_{Rabi} into the the diagonalizable part and the pertubation part $H_{Rabi} = H_0 + g(K_+ + L_+)$ where

$$\begin{aligned} H_0 &= \omega \hat{a}^\dagger \hat{a} + \frac{\omega_0}{2}\hat{\sigma}_z. \\ K_+ &= \hat{\sigma}^- \hat{a}^\dagger + \hat{\sigma}^+ \hat{a}. \\ L_+ &= \hat{\sigma}^+ \hat{a}^\dagger + \sigma^- \hat{a}. \end{aligned} \tag{5.2}$$

We define the unitary transformation

$$\hat{U} = e^{\lambda K_- + \bar{\lambda} L_-}, \tag{5.3}$$

where the small parameter $\lambda \equiv \frac{g}{\Delta}$, $\bar{\lambda} \equiv \frac{g}{\omega_0 + \omega}$ [53]. We have that $\lambda > \bar{\lambda}$, a small value of λ implies a small value of $\bar{\lambda}$ thus, $\lambda, \bar{\lambda}$ are of the same order.

Applying the unitary transformation to H_{Rabi} to get the dispersive Hamiltonian

$$\begin{aligned} H_{disp} &= \hat{U}^\dagger H_{Rabi} \hat{U} \\ &= \Big(1 - (\lambda K_- + \bar{\lambda} L_-) + \frac{1}{2}(\lambda K_- + \bar{\lambda} L_-)^2 - \dots \Big) H_{Rabi} \\ &\Big(1 + (\lambda K_- + \bar{\lambda} L_-) + \frac{1}{2}(\lambda K_- + \bar{\lambda} L_-)^2 + \dots \Big) \\ &= H_{Rabi} + \lambda \Big[H_{Rabi}, (K_+ L_-) \Big] + \frac{1}{2}\lambda^2 \Big[\Big[H_{Rabi}, (K_+ L_-) \Big], (K_+ L_-) \Big]. \end{aligned} \tag{5.4}$$

The unitary transformation can be seen as an interaction picture transformation. This allows us to the solve the system dynamics in a simpler manner. Using the commutation relations, we find Eq. (5.4) to be

$$H_{disp} = \omega \hat{a}^\dagger \hat{a} + \frac{\omega_0}{2}\hat{\sigma}_z + \frac{1}{2}\Big(\frac{g^2}{\Delta} + \frac{g^2}{2\omega_0 - \Delta}\Big)\hat{\sigma}_z(\hat{a}^\dagger + \hat{a})^2. \tag{5.5}$$

We next introduce the parameter $2\eta = \frac{g^2}{\Delta} + \frac{g^2}{2\omega_0 - \Delta}$ and rewrite H_{disp} as

$$H_{disp} = (\omega + 2\eta\hat{\sigma_z})\hat{a}^\dagger \hat{a} + (\frac{\omega_0}{2} + \eta)\hat{\sigma}_z + \eta\hat{\sigma}_z(\hat{a}^2 + \hat{a}^{\dagger 2}). \tag{5.6}$$

In Figure 5.1 we show the energy levels of the dispersive Hamiltonian. Eq. (5.6) clearly represents the cavity frequency shift which is the form used in dispersive qubit readout experiments [54]. Working with this form of Hamiltonian we do a comparison of the groundstates of the dispersive Hamiltonian and the quantum Rabi model and quantify the degree of squeezing in the groundstates.

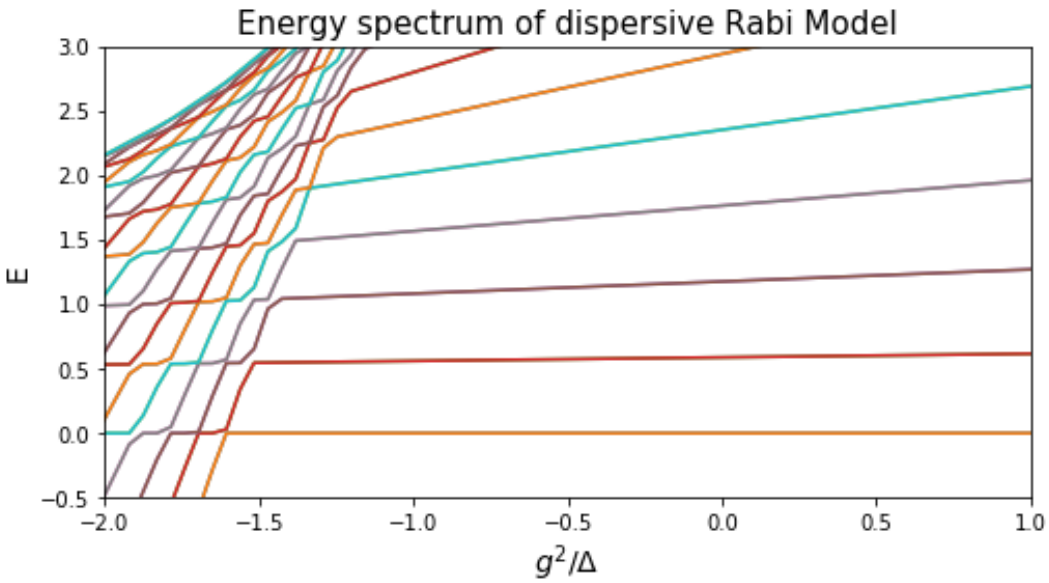

Figure 5.1: **Spectrum of dispersive** Rabi model.

In order to determine the eigenstates of the dispersive Hamiltonian and the quantum Rabi model we first rewrite the dispersive Hamiltonian in terms of the qubit states $|0\rangle, |1\rangle$ which are the + and - eigenstates of $\hat{\sigma}_z$

$$H_{disp} = H^{+}_{disp} |g\rangle \langle g| + H^{-}_{disp} |e\rangle \langle e|, \tag{5.7}$$

where $|g\rangle = |\uparrow\rangle = |1\rangle$, angular momentum state with z-component up.
$|e\rangle = |\downarrow\rangle = |0\rangle$, angular momentum state with z-component down.
and

$$H^{\pm}_{disp} = (\omega \pm 2\eta)\hat{a}^{\dagger}\hat{a} \pm (\frac{\omega_0}{2} + \eta) \pm \eta(\hat{a}^2 + \hat{a}^{\dagger 2}). \tag{5.8}$$

We then make use of the unitary squeezing operator $\hat{S}(r_{\pm})$ [55] defined to be

$$S(r_{\pm}) = e^{(r_{\pm}\hat{a}^{\dagger 2} - r_{\pm}\hat{a}^2)/2}, \tag{5.9}$$

to diagonalize $H^{\pm}_{disp}$. Some properties of $\hat{S}(r_{\pm})$ are

$$\begin{aligned} \hat{S}^{\dagger}(r_{\pm})\hat{a}\hat{S}(r_{\pm}) &= \hat{a}\cosh r_{\pm} + \hat{a}^{\dagger}\sinh r_{\pm}. \\ \hat{S}^{\dagger}(r_{\pm})\hat{a}^{\dagger}\hat{S}(r_{\pm}) &= \hat{a}^{\dagger}\cosh r_{\pm} + \hat{a}\sinh r_{\pm}. \end{aligned} \tag{5.10}$$

with the squeezing parameter $r_{\pm}$

$$r_{\pm} = \frac{1}{4}\ln\frac{\omega}{\omega \pm 4\eta}. \tag{5.11}$$

The resulting diagonal form of H_{disp} is

$$\tilde{H}_{disp} = \tilde{H}^{+}_{disp} |g\rangle \langle g| + \tilde{H}^{-}_{disp} |e\rangle \langle e|, \tag{5.12}$$

where

$$\tilde{H}^{\pm}_{disp} = \hat{S}^{\dagger}(r_{\pm})H^{\pm}_{disp}\hat{S}(r_{\pm}) = \sqrt{\omega(\omega \pm 4\eta)}\hat{a}^{\dagger}\hat{a} \pm \left(\frac{\omega_0}{2} + \eta\right). \tag{5.13}$$

The Hamiltonian in Eq. (5.13) is of a harmonic oscillator with the shifted frequency of the cavity corresponding to the qubit state $|0\rangle$ or $|1\rangle$.
The newly dispersive Hamiltonian $\tilde{H}_{disp}$ eigenstates are given by

$$|\tilde{\Psi}^{n,+}_{disp}\rangle = |n\rangle\,|g\rangle\,, \tag{5.14}$$

$$|\tilde{\Psi}^{n,-}_{disp}\rangle = |n\rangle\,|e\rangle\,, \qquad (n = 0, 1, 2, ...), \tag{5.15}$$

while those of $H^{\pm}_{disp}$ being

$$|\Psi^{n,\pm}_{disp}\rangle = \hat{S}(r_{\pm})\,|\tilde{\Psi}^{n,+}_{disp}\rangle\,. \tag{5.16}$$

This indicates that the groundstate is already in a squeezed vacuum state. In terms of the eigenvalues, $\tilde{H}_{disp}$ eigenvalues are approximated to eigenvalues of the quantum Rabi model since the unitary transformation leaves eigenvalues unchanged. The dispersive Hamiltonian $H^{\pm}_{disp}$ is related to the quantum Rabi Hamiltonian (Eq. (6.1)) by two unitary transformations so do the eigenstates that is to say,

$$|\Psi^{n,\pm}_{Rabi}\rangle \simeq \hat{U}\,|\Psi^{n,\pm}_{disp}\rangle = \hat{U}\hat{S}\,|\tilde{\Psi}^{n,\pm}_{disp}\rangle\,. \tag{5.17}$$

Expanding the $\hat{U}$ operator in Eq. (5.17) to first order in $\lambda, \bar{\lambda}$ we have

$$|\Psi^{n,\pm}_{Rabi}\rangle \simeq (1 + \lambda K_{+}\bar{\lambda}L)\hat{S}\,|\tilde{\Psi}^{n,\pm}_{disp}\rangle\,. \tag{5.18}$$

For the groundstate of $\tilde{H}_{disp}$, we have $|\tilde{\Psi}\rangle^{n,\pm}_{disp} = |0\rangle\,|\{g, e\}\rangle$ and the corresponding groundstate eigenstate of the quantum Rabi model to be

$$|\Psi^{0,-}_{Rabi}\rangle = \hat{S}(r_{-})\,|0\rangle\,|e\rangle + \hat{S}(r_{-})(\bar{\lambda}\cosh r_{-} - \lambda\sinh r_{-})\,|1\rangle\,|g\rangle\,. \tag{5.19}$$

$$|\Psi^{0,+}_{Rabi}\rangle = \hat{S}(r_{+})\,|0\rangle\,|g\rangle + \hat{S}(r_{+})(\bar{\lambda}\cosh r_{+} - \lambda\sinh r_{+})\,|1\rangle\,|e\rangle\,. \tag{5.20}$$

The above states are entangled states of the qubit and the field unlike the separable dispersive eigenstates. The groundstates are a superposition of qubit and cavity states, a squeezed vacuum state is apparent in the first term and squeezed number states are observed in the second term representing highly nonclassical state. Both the dispersive eigenstates and the quantum Rabi model eigenstates provide different elements for generation of squeezed states.

5.1.1 Degree of Squeezing in the Groundstates

In order to measure the degree of squeezing we review the quadrature operators for position and momentum namely,

$$X = (\hat{a}^{\dagger} + \hat{a}). \tag{5.21}$$

$$P = i(\hat{a}^{\dagger} - \hat{a}). \tag{5.22}$$

Using the results from the last chapter we find that for the groundstate in the qubit space $\hat{S}\,|0\rangle\,|0, 1\rangle$ the variance is

$$\begin{aligned}\left\langle(\Delta\hat{X})^2\right\rangle &= \langle e, g|\,\langle 0|\,\hat{S}^{\dagger}|(\Delta\hat{X})^2|\hat{S}\,|0\rangle\,|g, e\rangle \\ &= e^{2r_{\pm}},\end{aligned} \tag{5.23}$$

where $\Delta\hat{X} = \hat{X} - \left\langle\hat{X}\right\rangle$.

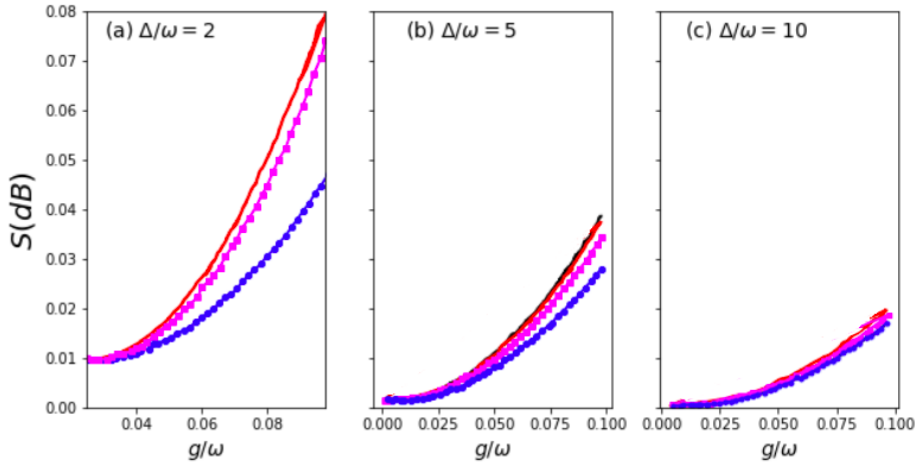

Figure 5.2: **Degree of Squeezing** S as a function of the coupling constant g for the dispersive Hamiltonian groundstates $|\Psi^{0,+}_{disp}\rangle$ (solid black line) and$|\Psi^{0,-}_{disp}\rangle$ (solid red line), the quantum Rabi model groundstates $|\Psi^{0,+}_{Rabi}\rangle$ (pink crosses) and $|\Psi^{0,-}_{Rabi}\rangle$ (dotted blue) with the detuning at (a) $\Delta/\omega = 2$, (b)$\Delta/\omega = 5$, (c)Δ/ω= 10.

and

$$\left\langle (\Delta P)^2 \right\rangle = e^{-2r_{\pm}}. \tag{5.24}$$

The above variance equations imply that for a positive detuning ($\Delta > 0$) the squeezing parameter value results in reduction of noise below the quantum limit in the momentum quadrature and increased fluctuations in the position quadrature. Experimentally the degree of squeezing is measured in decibels (dB) using the following formula

$$S = \max\left(0, -10\log_{10}\left(min\left(\left\langle \Delta X^2 \right\rangle, \left\langle \Delta P^2 \right\rangle\right)\right)\right) \tag{5.25}$$

Figure 5.2 shows the degree of squeezing in the groundstate of the dispersive Hamiltonian and that of the quantum Rabi model as a function of the coupling constant g. The degree of squeezing increases with the coupling strength and decreases as the detuning increases. Enhanced squeezing is observed for the ground state of the dispersive Hamiltonian compared to that of the quantum Rabi model.

5.2 Strong squeezing using sudden frequency jumps

In the last section we observed that both the disperisve Hamiltonian and the quantum Rabi model did not generate a significant amount of squeezing in the groundstates of the oscillator mode. In this section we consider a different approach to generate strong squeezing of the light field in a dispersive Hamiltonian. The basis

this approach uses follows from the work by Janszky et al. in [56] on generating squeezed states using repeated frequency jumps. The model Hamiltonian is that of a harmonic oscillator with unit mass. The scheme presented is based on the protocol developed in by Joshi et al. in [29] that generates strong squeezing using sudden changes in frequency with the dispersive Hamiltonian.We first rewrite the dispersive Hamiltonian (Eq. (5.7)) in terms of the field's creation and annihilation operators. The operators are expressed in position and momentum coordinates

$$\hat{a} = \frac{1}{2}\left(\sqrt{2\omega}\hat{X} + i\sqrt{\frac{2}{\omega}}\hat{P}\right). \tag{5.26}$$

$$\hat{a}^\dagger = \frac{1}{2}\left(\sqrt{2\omega}\hat{X} - i\sqrt{\frac{2}{\omega}}\hat{P}\right). \tag{5.27}$$

From Eq. (5.7) we have

$$\begin{aligned} H_{disp} &= H^+_{disp}\left|g\right\rangle\left\langle g\right| + H^-_{disp}\left|e\right\rangle\left\langle e\right| \\ &= \left(\frac{1}{2}\omega_+^2\hat{X}^2 + \frac{\hat{P}^2}{2}\right)\left|0\right\rangle\left\langle 0\right| + \left(\frac{1}{2}\omega_-^2\hat{X}^2 + \frac{\hat{P}^2}{2}\right)\left|1\right\rangle\left\langle 1\right| \\ &= \omega_+ a_+^\dagger a_+\left|0\right\rangle\left\langle 0\right| + \omega_- a_-^\dagger a_-\left|1\right\rangle\left\langle 1\right|. \end{aligned} \tag{5.28}$$

The resultant new potential is frequency shifted with

$$\hat{a}_\pm = \frac{1}{2}\left(\sqrt{2\omega_\pm}\hat{X} + i\sqrt{\frac{2}{\omega_\pm}}\hat{P}\right). \tag{5.29}$$

$$\hat{a}_\pm^\dagger = \frac{1}{2}\left(\sqrt{2\omega_\pm}\hat{X} - i\sqrt{\frac{2}{\omega_\pm}}\hat{P}\right), \tag{5.30}$$

being the creation and annihilation operators associated with the frequency shifted potential.
To apply the protocol we initialize the system to be in the dispersive groundstate $\left|\Psi^{0,-}_{disp}\right\rangle = \hat{S}\left|0\right\rangle\left|g\right\rangle$. For a qubit to be suddenly flipped we have

$$\left|\psi(t)\right\rangle = \left|g\right\rangle, t < 0. \tag{5.31}$$

$$\left|\psi(t)\right\rangle = \left|e\right\rangle, t \geq 0. \tag{5.32}$$

The way the field evolves is that at time t=0, $\omega_-\hat{a}_-^\dagger\hat{a}_-$ acts on the field and at $t \geq 0$ $\omega_+\hat{a}_+^\dagger\hat{a}_+$ acts on the field. Thus the qubit flip results in the change in frequency of the harmonic oscillator.

The steps of the protocol are discusses below (Figure 5.3)

- At $t < 0$ the system is in groundstate $|\Psi^{0,-}_{disp}\rangle = |0_-\rangle\,|g\rangle$, where $|0_-\rangle$ is the groundstate of the frequency-shifted oscillator potential $\omega_-\hat{a}^\dagger_-\hat{a}_-$.
- At $t = 0$ the qubit is flipped to an excited state with frequency shifted potential $\omega_+ a^\dagger_+ a_+$. The excited state is also squeezed.
- The newly squeezed excited state is evolved under the Hamiltonian $\omega_+ a^\dagger_+ a_+\,|e\rangle\,\langle e|$ at time ΔT_+.
- The qubit is then flipped back to $|g\rangle$ with the frequency change from $\omega_+ \to \omega_-$ in which the squeezed state is produced in respect to the potential $\omega_- a^\dagger_- a_-$.
- A time evolution of ΔT_- is applied to the groundstate $|g\rangle$ with the frequency shifted potential $\omega_- a^\dagger_- a_-\,|g\rangle\,\langle g|$ as it completes the first cycle.

The field operators evolve over time as such they are represented in the following manner

$$\hat{a}_-(\Delta T_-, \Delta T_+) = \hat{a}_-(\Delta T_+)e^{-i\omega_-\Delta T_-}. \tag{5.33}$$

$$\hat{a}^\dagger_-(\Delta T_-, \Delta T_+) = \hat{a}^\dagger_-(\Delta T_+)e^{i\omega_-\Delta T_-}, \tag{5.34}$$

with

$$\hat{a}_-(\Delta T_+) = \cos(\omega_+\Delta T_+)\hat{a}_-(0) - i\sin\omega_+\Delta T_+[u^2_+\hat{a}_-(0) + u^2_-\hat{a}^\dagger_-(0)]. \tag{5.35}$$

$$\hat{a}^\dagger_-(\Delta T_+) = \cos(\omega_+\Delta T_+)\hat{a}^\dagger_-(0) - i\sin\omega_+\Delta T_+[u^2_+\hat{a}^\dagger_-(0) + u^2_-\hat{a}^\dagger_-(0)]. \tag{5.36}$$

The quadrature operators take the following form

$$\hat{X}_-(\Delta T_-, \Delta T_+) = (\hat{a}^\dagger(\Delta T_-, \Delta T_+) + \hat{a}_-(\Delta T_-, \Delta T_+)). \tag{5.37}$$

$$\hat{P}_-(\Delta T_-, \Delta T_+) = i(\hat{a}^\dagger(\Delta T_-, \Delta T_+) - \hat{a}_-(\Delta T_-, \Delta T_+)). \tag{5.38}$$

We have the variances to be

$$\left\langle \Delta\hat{X}_-(\Delta T_-, \Delta T_+)^2 \right\rangle = \left(\frac{\omega_+}{\omega_-}\right)^2. \tag{5.39}$$

$$\left\langle \Delta\hat{P}_-(\Delta T_-, \Delta T_+)^2 \right\rangle = \left(\frac{\omega_-}{\omega_+}\right)^2. \tag{5.40}$$

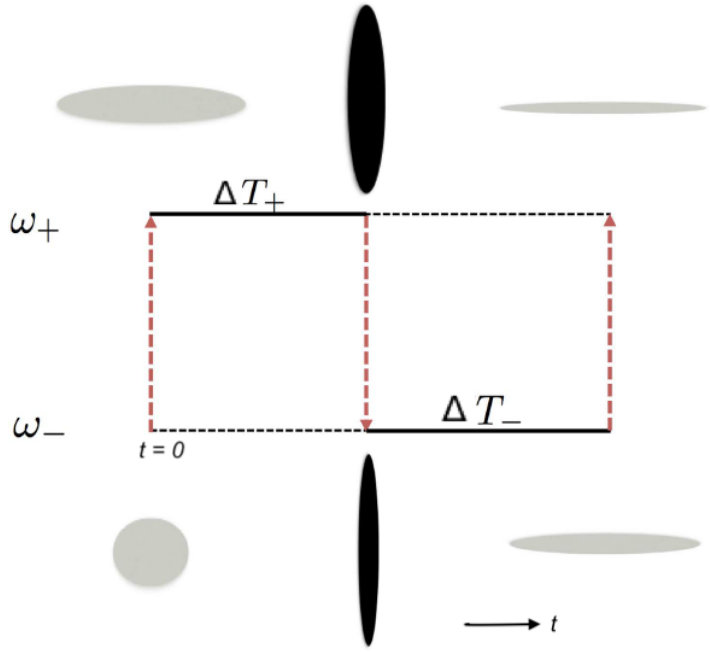

Figure 5.3: **Schematic diagram of the squeezing protocol** with the circle and ellipses representing the field states.

Substituting Eqs. (5.39) and (5.40) into the squeezing formula Eq. (5.25) we can analyze numerically the degree of squeezing that occurs for a full cycle of the protocol.
It is clearly seen that implementing qubit flips greatly enhances the degree of squeezing. More squeezing can be achieved by repeating the protocol for N cycles with the variances scaling up as $\left\langle \Delta\hat{X}_-(\Delta T_-, \Delta T_+)^2 \right\rangle^N$ and $\left\langle \Delta\hat{P}_-(\Delta T_-, \Delta T_+)^2 \right\rangle^N$.

The above protocol was applied to the dispersive Hamiltonian it can be extended to the quantum Rabi model to analyze the degree of squeezing. It is worth to note that the state of the Rabi Hamiltonian after one cycle is

$$|\Psi_{Rabi}(\Delta T_-, \Delta T_+)\rangle = e^{-iH_{Rabi}\Delta_-}\hat{\sigma}_x e^{-iH_{Rabi}\Delta_+}\hat{\sigma}_x |\Psi^0_{Rabi}\rangle\,. \tag{5.41}$$

Figure 5.4 shows the comparison of the degree of squeezing generated in the groundstate $|\Psi^{0,-}_{disp}\rangle$ with that of obtained after one cycle of the protocol. It can be clearly seen that the protocol using sudden frequency flips can significantly increase the degree of squeezing of the field mode over that naturally present in the groundstate. (In Figure 5.6 we show the comparison of the degree of squeezing S for the dispersive Hamiltonian and the Rabi Hamiltonian. Significant squeezing is achieved in the approximate Rabi Hamiltonian than the dispersive Hamiltonian). Illustrated in

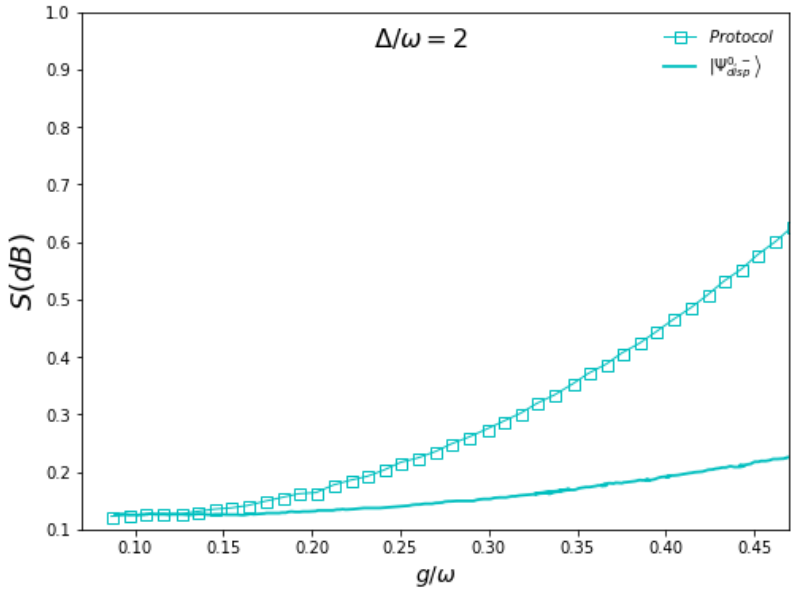

Figure 5.4: **Degree of squeezing** S present in the ground state $|\Psi^{0,-}_{disp}\rangle$ versus that obtained after one cycle of the protocol.

Figure 5.5 are the Wigner functions of the field states using the Rabi Hamiltonian for (a). $|g\rangle$ and (b). $|e\rangle$ qubit states. The Wigner function used is defined in the following form

$$W(\alpha) = \frac{2}{\pi} Tr\Big[\hat{D}^{\dagger}(\alpha)\rho_{Rabi}\hat{D}(\alpha)(-1)^{\hat{a}^{\dagger}\hat{a}}\Big], \tag{5.42}$$

where $\hat{D}(\alpha) = e^{(\alpha\hat{a}^{\dagger} - \alpha^{*}\hat{a})}$ (displacement operator), ρ_{Rabi} is the density matrix of the field, $\alpha = \alpha_r + i\alpha_m$ (complex parameter).
The component of the field along $|g\rangle$ qubit state is similar to the Wigner function of a squeezed state as in Figure 4.1a, and the component of the field along $|e\rangle$ state shows peaks in the negative region an indication of a highly nonclassical state.

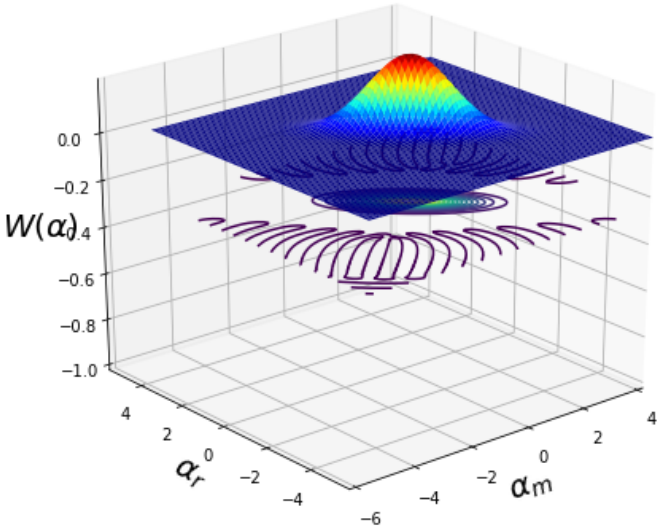

(a)

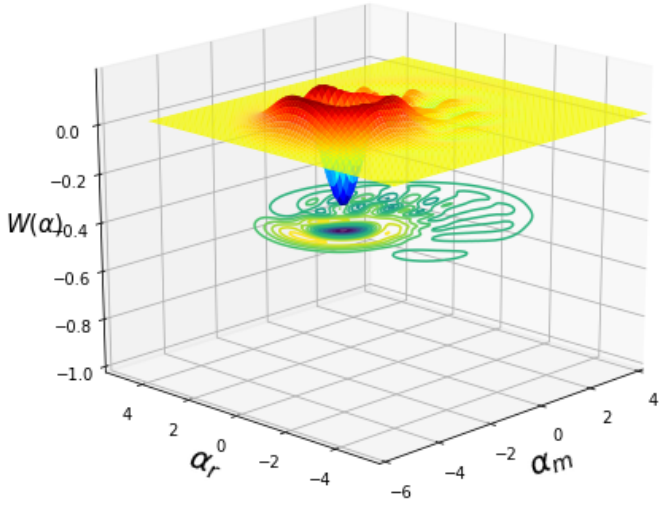

(b)

Figure 5.5: (a) **Wigner function** of the field along the $|g\rangle$ component of the qubit for 15 cycles of the protocol using the Rabi Hamiltonian. (b) Wigner function of the field along the $|e\rangle$ component with $g/\omega = 0.1, \Delta/\omega = 2$.

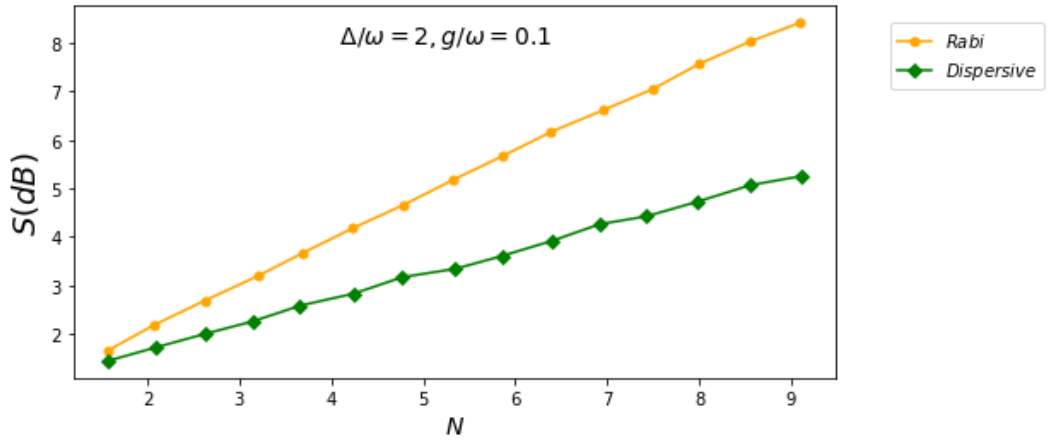

Figure 5.6: **Degree of squeezing** S for the dispersive and Rabi version of the squeezing protocol.

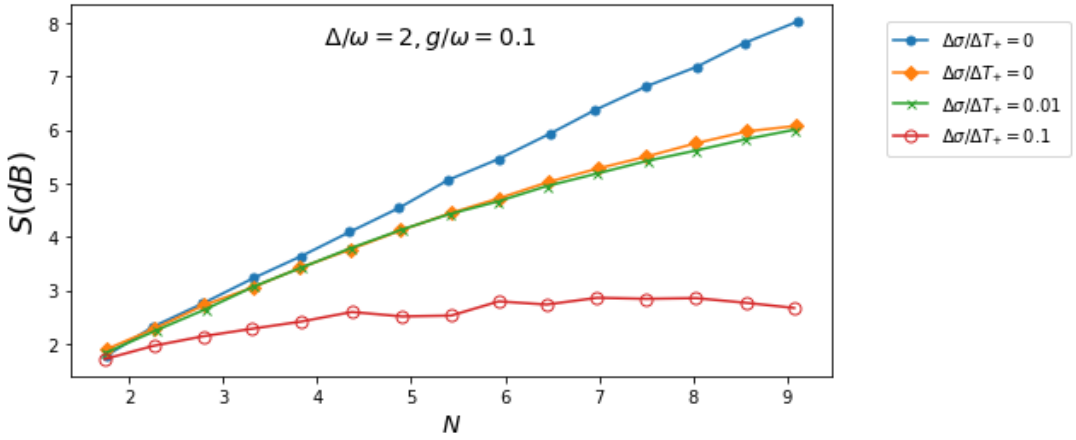

Figure 5.7: **Cavity photon losses** on the average degree of squeezing $\langle S \rangle$ produced by N cycles of the Rabi protocol.

5.3 Discussion

In this section we discuss the errors arising from fully implementing the above protocol. In a physical setting the protocol will suffer from cavity imperfections that are prone to photon losses, dephasing of the qubit and qubit relaxation which affect the protocol outcome. The photon loss is integrated into the model by making use of the master equation at time intervals of $\Delta T_{\pm}$ with a decay rate of Γ. A simulation of the master equation at $\Gamma = 0.01/\Delta T_+$ is shown in Figure 5.7. The degree of squeezing becomes non-linear in the cycle number N due to photon loss in the cavity and saturates for an increases cycle number N at an additional round of protocol. To achieve maximum squeezing we introduce time delays of random offset ϵ to account for inaccuracies in the protocol. The choice of the ϵ is taken from a normal distribution of mean zero and standard deviation $\Delta\sigma$.

Within the dispersive version of the protocol, the qubit is often in one of its eigen-

states which means that dephasing does not affect the protocol and solely the energy relaxation time T_1 should be considered. In the Rabi case qubit dephasing might contribute to noise and as such it is difficult to know exactly which eigenstate is the qubit is in. In the time evoultion interval ΔT_+ the qubit remains coherent throughout the total N cycles of the protocol.
By selecting a cavity frequency $\omega \sim$1GHz and coupling strength $g = 0.1\omega$ offers $\Delta T_\pm$ relevance to superconducting circuit QED experiments. Qubit losses should not be a limiting factor for the protocol in the experimental implementation given that superconducting qubits are routinely achieving dephasing and relaxation times of tens of microseconds [57–60]. Thus, the degree of squeezing that may be achieved cannot be hindered by the protocol.
The cavity photon loss incorporates an additional effect in the protocol imperfection as a result of the field state made up over sequential cycles and so should retain coherence over the total N cycles of the protocol. To include the cavity photon losses in the protocol for squeezing generation we use the master equation [55], presumptuous that the bosonic mode couples to zero temperature reservoir under the damping rate Γ in the interval $\Delta T_\pm$.
The master equation simulation with $\Gamma = 0.1/\Delta T_+$ is shown in Figure 5.7, where the degree of squeezing within the presence of photon loss is not any longer linear within the range of N cycles. As N increases, the additional squeezing generated begins to saturate. However, a considerable increase in squeezing over that present within the initial state will still be obtained.

To ensure maximum squeezing of the bosonic mode the protocol needs rigorously designed time delays. Modeling the inaccuracies in timing means we have to add a random offset ϵ, chosen from a standard deviation with the mean centered at zero and variance $\Delta\sigma$ to every time delay $\Delta T_\pm$. The mean degree of squeezing of the bosonic mode is calculated by taking an ensemble average over multiple runs of the N-cycle protocol as shown in Figure 5.7 where the mean degree of squeezing for cavity photon losses and random time delays are included in the protocol. Once the error in timing is on the order of 1%, the timing noise has very little impact on the degree of squeezing. However, larger timing errors dramatically scale back the degree of squeezing generated. Therefore the flexibility to manage the timing of qubit flips to a fairly precise degree are vital for experimental implements of the protocol.
The preceding calculations have relied on the idea of instant qubit state flips that result in sudden changes within the frequency of the oscillator. Ideally finite however small change $\tilde{t}$ is required for sudden frequency change this is when $\tilde{t} \ll min(\omega_+, \omega_-)/|\omega_+^2 - \omega_-^2|$ with the change from $\omega_+ \to \omega_-$ being a good approximation.
Modification of the sudden frequency shift [56] have been mentioned in literature. The sinusoidal modulation has been studied extensively in [61, 62]. Both above schemes are less hard from an experimental position but don't seem efficient as the sudden jump protocol

5.4 Conclusion

Squeezed light has been traditionally generated through optical interactions, however over the years completely different physical systems are presently pursued in this direction together with superconducting microwave cavities. Experimental developments achieved significant squeezing in optical oscillators [63, 64].
In this chapter we presented a new technique of generating squeezing of the light field in a dispersive regime interacting with the qubit under the Rabi model. Beneath this interaction, the dispersive frequency shift allows the frequency of the cavity mode to be modified by flipping the state of the qubit. In absence of noise , significant squeezing is produced from the frequency shifts of the sudden frequency jumps. Even within the presence of a protocol level noise and experimental imperfection, the degree of squeezing made beneath this protocol is similar to the degree of squeezing studied in [65, 66] and thus, our methodology of squeezed state generation could have possible applications in ultra-precise sensing and measurements.

Chapter 6

Hybrid Quantum Circuits

In this chapter we combine the idea of squeezed light into feasible quantum circuit geometry that enables quantum computation and measurement. We consider hybrid systems (Figure 6.1) because of their distinguished properties such as coherence of qubit states and better experimental implementation than other systems. One of the ways to quantify or observe squeezed states of light it is through entangled states [67] as shown in the previous chapters although within a hybrid quantum system is important to fully understand the entanglement dynamics of the interacting systems. Thus, in the first section of this chapter we study the entanglement dynamics of a hybrid system consisting of flux qubits together with NVE and measure entanglement of the system. We then use the results of this section to build and understand the generation of squeezed states within such hybrid structure in the second section. A single-mode squeezed state of NVE is generated through entangled bosonic mode of the transmission line resonator (TLR) [68, 69].

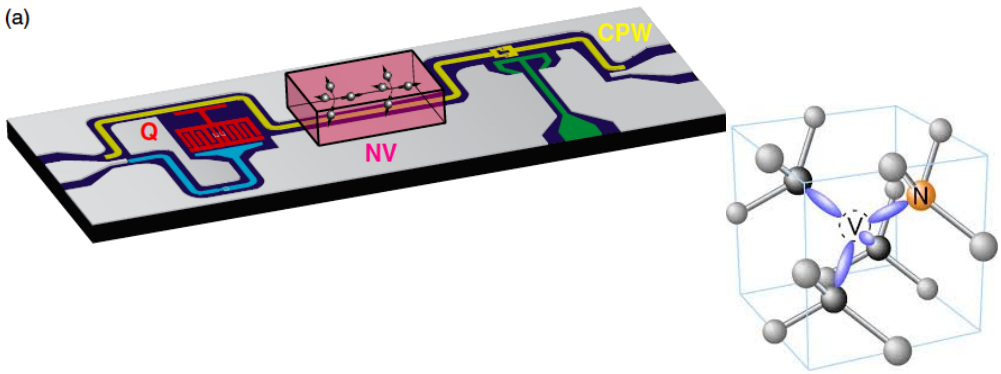

Figure 6.1: (a) **Experimental circuit design** where NV,Q and CPW denote the NV center ensemble in diamond (with its zoomed in image on the right), transmon qubit and the coplanar wavequide resonator.

6.1 Entanglement dynamics of flux qubits and a nitrogen-vacancy-center ensemble

Quantum entangled states are crucially important in quantum information processes [70, 71]. Extensive research has been done on pure bipartite entangled states [72]. A real quantum system is subjected to decoherence through its environment (dissipation) and is generally in a mixed state. To effectively build a quantum circuit that has long coherence times and structural design that allows for scability of the circuit, tunability of the superconducting qubit devices and large couplings of the quantum processor for fast manipulation [73, 74] requires combing two worlds, that of superconducting flux qubits and microscopic systems (spin systems) together termed 'hybrid' quantum system as proposed by Xiang et al. in [74] and experimentally achieved [75, 76]. A hybrid quantum system that will be studied in this thesis is that consisting of an NVE (nitrogen-vacancy center ensemble) acting as a quantum memory together with a superconducting flux qubit that acts as a quantum processor. NV centers in diamond have long coherence times of approximately 1 s at 77 K [77].

In this section we study a hybrid bipartite and three-qubit quantum systems to investigate dynamical properties of maximally entangled states, whether they are pure entangled states or mixed states. The measure of entanglement used is concurrence C(t) as one of the quantifiable measure and entropy of states [78, 79]. We further investigate whether the hybrid entanglement is of geometric nature [80].

6.1.1 Model

The hybrid quantum system that is studied consists of two flux qubits Qubit M and Qubit C (Figure 6.2) together with an NV ensemble. Qubit C is the quantum processor with the NV center ensemble coupled to Qubit M as a spin quantum memory. Qubit C is tunably coupled to Qubit M with coupling strength J. It is important to mention that the quantum processing (computing) part of the above system and the quantum memory system (NV center ensemble) influence each other thus making it difficult to effectively store a quantum state on single NV center as well as to perform quantum computation. The external magnetic field I_{ext} induces a splitting between $m = 0$ and $m = -1$ sublevels [73].

The flux Qubit C is considered to be in an initial state $|\Psi\rangle_C = \sin\theta\,|0\rangle_C + \cos\theta\,|1\rangle_C$ with both the flux Qubit M and NVE in a groundstate $|\Psi\rangle_{MNV} = |0\rangle_M\,|0\rangle_{NV}$. The initial state of the system in a coherent superposition

$$|\Psi(0)\rangle = \sin\theta\,|0\rangle_C\,|0\rangle_M\,|0\rangle_{NV} + \cos\theta\,|1\rangle_C\,|0\rangle_M\,|0\rangle_{NV}\,. \tag{6.1}$$

At time t,

$$\begin{aligned}|\Psi(t)\rangle = a_0\,|0\rangle_C\,|0\rangle_M\,|0\rangle_{NV} + a_1\,|1\rangle_C\,|0\rangle_M\,|0\rangle_{NV}\\ + a_2\,|0\rangle_C\,|1\rangle_M\,|0\rangle_{NV} + a_3\,|0\rangle_C\,|0\rangle_M\,|1\rangle_{NV}\,.\end{aligned} \tag{6.2}$$

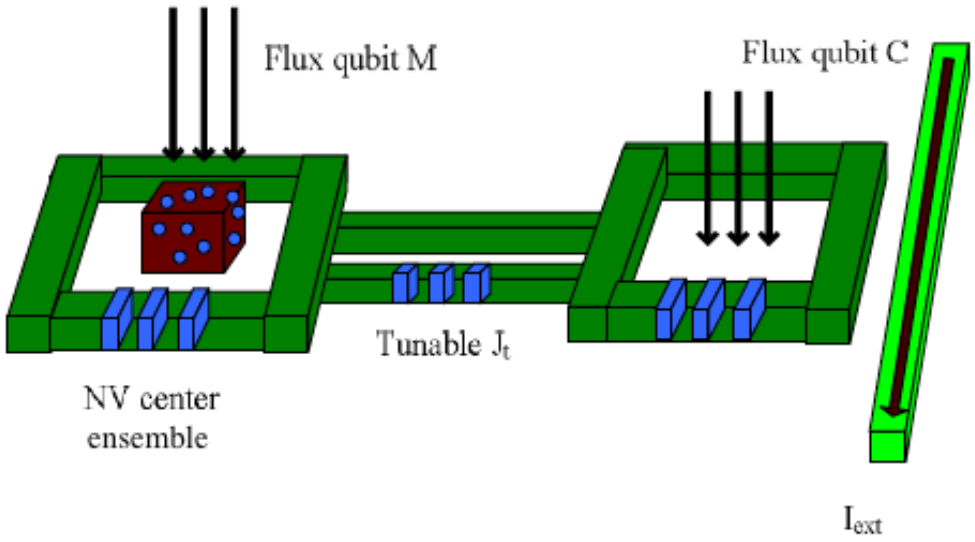

Figure 6.2: **Physical quantum system** consisting of two superconducting flux qubits and an NV center ensemble.

The time evolution of the state is given by $|\Psi(t)\rangle = e^{-iHt}|\Psi(0)\rangle$ where H is the resonant-interaction Hamiltonian

$$H = g\big(\hat{b}^{+}\hat{\sigma}_M^{-} + \hat{b}\hat{\sigma}_M^{+}\big) + J\big(\hat{\sigma}_C^{-}\hat{\sigma}_M^{+} + \hat{\sigma}_C^{+}\hat{\sigma}_M^{-}\big), \tag{6.3}$$

where g, J represent the coupling between the flux Qubit M and NVE, the tunable coupling between flux Qubit C and flux Qubit M. The NVE system is considered as a bosonic mode because of the collective excitations [81] of the electron cloud with $\hat{b}, \hat{b}^{+}$ obeying the commutation relations, $\hat{\sigma}_C^{+}(\hat{\sigma}_C^{-})$ and $\hat{\sigma}_M^{+}(\hat{\sigma}_M^{-})$ represent the atomic spin operators.

Working in the following basis set

$$\{|0\rangle_C|0\rangle_M|0\rangle_{NV}, |1\rangle_C|0\rangle_M|0\rangle_{NV}, |0\rangle_C|1\rangle_M|0\rangle_{NV}, |0\rangle_C|0\rangle_M|1\rangle_{NV}\}.$$

The Hamiltonian H in Eq. (6.3) can be represented in terms of this basis

$$H = \langle i|H|j\rangle, \qquad i,j\epsilon\{|0\rangle_C|0\rangle_M|0\rangle_{NV}, ..., |0\rangle_C|0\rangle_M|1\rangle_{NV}\}. \tag{6.4}$$

In matrix form H,

$$H = \begin{pmatrix} \alpha & \beta & \gamma & \delta \\ \epsilon & \zeta & \eta & \theta \\ \iota & \kappa & \lambda & \mu \\ \nu & \xi & \tau & \pi \end{pmatrix}, \tag{6.5}$$

where

$$\begin{aligned}
\alpha &= \langle 0|_C \langle 0|_M \langle 0_{NV}| H |0\rangle_C |0\rangle_M |0\rangle_{NV}, \quad \beta = \langle 1|_C \langle 0|_M \langle 0_{NV}| H |0\rangle_C |0\rangle_M |0\rangle_{NV}. \\
\gamma &= \langle 0|_C \langle 1|_M \langle 0_{NV}| H |0\rangle_C |1\rangle_M |0\rangle_{NV}, \quad \delta = \langle 0|_C \langle 0|_M \langle 1_{NV}| H |0\rangle_C |0\rangle_M |1\rangle_{NV}. \\
\epsilon &= \langle 0|_C \langle 0|_M \langle 0_{NV}| H |1\rangle_C |0\rangle_M |0\rangle_{NV}, \quad \zeta = \langle 1|_C \langle 0|_M \langle 0_{NV}| H |1\rangle_C |0\rangle_M |0\rangle_{NV}. \\
\iota &= \langle 0|_C \langle 0|_M \langle 0_{NV}| H |0\rangle_C |1\rangle_M |0\rangle_{NV}, \quad \kappa = \langle 1|_C \langle 0|_M \langle 0_{NV}| H |0\rangle_C |1\rangle_M |0\rangle_{NV}. \\
\lambda &= \langle 0|_C \langle 1|_M \langle 0_{NV}| H |0\rangle_C |1\rangle_M |0\rangle_{NV}, \quad \mu = \langle 0|_C \langle 0|_M \langle 1_{NV}| H |0\rangle_C |1\rangle_M |0\rangle_{NV}. \\
\nu &= \langle 0|_C \langle 0|_M \langle 0_{NV}| H |0\rangle_C |0\rangle_M |1\rangle_{NV}, \quad \xi = \langle 1|_C \langle 0|_M \langle 0_{NV}| H |0\rangle_C |0\rangle_M |1\rangle_{NV}. \\
\tau &= \langle 0|_C \langle 1|_M \langle 0_{NV}| H |0\rangle_C |0\rangle_M |1\rangle_{NV}, \quad \pi = \langle 0|_C \langle 0|_M \langle 1_{NV}| H |1\rangle_C |0\rangle_M |1\rangle_{NV}.
\end{aligned} \tag{6.6}$$

Using the ladder photonic and atomic spin operators defined in Eq. (2.44) we can simplify H to be

$$H = \begin{pmatrix} 0 & 0 & 0 & 0 \\ 0 & 0 & J & 0 \\ 0 & J & 0 & g \\ 0 & 0 & g & 0 \end{pmatrix}. \tag{6.7}$$

The eigenvalues of matrix H in Eq. (6.7) are

$$\lambda_0 = 0, \qquad \lambda_1 = 0, \qquad \lambda_2 = -\sqrt{g^2 + J^2}, \qquad \lambda_3 = \sqrt{g^2 + J^2}. \tag{6.8}$$

The corresponding normalized eigenvectors are

$$\begin{aligned}
x_0 &= \left[0, \frac{-g}{J\sqrt{1 + \left|\frac{g}{J}\right|^2}}, 0, \frac{1}{\sqrt{1 + \left|\frac{g}{J}\right|^2}}\right], \\
x_1 &= [1, 0, 0, 0], \\
x_2 &= \left[0, \frac{J}{g\sqrt{\left|\frac{g^2+J^2}{g}\right|^2 + \left|\frac{J}{g}\right|^2 + 1}}, -\frac{\sqrt{g^2+J^2}}{g\sqrt{\left|\frac{g^2+J^2}{g}\right|^2 + \left|\frac{J}{g}\right|^2 + 1}}, \frac{1}{\sqrt{\left|\frac{g^2+J^2}{g}\right|^2 + \left|\frac{J}{g}\right|^2 + 1}}\right], \\
x_3 &= \left[0, \frac{J}{g\sqrt{\left|\frac{g^2+J^2}{g}\right|^2 + \left|\frac{J}{g}\right|^2 + 1}}, \frac{\sqrt{g^2+J^2}}{g\sqrt{\left|\frac{g^2+J^2}{g}\right|^2 + \left|\frac{J}{g}\right|^2 + 1}}, \frac{1}{\sqrt{\left|\frac{g^2+J^2}{g}\right|^2 + \left|\frac{J}{g}\right|^2 + 1}}\right].
\end{aligned} \tag{6.9}$$

Applying the time evolution $e^{-iHt/\hbar}(\hbar = 1)$ we have

$$\begin{aligned}
e^{-iHt/\hbar} &= e^{-i\lambda_0 t} x_0 x_0^\dagger + e^{-i\lambda_1 t} x_1 x_1^\dagger + e^{-i\lambda_2 t} x_2 x_2^\dagger + e^{-i\lambda_3 t} x_3 x_3^\dagger \\
&= \begin{pmatrix} 1 & 0 & 0 & 0 \\ 0 & a & 0 & 0 \\ 0 & 0 & b & 0 \\ 0 & 0 & 0 & c \end{pmatrix},
\end{aligned} \tag{6.10}$$

where

$$
\begin{aligned}
a &= \cos\theta\left[\frac{g^2}{J^2\left(1+\left|\frac{g}{J}\right|^2\right)}+\frac{J^2}{g^2\left(\sqrt{\left|\frac{g^2+J^2}{g}\right|^2+\left|\frac{J}{g}\right|^2+1}\right)}\right](e^{i\sqrt{g^2+J^2}t}+e^{-i\sqrt{g^2+J^2}t}),\\
b &= \cos\theta\left[\frac{J\sqrt{g^2+J^2}}{g\sqrt{\left|\frac{g^2+J^2}{g}\right|^2+\left|\frac{J}{g}\right|^2+1}}\right](e^{-i\sqrt{g^2+J^2}t}-e^{i\sqrt{g^2+J^2}t}),\\
c &= \cos\theta\left[\frac{g}{J\left(1+\left|\frac{-g}{J}\right|^2\right)}+\frac{J}{g\left(\sqrt{\left|\frac{g^2+J^2}{g}\right|^2+\left|\frac{J}{g}\right|^2+1}\right)}\right](e^{-i\sqrt{g^2+J^2}t}+e^{i\sqrt{g^2+J^2}t}).
\end{aligned}
\tag{6.11}
$$

Using the trigonometric identities $\sin\theta=\frac{e^{i\theta}-e^{-i\theta}}{2i}$ and $\cos\theta=\frac{e^{i\theta}+e^{-i\theta}}{2}$ we find the coefficients of the system's state at time t to be

$$
\begin{aligned}
a_0(t) &= \sin\theta,\\
a_1(t) &= \frac{\cos(\theta)(g^2+J^2\cos\sqrt{g^2+J^2}t)}{g^2+J^2},\\
a_2(t) &= -\frac{iJ\cos(\theta)\sin\sqrt{g^2+J^2}t}{\sqrt{g^2+J^2}},\\
a_3(t) &= \frac{gJ\cos(\theta)[-1+\cos\sqrt{g^2+J^2}t]}{g^2+J^2}.
\end{aligned}
\tag{6.12}
$$

To determine the entanglement dynamics of the system we first evaluate the density matrix of the system at time t

$$
\begin{aligned}
|\Psi(t)\rangle\langle\Psi(t)| = {} & a_0a_0^*\,|0_M\rangle\langle 0|_M\otimes|0_C\rangle\langle 0|_C\otimes|0_{NV}\rangle\langle 0|_{NV}+a_0a_1^*\,|0_M\rangle\langle 0|_M\otimes|0_C\rangle\langle 1|_C\\
&\otimes|0_{NV}\rangle\langle 0|_{NV}+a_0a_2^*\,|0_M\rangle\langle 1|_M\otimes|0_C\rangle\langle 0|_C\otimes|0_{NV}\rangle\langle 0|_{NV}+a_0a_3^*\,|0_M\rangle\langle 0|_M\\
&\otimes|0_C\rangle\langle 0|_C\otimes|0_{NV}\rangle\langle 1|_{NV}+a_1a_0^*\,|0_M\rangle\langle 0|_M\otimes|1_C\rangle\langle 0|_C\otimes|0_{NV}\rangle\langle 0|_{NV}\\
&+a_1a_1^*\,|0_M\rangle\langle 0|_M\otimes|1_C\rangle\langle 1|_C\otimes|0_{NV}\rangle\langle 0|_{NV}+a_1a_2^*\,|0_M\rangle\langle 1|_M\otimes|0_C\rangle\langle 0|_C\\
&\otimes|0_{NV}\rangle\langle 0|_{NV}+a_1a_3^*\,|0_M\rangle\langle 0|_M\otimes|1_C\rangle\langle 0|_C\otimes|0_{NV}\rangle\langle 1|_{NV}+a_2a_0^*\,|1_M\rangle\langle 0|_M\\
&\otimes|0_C\rangle\langle 0|_C\otimes|0_{NV}\rangle\langle 0|_{NV}+a_2a_1^*\,|0_M\rangle\langle 0|_M\otimes|1_C\rangle\langle 0|_C\otimes|0_{NV}\rangle\langle 0|_{NV}\\
&+a_2a_2^*\,|1_M\rangle\langle 1|_M\otimes|0_C\rangle\langle 0|_C\otimes|0_{NV}\rangle\langle 0|_{NV}+a_2a_3^*\,|1_M\rangle\langle 0|_M\otimes|0_C\rangle\langle 0|_C\\
&\otimes|0_{NV}\rangle\langle 1|_{NV}+a_3a_0^*\,|0_M\rangle\langle 0|_M\otimes|0_C\rangle\langle 0|_C\otimes|1_{NV}\rangle\langle 0|_{NV}+a_3a_1^*\,|0_M\rangle\langle 0|_M\\
&\otimes|0_C\rangle\langle 1|_C\otimes|1_{NV}\rangle\langle 0|_{NV}+a_3a_2^*\,|0_M\rangle\langle 1|_M\otimes|0_C\rangle\langle 0|_C\otimes|1_{NV}\rangle\langle 0|_{NV}\\
&+a_3a_3^*\,|0_M\rangle\langle 0|_M\otimes|0_C\rangle\langle 0|_C\otimes|1_{NV}\rangle\langle 1|_{NV}\,.
\end{aligned}
\tag{6.13}
$$

Entanglement between Qubit C and NVE is calculated by tracing out Qubit M in Eq. (6.13) to give the reduced density matrix ρ_{CNV}. Using the basis $|1\rangle = |1_C\rangle\,|1_{NV}\rangle$, $|2\rangle = |1_C\rangle\,|0_{NV}\rangle$, $|3\rangle = |0_C\rangle\,|1_{NV}\rangle$, $|4\rangle = |0_C\rangle\,|0_{NV}\rangle$ we find the density matrix to be

$$\begin{aligned}\rho_{CNV} &= Tr_M\,|\Psi(t)\rangle\,\langle\Psi(t)| \\ &= a_0a_0^*\,|0_C\rangle\langle 0|_C \otimes |0_{NV}\rangle\langle 0|_{NV} + a_0a_1^*\,|0_C\rangle\langle 1|_C \otimes |0_{NV}\rangle\langle 0|_{NV} \\ &+ a_0a_3^*\,|0_C\rangle\langle 0|_C \otimes |0_{NV}\rangle\langle 1|_{NV} + a_1a_0^*\,|1_C\rangle\langle 0|_C \otimes |0_{NV}\rangle\langle 0|_{NV} \\ &+ a_1a_1^*\,|1_C\rangle\langle 1|_C \otimes |0_{NV}\rangle\langle 0|_{NV} + a_1a_3^*\,|1_C\rangle\langle 0|_C \otimes |0_{NV}\rangle\langle 1|_{NV} \\ &+ a_2a_2^*\,|0_C\rangle\langle 0|_C \otimes |0_{NV}\rangle\langle 0|_{NV} + a_3a_0^*\,|0_C\rangle\langle 0|_C \otimes |1_{NV}\rangle\langle 0|_{NV} \\ &+ a_3a_1^*\,|0_C\rangle\langle 1|_C \otimes |1_{NV}\rangle\langle 0|_{NV} + a_3a_3^*\,|0_C\rangle\langle 0|_C \otimes |1_{NV}\rangle\langle 1|_{NV}\,.\end{aligned} \tag{6.14}$$

In the standard basis term defined above we find Eq. (6.14)

$$\begin{aligned}\rho_{CNV} &= a_0a_0^*\,|4\rangle\,\langle 4| + a_0a_1^*\,|4\rangle\,\langle 2| + a_0a_3^*\,|4\rangle\,\langle 3| + a_1a_0^*\,|2\rangle\,\langle 4| \\ &+ a_1a_1^*\,|2\rangle\,\langle 2| + a_1a_3^*\,|2\rangle\,\langle 3| + a_2a_2^*\,|4\rangle\,\langle 4| \\ &+ a_3a_0^*\,|3\rangle\,\langle 4| + a_3a_1^*\,|3\rangle\,\langle 2| + a_3a_3^*\,|3\rangle\,\langle 3| \\ &= \begin{pmatrix} 0 & 0 & 0 & 0 \\ 0 & a_1a_1^* & a_1a_3^* & a_1a_0^* \\ 0 & a_3a_1^* & a_3a_3^* & a_3a_0^* \\ 0 & a_0a_1^* & a_0a_3^* & a_0a_0^* + a_2a_2^* \end{pmatrix}.\end{aligned} \tag{6.15}$$

To measure the quantity of entanglement of a two-particle system or bipartite system we turn to the definition introduced by Wootters [78, 79] of Concurrence $C(t)$ defined as

$$C(t) = \max[0, \lambda_1(t) - \lambda_2(t) - \lambda_3(t) - \lambda_4(t)], \tag{6.16}$$

where the $\lambda_i(t)$ are eigenvalues of the matrix in decreasing order

$$\sqrt{\sqrt{\rho}\tilde{\rho}\sqrt{\rho}}, \qquad\qquad \tilde{\rho} = (\sigma_y \otimes \sigma_y)\rho^*(\sigma_y \otimes \sigma_y). \tag{6.17}$$

The Concurrence values range from 0 to 1 with 1 being the maximally entangled states and 0 having no entanglement.
Evaluating the matrix in Eq. (6.17) for the reduced density matrix of the flux Qubit C and NVE ρ_{CNV} and the concurrence we get the following expression

$$C_{CNV}(t) = 2\left|\frac{\cos(\theta)^2 gJ\left[(g^2 - J^2)(\cos\sqrt{g^2 + J^2}t - 1) + \frac{J^2}{2}(\cos 2\sqrt{g^2 + J^2}t - 1)\right]}{(g^2 + J^2)}\right|. \tag{6.18}$$

Using Eq. (6.13) we can find the reduced density matrix of the flux Qubit M and

the NVE by tracing out the flux Qubit C

$$\begin{aligned}\rho_{MNV} &= Tr_C \left|\Psi(t)\right\rangle \left\langle\Psi(t)\right| \\ &= a_0 a_0^* \left|0_M\right\rangle\!\left\langle 0\right|_M \otimes \left|0_{NV}\right\rangle\!\left\langle 0\right|_{NV} + a_0 a_2 * \left|0_M\right\rangle\!\left\langle 1\right|_M \otimes \left|0_{NV}\right\rangle\!\left\langle 0\right|_{NV} \\ &+ a_0 a_3^* \left|0_M\right\rangle\!\left\langle 0\right|_M \otimes \left|0_{NV}\right\rangle\!\left\langle 1\right|_{NV} + a_1 a_1^* \left|0_M\right\rangle\!\left\langle 0\right|_C \otimes \left|0_{NV}\right\rangle\!\left\langle 0\right|_{NV} \\ &+ a_1 a_2^* \left|0_M\right\rangle\!\left\langle 1\right|_M \otimes \left|0_{NV}\right\rangle\!\left\langle 0\right|_{NV} + a_2 a_0^* \left|1_M\right\rangle\!\left\langle 0\right|_M \otimes \left|0_{NV}\right\rangle\!\left\langle 0\right|_{NV} \\ &+ a_2 a_2^* \left|1_M\right\rangle\!\left\langle 1\right|_M \otimes \left|0_{NV}\right\rangle\!\left\langle 0\right|_{NV} + a_2 a_3^* \left|1_M\right\rangle\!\left\langle 0\right|_M \otimes \left|0_{NV}\right\rangle\!\left\langle 1\right|_{NV} \\ &+ a_3 a_0^* \left|0_M\right\rangle\!\left\langle 0\right|_M \otimes \left|1_{NV}\right\rangle\!\left\langle 0\right|_{NV} + a_3 a_2^* \left|0_M\right\rangle\!\left\langle 1\right|_C \otimes \left|1_{NV}\right\rangle\!\left\langle 0\right|_{NV} \\ &+ a_3 a_3 * \left|0_M\right\rangle\!\left\langle 0\right|_M \otimes \left|1_{NV}\right\rangle\!\left\langle 1\right|_{NV},\end{aligned} \tag{6.19}$$

which in the basis $|1\rangle = |1_M\rangle|1_{NV}\rangle$, $|2\rangle = |1_M\rangle|0_{NV}\rangle$, $|3\rangle = |0_M\rangle|1_{NV}\rangle$, $|4\rangle = |0_M\rangle|0_{NV}\rangle$ reduced density matrix ρ_{MNV}

$$\begin{aligned}\rho_{CNV} &= a_0 a_0^* \left|4\right\rangle\left\langle 4\right| + a_0 a_2^* \left|4\right\rangle\left\langle 2\right| + a_0 a_3^* \left|4\right\rangle\left\langle 3\right| + a_1 a_1^* \left|4\right\rangle\left\langle 4\right| \\ &+ a_1 a_2^* \left|4\right\rangle\left\langle 2\right| + a_2 a_0^* \left|2\right\rangle\left\langle 4\right| + a_2 a_2^* \left|2\right\rangle\left\langle 2\right| + a_2 a_3^* \left|2\right\rangle\left\langle 3\right| \\ &+ a_3 a_0^* \left|3\right\rangle\left\langle 4\right| + a_3 a_2^* \left|3\right\rangle\left\langle 2\right| + a_3 a_3^* \left|3\right\rangle\left\langle 3\right| \\ &= \begin{pmatrix} 0 & 0 & 0 & 0 \\ 0 & a_2 a_2^* & a_2 a_3^* & a_2 a_0^* \\ 0 & a_3 a_2^* & a_3 a_3^* & a_3 a_2^* \\ 0 & a_0 a_2^* & a_2 a_3^* & a_0 a_0^* + a_1 a_1^* \end{pmatrix}.\end{aligned} \tag{6.20}$$

The concurrence expression of the flux Qubit M and the NVE is

$$C_{MNV}(t) = 2\left|\frac{\cos(\theta)^2 g J^2 \left(\frac{1}{2}\sin 2\sqrt{g^2+J^2}t - \sin\sqrt{g^2+J^2}t\right)}{(g^2+J^2)^{\frac{3}{2}}}\right|. \tag{6.21}$$

For a three-particle system or we measure the '3-way' entanglement of the flux Qubit C, flux Qubit M and the NVE using the three-tangle measure defined as [82]

$$\tau(\Psi_{CMNV}) = \tau_{C(\rho_C)} - C_{CM}^2 - C_{CNV}^2, \tag{6.22}$$

where the first term is the linear entropy defined as

$$\tau_{C(\rho_C)} = 2[1 - Tr\rho_C^2]. \tag{6.23}$$

The reduced density matrix ρ_C in Eq. (6.23) is found by taking the partial trace of the flux Qubit M of the reduced density matrix ρ_{CM}

$$\begin{aligned}\rho_C = Tr_M \rho_{CM} &= a_1 a_1^* \left|1\right\rangle\left\langle 1\right| + a_1 a_0^* \left|1\right\rangle\left\langle 0\right| + a_2 a_2^* \left|0\right\rangle\left\langle 0\right| \\ &+ a_0 a_1^* \left|0\right\rangle\left\langle 1\right| + (a_0 a_0^* + a_3 a_3^*) \left|0\right\rangle\left\langle 0\right|.\end{aligned} \tag{6.24}$$

In which,

$$Tr\rho_C^2 = (a_1 a_1^*)^2 + (a_2 a_2^* + a_0 a_0^* + a_3 a_3^*)^2 + 2 a_1 a_0^* a_0 a_1^*. \tag{6.25}$$

Within the three-qubit interaction of the system we also interested in dissipation that the total system undergoes. For this we consider the Lindblad master equation for j qubits

$$\frac{d\rho}{dt} = -i[H,\rho] + \sum_{j=C,M} \frac{\gamma_j}{2}\Big(2\sigma_j^- \rho \sigma_j^+ - \{\sigma_j^+\sigma_j^-,\rho\}\Big), \tag{6.26}$$

wth the density matrix ρ is denoted by

$$\rho(t) = \begin{pmatrix} \rho_{11} & \rho_{12} & \rho_{13} & \rho_{14} \\ \rho_{21} & \rho_{22} & \rho_{23} & \rho_{24} \\ \rho_{31} & \rho_{32} & \rho_{33} & \rho_{34} \\ \rho_{41} & \rho_{42} & \rho_{43} & \rho_{44} \end{pmatrix}, \tag{6.27}$$

where the basis $|1\rangle = |000\rangle, |2\rangle = |100\rangle, |3\rangle = |010\rangle, |4\rangle = |001\rangle$.

The corresponding matrix elements of the time evolution of the density matrix ρ in Eq. (6.26) are

$$\begin{aligned}
\dot{\rho_{11}} &= \gamma_C\rho_{22} + \gamma_M\rho_{33}, \\
\dot{\rho_{12}} &= iJ\rho_{13} - \frac{\gamma_M}{2}\rho_{33}, \\
\dot{\rho_{13}} &= i(g\rho_{14} + J\rho_{12}) - \frac{\gamma_M}{2}\rho_{13}, \\
\dot{\rho_{14}} &= ig\rho_{143}, \\
\dot{\rho_{21}} &= -iJ\rho_{31} - \frac{\gamma_C}{2}\rho_{21}, \\
\dot{\rho_{22}} &= iJ(\rho_{23} - \rho_{32}) - \gamma_C\rho_{22}, \\
\dot{\rho_{23}} &= i[g\rho_{24} + J(\rho_{22} - \rho_{33})] - \frac{1}{2}(\gamma_C + \gamma_M)\rho_{23}, \\
\dot{\rho_{24}} &= i(g\rho_{23} - J\rho_{34}) - \frac{\gamma_C}{2}\rho_{24}, \\
\dot{\rho_{31}} &= i(g\rho_{41} + J\rho_{21}) - \frac{\gamma_M}{2}\rho_{31}, \\
\dot{\rho_{32}} &= -i[g\rho_{42} + J(\rho_{22} - \rho_{33})] - \frac{\gamma_M}{2}\rho_{32} - \frac{\gamma_C}{2}\rho_{32}, \\
\dot{\rho_{33}} &= i[g(\rho_{34} - \rho_{43}) + J(\rho_{32} - \rho_{23})] - \gamma_M\rho_{33}, \\
\dot{\rho_{34}} &= i[g(\rho_{33} - \rho_{44}) - J\rho_{24}] - \frac{\gamma_M}{2}\rho_{34}, \\
\dot{\rho_{41}} &= ig\rho_{31}, \\
\dot{\rho_{42}} &= ig\rho_{23} - \frac{\gamma_C}{2}\rho_{42}, \\
\dot{\rho_{43}} &= i[g(\rho_{44} - \rho_{33}) + J\rho_{42}] - \frac{\gamma_M}{2}\rho_{43}, \\
\dot{\rho_{44}} &= i[(g+J)\rho_{43} - G\rho_{34}.
\end{aligned} \tag{6.28}$$

6.1.2 Results and Discussion

In this section we present and discuss the results of concurrences $C(t)$ for the bipartite and residual entanglement of the flux Qubit C, flux Qubit M and NVE in the absence and presence of dissipation as calculated from the last section.

Bipartite Entanglement - Without Dissipation

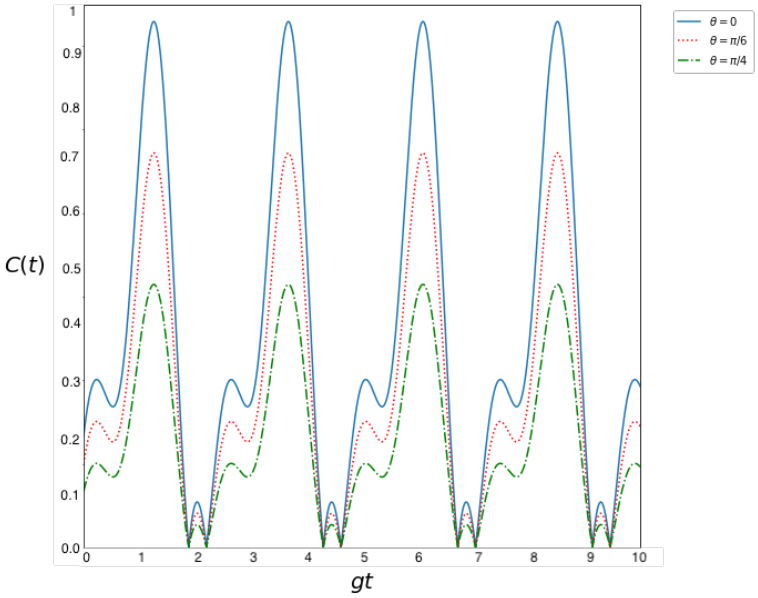

Figure 6.3: **Concurrence C(t)** measure between the flux Qubit C and NVE at a tunable coupling of $J = 2.4g$ with $\theta = 0, \pi/6, \pi/4$.

Figure 6.3 shows the time evolution of the concurrence of the flux qubit C and the NVE.The periodic time of the concurrence of Qubit C and NVE is $\frac{2\pi}{\sqrt{g^2+J^2}}$.It can be seen that for different θ the oscillation frequency of the entanglement remains the same. Increasing the initial entanglement degree from $\theta = 0$, the entanglement gets smaller this is only for a bipartite system. The concurrence measures the degree of entanglement of a system. A maximal entangled state of the flux Qubit C and the NVE can be can be obtained from the concurrence Eq. (6.18) and takes the following form $|\Psi(t)\rangle = \frac{1}{\sqrt{2}}(|1\rangle_C |0\rangle_{NV} + |0\rangle_C |1\rangle_{NV})$. The initial paper [31] did not address whether the degree of entanglement has an influence or not on the quantum memory unit(NV ensemble) and the computing unit(Qubit C). This question can possibly be addressed by a study on whether current preferred geometry of the hybrid quantum system does influence the degree of entanglement within a bipartite system.

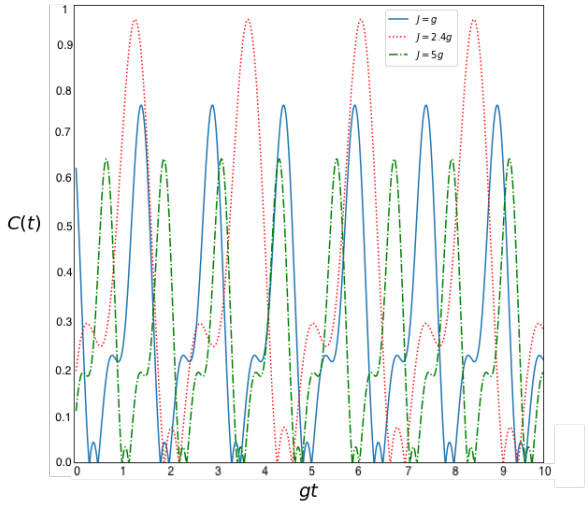

Figure 6.4: **Concurrence C(t)** measure between the flux Qubit C and NVE at $\theta = 0$ with $J = g, 2.4g, 5g$.

In Figure 6.4 the periodic time of the flux Qubit C and NVE is $\frac{2\pi}{\sqrt{g^2+J^2}}$.By keeping the coupling strength g between the NVE and flux Qubit C fixed, the oscillation frequency becomes larger with the increase of the coupling strength J this is because the exchange of energy between the flux Qubit C and NVE becomes faster with the increase of the coupling strength. The amount of entanglement is firstly increased and then decreased with the increase of the coupling strength J . In this case the amount entanglement can be controlled by adjusting the coupling strength J and g.

In Figure 6.5, the oscillation frequency of the flux Qubit M and the NVE does not change. With the increase of the initial entanglement degree of the flux Qubit C , the amount of entanglement is smaller. At initial entanglement degree $\theta = 0$ we have a maxima, a maximally entangled state $|\Psi(t)\rangle = \frac{1}{\sqrt{2}}(|1\rangle_M |0\rangle_{NV} + |0\rangle_M |1\rangle_{NV})$.

Increasing the coupling strength J in Figure 6.6, the exchange of energy between the flux qubit M and the NVE becomes faster contributing to the increase of the oscillation frequency. The amount of entanglement is firstly increased then decreased. At a coupling strength J= $1.42g$ the maxima can be achieved implying that by changing the magnetic field we can effectively control and manipulate the entanglement between the flux qubit M and NVE.

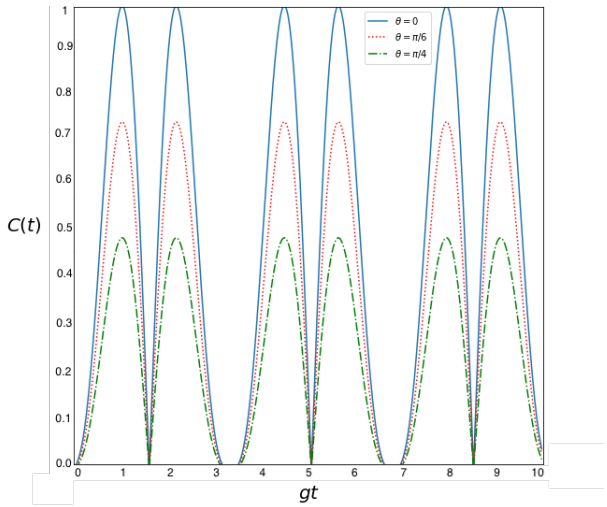

Figure 6.5: **Concurrence C(t)** measure between the flux Qubit M and NVE at a tunable coupling of $J = 1.42g$ with $\theta = 0, \pi/6, \pi/4$.

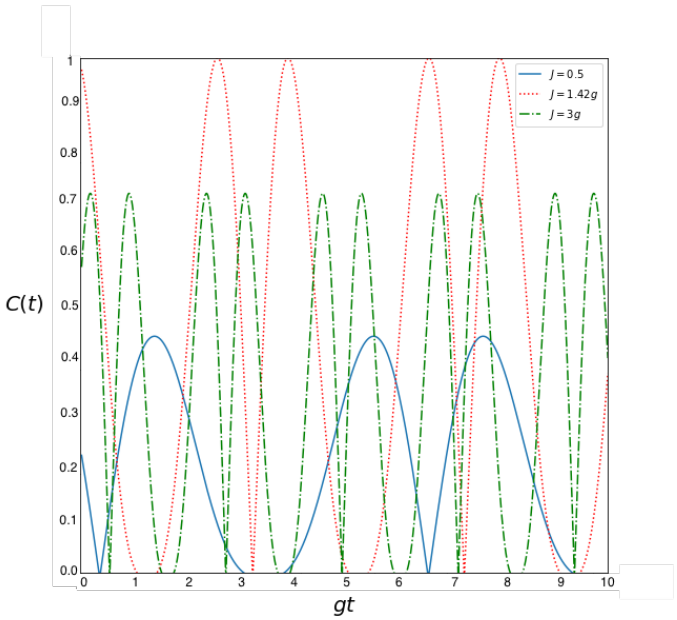

Figure 6.6: **Concurrence C(t)** measure between the flux Qubit M at $\theta = 0$ with $J = 0.5g, 1.42g, 3g$.

Three-tangle - Without Dissipation

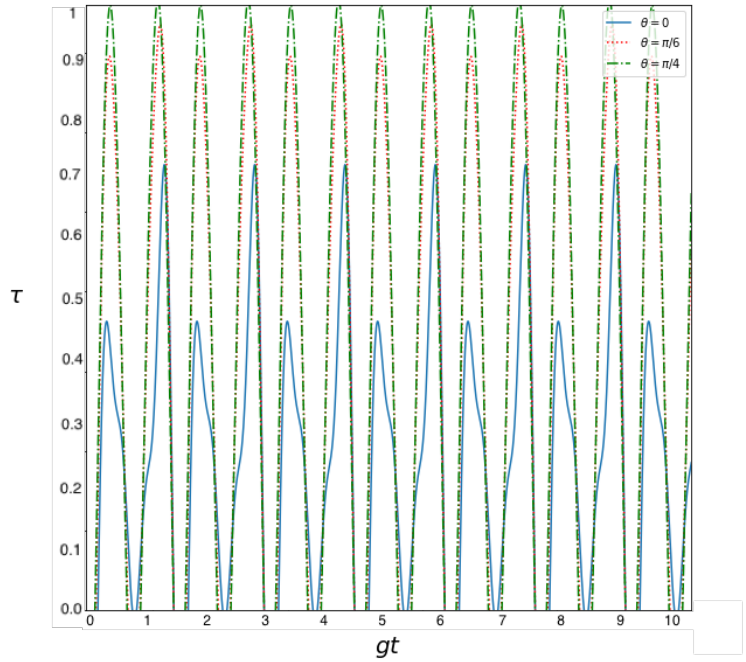

Figure 6.7: **Three-tangle** τ measure between the flux Qubit C, flux Qubit M and NVE at a tunable coupling of $J = 2.4g$ with $\theta = 0, \pi/6, \pi/4$.

In Figure 6.7 we show the time evolution of the three-tangle measure of the flux Qubit M, flux Qubit C and the NVE at the coupling strength $J = 2.4g$ for entanglement degree $\theta \in [0, \pi/6, \pi/4]$. The three-tangle is of a periodic function with period $T = 2\pi/\sqrt{g^2 + J^2}$ and an invariable oscillation frequency between the entanglement degrees. By increasing the initial entanglement degree of flux Qubit C the residual entanglement of the system gets larger. Maximum three-tangle of the flux is achieved with entanglement degree $\theta = \pi/4$.

Keeping the entanglement degree $\theta = 0$ and varying the coupling strengths J in Figure 6.8 results in the oscillation frequency that varies rapidly for $J = 5g$, increasing the coupling J results in the oscillation frequency becoming smaller and decreased residual tangle of the three-qubit system. We have kept the coupling g constant during the system's evolution.

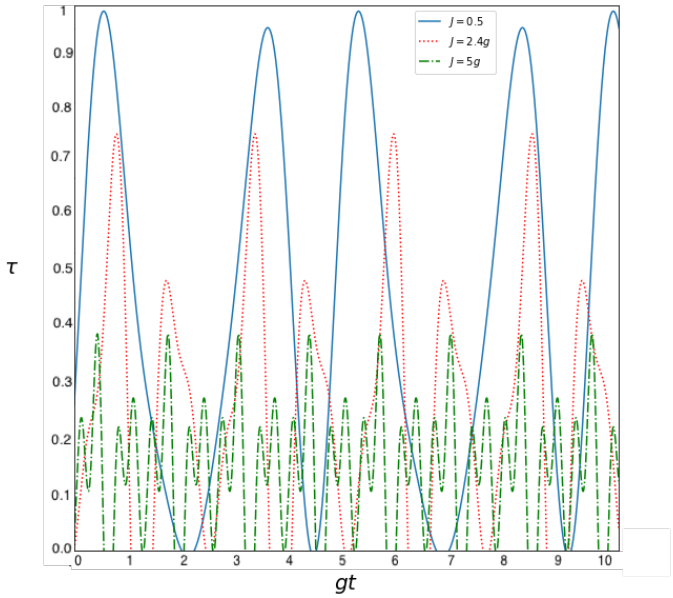

Figure 6.8: **Three-tangle** τ measure between the flux Qubit C, flux Qubit M and NVE at an entanglement degree $\theta = 0$ with $J = 0.5g, 2.4g, 5g$

Bipartite and Residual Entanglement - With Dissipation

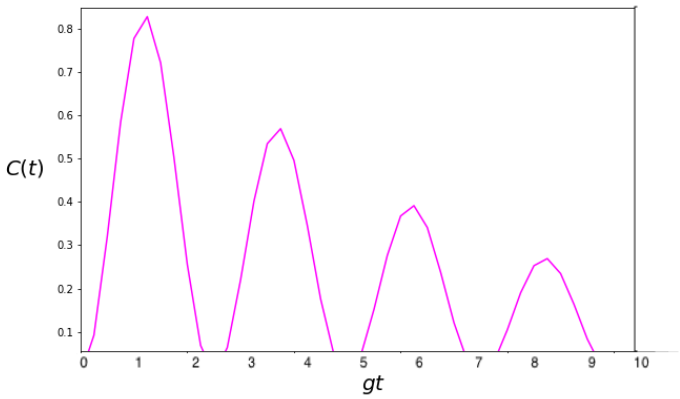

Figure 6.9: **Concurrence C(t)** measure of the flux qubit C and NVE at a tunable coupling of $J = 2.4g$

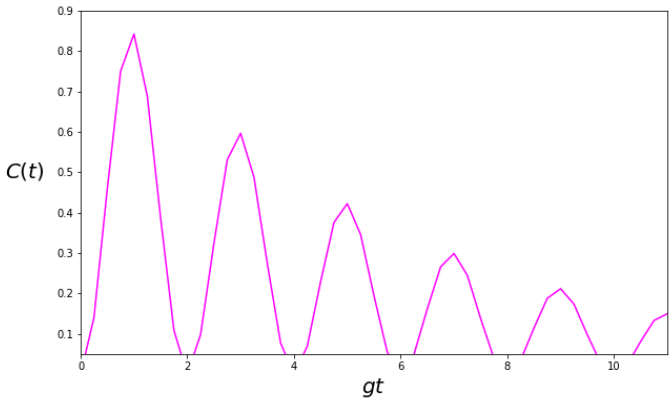

Figure 6.10: **Concurrence C(t)** measure of the flux qubit M and NVE at a tunable coupling of $J = 1.42g$, decay rate $\gamma_M = 0.8$G

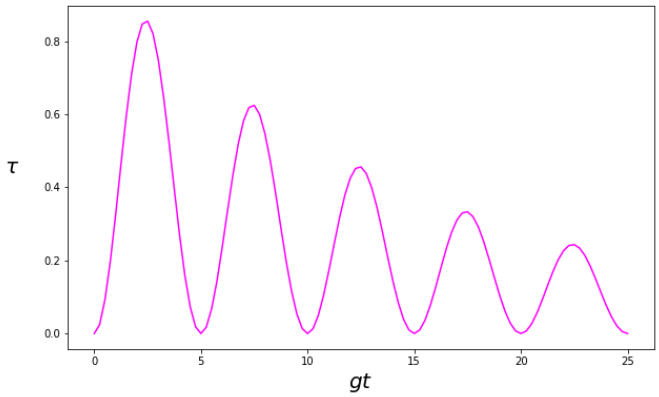

Figure 6.11: **Three-tangle** measure of the flux qubit C, flux qubit M and NVE at a tunable coupling of $J = 3g$ and decay rates $\gamma_C = 0.5$g, γ_M=0.5g

The bipartite entanglement of the flux Qubit C and NVE is evolved in presence of dissipation. Shown in Figure 6.9 is the concurrence of the flux Qubit C and NVE for the decay rate $\gamma_C = 0.3g$. For $\theta = 0$ the concurrence follows the time evolution of a typical dissipative dynamical system with the periodic oscillations in Figure 6.3 now decreasing and tending to zero with the entanglement between the flux qubit C and NVE decreasing over time.

Figure 6.10 shows the time evolution of the concurrence of the flux Qubit M and NVE under dissipation with the tunable coupling $J = 1.42g$ and at $\theta = 0$. Comparison with Figure 6.5 the decay rate γ_M affects the frequency oscillations and thus weaken the rapid decay of the entanglement this is known as the sudden death effect. The entanglement strength tends to zero. There is also not much difference between the concurrence measure of the flux Qubit C with NVE and flux Qubit M with NVE under dissipation for different decay rates between the two. The reason for this is because of the similar design and structure the superconducting flux qubits.

We lastly measure the residual entanglement under dissipation of the system. In Figure 6.11 the oscillation frequency decreases and eventually tends to zero for the coupling strength $J = 3g$ and decay rates $\gamma_C = 0.5g, \gamma_M = 0.5g$. Three-tangle measure decreases compared with the ideal case where constant frequency oscillations were observed and thus the entanglement did not change over time.

6.1.3 Conclusion

In this section we calculated and analysed concurrence as a quantifiable measure of entanglement of quantum systems including hybrid ones. From entanglement dynamics we are able to construct quantum systems that are suitable for quantum information processes. It is where in the next section we will use entanglement measures of the flux qubits and NVE to generate squeezed states of NVE, we will be specifically looking at an entangled squeezed state with the modes of the resonator, since we know how qubits are entangled with spin ensembles we therefore can investigate those with bosonic modes and perform another form of entanglement measure through what is known as logarithmic negavitity.

6.2 Single-mode squeezed state of NVE coupled to resonator

We propose a method of generating a single-mode squeezed state of an NVE coupled to transmission line resonator (TLR) through a flux qubit (Figure 6.12a,b). External driving field is applied to induce the Raman transitions of the groundstate of the NVE and the dissipative process allows the resonator to be entangled with the NVE state and thus generate a squeezed state of the NVE.

6.2.1 Model

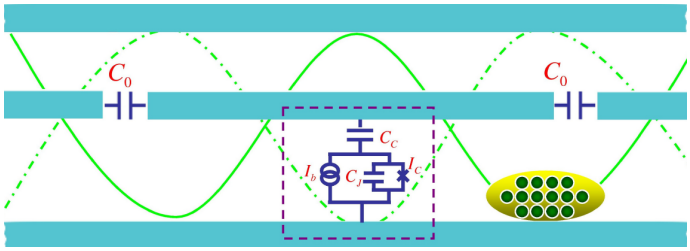

(a)

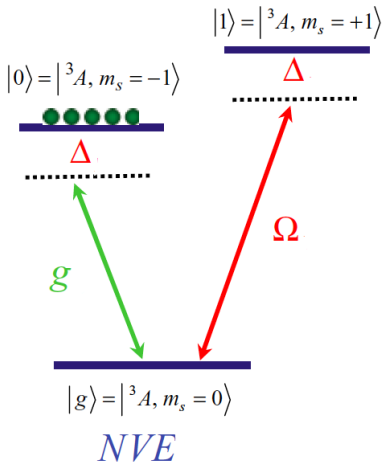

(b)

Figure 6.12: (a) **Schematic** of the CBJJ qubit and NVE coupled to the transmission line resonator (TLR) [76]. (b) **The NVE** level structure consisting of the groundstate and first two excited states with vacuum Rabi frequency g, driving field Ω and detuning δ [83].

The TLR is made of conductors with lateral ground plates of capacitance C and evenly distributed inductor L with the model Hamiltonian given by

$$H_{RES} = \frac{1}{2}\omega_r \hat{a}^\dagger \hat{a}, \tag{6.29}$$

where $\omega_r = \frac{2\pi}{\sqrt{LC}}$.

The current-biased Josephson junction (CBJJ) qubit model Hamiltonian is given by

$$H_Q = \frac{1}{2}\omega_q \hat{\sigma}_z. \tag{6.30}$$

Figure 6.12b shows the energy level structure of the NVE. It has a groundstate that is a spin triplet $|m_s = 0, \pm 1\rangle$ with degenerate sublevels $|m_s = \pm 1\rangle$. By inducing an energy splitting $D_B = \chi_e |B_{ex}|$ brought by an external magnetic field B_e, the degeneracy of the levels can be lifted resulting in in the three level system $|m_s = 0\rangle \equiv |g\rangle$, $|m_s = -1\rangle \equiv |0\rangle$ and $|m_s = +1\rangle \equiv |1\rangle$. The model Hamiltonian governing a single NVE center is given by,

$$H_{NVE} = \sum_{j=1}^{N} \omega_0 \left|g\right\rangle_j \left\langle g\right| + \omega_g \left|0\right\rangle_j \left\langle 0\right| + \omega_e \left|1\right\rangle_j \left\langle 1\right|, \tag{6.31}$$

where j denotes the jth NV center in the NVE.

The total Hamiltonian describing the hybrid quantum system is

$$H_T = H_0 + H_I, \tag{6.32}$$

with

$$\begin{aligned} H_0 &= H_Q + H_{RES} + H_{NVE}. \\ H_I &= \sum_{i=1}^{N} \left[\frac{g^2}{\Delta} \hat{a}^\dagger \hat{a} \left|0\right\rangle_i \left\langle 0\right|_i + \frac{\Omega^2}{4\Delta} \left|1\right\rangle_i \left\langle 1\right|_i + \frac{\Omega g \hat{a}^\dagger}{2\Delta} \left|0\right\rangle_i \left\langle 1\right|_i + H.c \right], \end{aligned} \tag{6.33}$$

where Ω is the Rabi frequency with of the driving field and Δ is the detuning. H_I describes the interaction of the NV centers with the resonator mode in an interaction picture.

We use the Holstein-Primakoff transformation [84–86] to map the collective spin operator $\hat{S}^{\pm}$ into boson operators $\hat{b}^\dagger \hat{b}$,

$$\begin{aligned} \hat{S}^\dagger &= \hat{b}^\dagger \sqrt{N - \hat{b}^\dagger \hat{b}} \simeq \sqrt{N} \hat{b}^\dagger, \\ \hat{S}^- &= \hat{b} \sqrt{N - \hat{b}^\dagger \hat{b}} \simeq \sqrt{N} \hat{b}, \\ \hat{S}^z &= \left(\hat{b}^\dagger \hat{b} - \frac{N}{2} \right). \end{aligned} \tag{6.34}$$

Applying the above transformations and neglecting the constant energy terms in H_I we have the effective Hamiltonian to be

$$H_{eff} = \sqrt{N} \frac{\Omega g}{2\Delta} \left(\hat{a}^\dagger \hat{b} + \hat{a} \hat{b}^\dagger \right) + H.c. \tag{6.35}$$

Single-mode squeezed states can be generated from the entangled bosonic mode b in the NVE with the TLR. Due to imperfections of the cavity we take into account the resonator photon decay by evolving the density matrix ρ through the master equation

$$\frac{d\rho}{dt} = -i[H_{eff}, \rho] + \kappa D[a]\rho, \tag{6.36}$$

where $D[\hat{O}]\rho = 2\hat{O}\rho\hat{O}^\dagger - \hat{O}^\dagger\hat{O}\rho - \rho\hat{O}^\dagger\hat{O}$, κ is the decay rate of the resonator. We define a unitary squeezing operator $\hat{S}(z) = e^{(z\hat{a}^2 - z\hat{a}^{\dagger 2})}$ where $z = \arctan\zeta$ is the squeezing parameter. Under the action of this transformation the density operator transforms as

$$\tilde{\rho} = \hat{S}^\dagger(z)\rho\hat{S}(z). \tag{6.37}$$

After the transformation $\hat{S}$ is applied, the master equation (Eq. (6.36)) becomes

$$\frac{d\tilde{\rho}}{dt} = -i[\tilde{H}_{eff}, \rho] + \kappa D[\hat{a}]\tilde{\rho}. \tag{6.38}$$

For any dissipative dynamical process it will eventually reach a stationary state where $\frac{d\tilde{\rho}}{dt} = 0$. The stationary states of the resonator and NVE are represneted by $|\psi\rangle = |\varphi\rangle \otimes |\phi\rangle$, where $|\varphi\rangle$ is that of NVE and $|\phi\rangle$ is of the resonator. Both states are in a vacuum state. We thus have the stationary state of the total system to be

$$|\Psi\rangle_S = e^{(z\hat{a}^2 - z\hat{a}^{\dagger 2})}\,|0\rangle_{NVE} \otimes |0\rangle_{RES} \tag{6.39}$$

Eq. (6.39) represents the single-mode squeeze state of the collective excitations of the NVE generated by the resonator decay.

To analyze the squeezed state of the NVE we define the position and momentum quadrature operators

$$\begin{aligned} X &= \frac{1}{\sqrt{2}}(\hat{b} + \hat{b}^\dagger), \\ P &= \frac{1}{i\sqrt{2}}(\hat{b} - \hat{b}^\dagger). \end{aligned} \tag{6.40}$$

We investigate the time evolution of the variance of the system in presence and absence of the decay rate of the spin ensemble (NVE) and the collective coupling strength in the Results section.

6.2.2 Results and Discussion

To quantify the single-mode squeeze state of the NVE we analyze the variance, $\langle(\Delta X)^2 + (\Delta P)^2\rangle$ as the function of κt in Figure 6.13 with decay rates of the spin ensemble γ. We assume that the system is in the initial groundstate $|0\rangle_{NVE} \otimes |0\rangle_{RES}$. In lack of the decay of NVE, the Variance deviates from the ideal case at $t < 1$. In presence of the decay rate $\gamma = 0.1\kappa$ the ideal case is achieved for a squeezed state. From the squeezing parameter $z = \arctan\zeta$ with $\zeta = 0.4$ and $z = 1.01$ the squeezing degree becomes 4.25 dB tuned by the external driving field Ω. We can measure the squeezing degree to a larger amount by adjusting or varying the Ω parameter from 0.4 to 0.520.

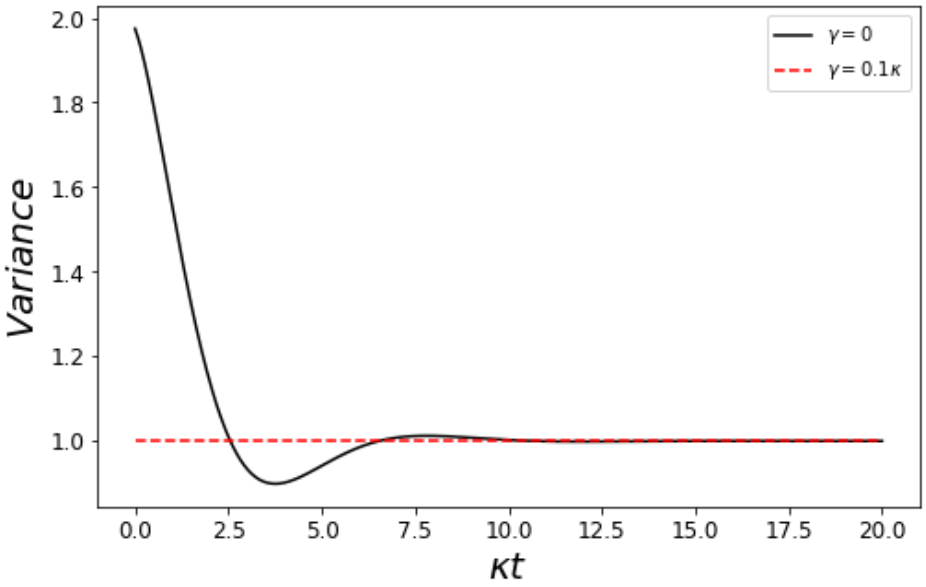

Figure 6.13: **Time evolution of Variance** $\langle(\Delta X)^2 + (\Delta P)^2\rangle$ as a function of κt for the NVE decay rate $\gamma = 0, 0.1$.

For various values of the decay rate κ of the transmission line resonator (TLR) we plot the variance of the system as a function of time in Figure 6.14. The variance is less than the value 2.5 satisfying the entanglement criterion [87] for the system. We take note that when κ is a unit value, one of the respective interactions of Hamiltonian H (Eq. (6.35)) takes importance, namely the parametric amplification. We can conclude that the entangled state does not stay for a long period at most $t < 1.5$. By introducing a parametric amplification mechanism we expect the degeneracy of the eigenstates of the effective Hamiltonian (Eq. (6.35)) to be represented by the dotted dashed thin curves in the Figure 6.14. Essentially these will be the polaritons brought by the Holstein-Primakoff transformation that was mentioned above.

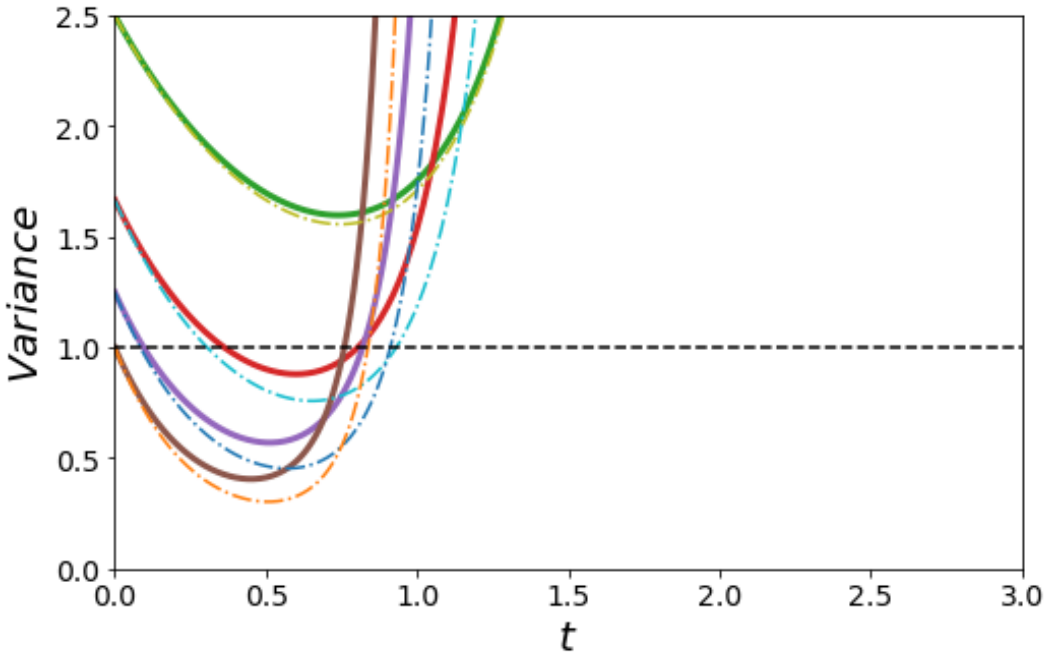

Figure 6.14: **Variance** $\langle(\Delta X)^2 + (\Delta P)^2\rangle$ as a function of t for the resonator decay rates $\kappa = 0.2, 0.4, 0.6, 0.8$.

In Figure 6.15 we plot the effect of two dynamic processes on the entangled squeeze state of NVE. Two of these dynamics include the collective excitation of NVE, (purple curve) and the other of local excitation (blue dashed curve) for the initial state $|0\rangle_{NVE} \otimes |0\rangle_{RES}$. In both cases, we see that the maximally entangled squeezed state of NVE (thin curve) can be obtained under the parametric amplification mechanism and a larger entangled state time for such a state (thick curves). This is in accordance with a study performed in [88] and [89].

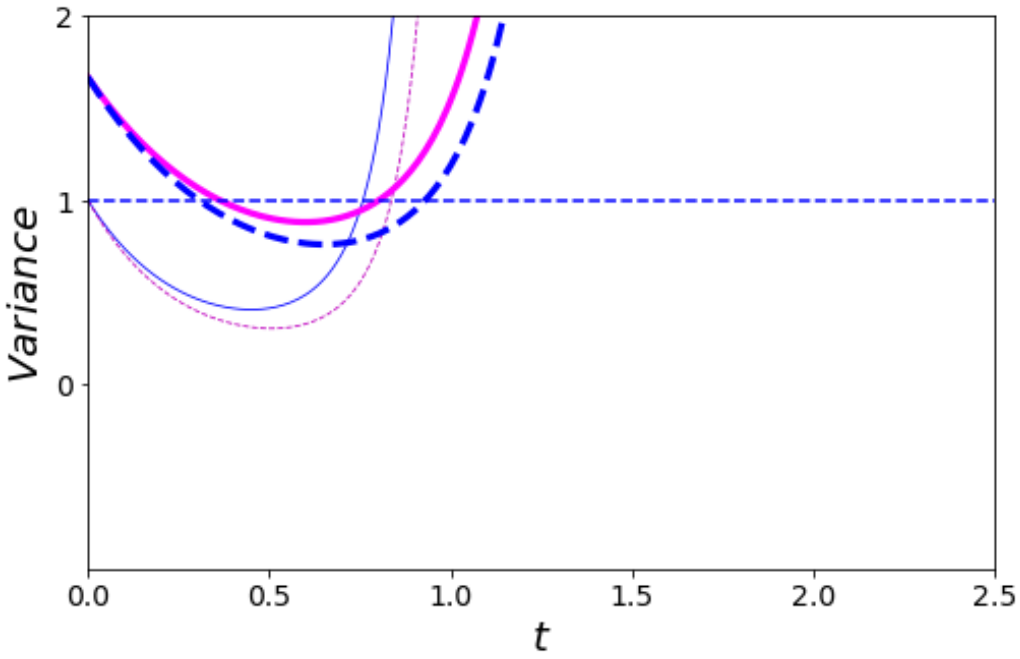

Figure 6.15: **Time evolution of the Variance** $\langle(\Delta X)^2 + (\Delta P)^2\rangle$ as a function of time for two different dynamical processes of the NVE.

Logarithmic Negativity

We introduce and compute another quantifiable measure of entanglement - logarithmic negativity defined as $L_N = \log ||\rho||$ [90] where ρ is the density matrix of the total system. In Figure 6.16, 6.17 we show that the time evolution of L_N of the NVE with two different decay rates γ. In the first figure the standard negativity is observed when the system is driven by a constant field Ω, in absence of the dissipation in the spin ensemble the logarithmic negativity takes a constant 0.60 value, the highest entangled state. For $\gamma = 0.1\kappa$ the logarithmic negativity shows an unentangled squeeze state of the NVE.

For a single collective excitation process the L_N takes a value below zero in the ideal case and -1.0 for $\gamma = 0.1\kappa$ shown in Figure 6.17. Similar with the collective excitation in Figure 6.16 there is emergence of distinct dynamical processes happening when dissipation of the spin ensemble is turned on.

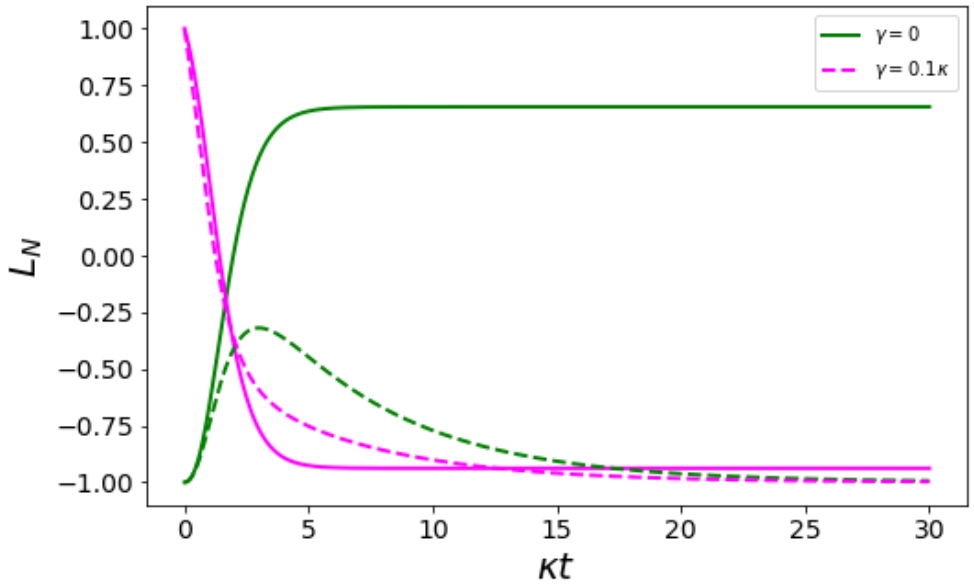

Figure 6.16: **Logarithmic negativity** L_N as a function of time for the decay rates $\gamma = 0, \gamma = 0.1\kappa$ of the NVE through the collective excitation of the spin ensemble.

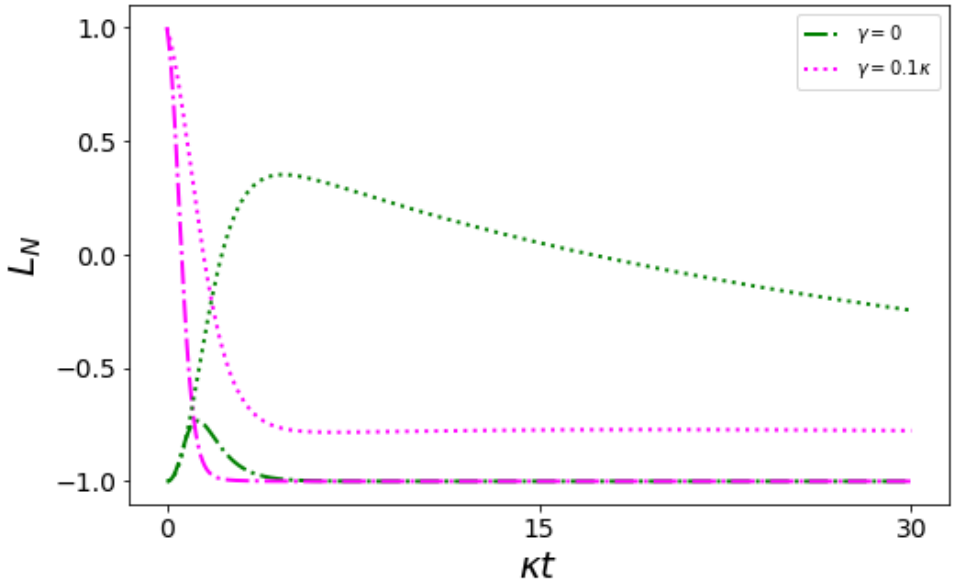

Figure 6.17: **Logarithmic negativity** L_N as a function of time for the decay rates $\gamma = 0, \gamma = 0.1\kappa$ of the NVE through a single excitation of the spin ensemble.

6.2.3 Conclusion

We have studied the generation of single-mode squeezed states of spin ensemble (NVE) in a hybrid system consisting of a qubit, transmission line resonator and NVE. The dissipation of the resonator is used to realize a single-mode squeeze state through the dissipative dynamical process at hand. We note that two of these processes were in effect and as a result influenced the degree of produced by the amount and period of the entangled squeezed state produced. The current model is in line with experimental feasibility as well as design scalability.

Chapter 7

Conclusion

The rudimentary single-mode generation of squeezed states of NVE is the first step towards hybrid quantum systems being used in quantum information applications especially within circuit QED systems. By capturing the full dissipative dynamics in a single qubit-cavity system we are then able to scale that up to lattice cavities thus simulating many-body interaction physics. The dissipativeness of quantum systems is a resource in the developments of quantum states used in quantum computing and quantum information processing. Dissipative processes capture the full information that a quantum system has whether this is loss of information to reservoir or environment or whether feedback to the system of interest as it can influence the outcomes of the measurements, hence the motivation to do a formal derivation of the JC model in this thesis. We were able to show the generation of exotic quantum states known as squeezed states by solving the the time-convolutionless master equation in a dissipating atom-cavity system. The basic light-matter interaction Hamiltonian of the Jaynes-Cummings model and the use of open quantum system dynamics enables us to reproduce these fundamental states of quantum mechanics.

Advancements in the field of experimental design of superconducting qubits meant that different quantum systems can be tested for their coherence and effective use in quantum information processing. The once unsolvable Rabi model Hamiltonian forms the basis of generating squeezed states of light under the protocol presented in this work. By applying a mathematical transformation onto the original Rabi Hamiltonian and limiting the interaction of atom (qubit) with the light field to a dispersive regime where the detuning is much greater than the coupling between the atom and the cavity ($\Delta >> g$), we were able to construct a protocol that generates squeezed states of light in a cavity system. We simulated the process and analyzed the exact measurements such as frequency shifts in the scheme that indicate the degree of squeezing produced. This work was prompted by the possible full experimental implementation of the frequency based qubit flips protocol presented because it suffers less decoherence of the qubits and noise as compared with squeezing generation experiments in literature [65, 66].

To realize quantum computing or better yet perform quantum mechanical simulations a need for an architecture that hosts individual components of quantum systems is required. Quantum circuits offer the ability to realize computation of hybrid quantum systems. Using superconducting qubits together with microwave bus resonators a basic computing system is produced. However, many research studies have indicated that basic circuit components of quantum systems including only qubits and resonators suffer from decoherence and memory loss. The solution to this is the incorporation of spin systems in the circuit structure because of the amazing properties of the spin systems. Since entanglement is crucial to every quantum system that is based on communication with subsystems we then studied all possible entanglement dynamics that a quantum system will possess. Out of this beautiful mathematics emerge the density matrices that we used to describe the measure of entanglement through concurrence. Through bipartite and residual entanglement measurements we were able to reveal the behaviour of a real quantum circuit made up of multi-partite entangled quantum systems

Squeezed states of light being the theme of this thesis we incorporate them in a hybrid quantum system through the generation of single-mode squeeze state of the spin ensemble (NVE). This is a novel technique that requires a mathematical transformation of the interacting Hamiltonian of the flux qubit, transmission line resonator (TLR) and the NVE provided necessary framework to realize squeezed states of the NVE in a form of an entangled state with the resonator (bosonic) mode. Even though most of the results showed a short lived entangled squeeze state of the NVE, a much longer lived state would put the above scheme out of the confines of experimental implementation and realization although Ref [91] have taken a similar approach.

Some of the simulations in this thesis especially those of dissipative processes and systems were based on an open quantum system software tool called QuTiP [92]. At the heart of the software is quantum object called Qobj representing quantum objects such as states and operators. We higly recommend this tool for any open or closed quantum systems work.

The goal of this thesis is to provide elementary introduction to simulations of condensed matter models. From this work simulations on models such as the Dicke Model, Anderson Model and the famous Kondo Problem Model [19] on many-body physics can be implemented. In fact, it was the initial study and interest in the Dicke Model that motivated the study of the Jaynes-Cummings physics and its applications in the field of quantum information processing. Our group at the Nano-Scale Transport Physics Laboratory (NSTPL) is currently working on the study of quantum phase transitions that occur in spin-boson systems [93, 94] this also includes the simulation of the Jaynes-Cummings lattice [18]. This theoretical work should culminate in a practical quantum device that emulates these systems as part of the quantum technology research of the group.

Digital quantum simulations of circuit QED are gaining attention from researchers [95] with a major study conducted on the weak localization phenomena [96]. Digital quantum simulation is now very much possible to implement thanks to devices made available by IBM, Rigetti, Alibaba and others online. The IBM Q flagship project has availed various quantum device architectures which are open for access by researchers and quantum enthusiasts. The future research direction of my work will entail using software such as these to study and digitise quantum phase transitions in spin systems as these platforms will offer the ability to first test models/ algorithms on real quantum system on the cloud before experimentally being carried out.

References

1. Feynman, R. P. Simulating physics with computers. *International journal of theoretical physics* **21,** 467–488 (1982).
2. Las Heras, U. *Digital quantum simulations of spin models in superconducting circuits* PhD thesis (Master's thesis, University of the Basque Country, 2013).
3. Georgescu, I. M., Ashhab, S. & Nori, F. Quantum simulation. *Reviews of Modern Physics* **86,** 153 (2014).
4. Schumacher, B. Quantum coding. *Physical Review A* **51,** 2738 (1995).
5. Weimer, H., Müller, M., Lesanovsky, I., Zoller, P. & Büchler, H. P. A Rydberg quantum simulator. *Nature Physics* **6,** 382 (2010).
6. Blatt, R. & Wineland, D. Entangled states of trapped atomic ions. *Nature* **453,** 1008 (2008).
7. Li, Z. *et al.* Solving quantum ground-state problems with nuclear magnetic resonance. *Scientific reports* **1,** 88 (2011).
8. Peng, X.-h. & Suter, D. Spin qubits for quantum simulations. *Frontiers of physics in China* **5,** 1–25 (2010).
9. Hanson, R. & Awschalom, D. D. Coherent manipulation of single spins in semiconductors. *Nature* **453,** 1043 (2008).
10. Imamog, A. *et al.* Quantum information processing using quantum dot spins and cavity QED. *Physical review letters* **83,** 4204 (1999).
11. Fink, J. *et al.* Climbing the Jaynes–Cummings ladder and observing its nonlinearity in a cavity QED system. *Nature* **454,** 315 (2008).
12. Ashhab, S. *et al.* Interqubit coupling mediated by a high-excitation-energy quantum object. *Physical Review B* **77,** 014510 (2008).
13. You, J. & Nori, F. Superconducting circuits and quantum information. *arXiv preprint quant-ph/0601121* (2006).
14. Clarke, J. & Wilhelm, F. K. Superconducting quantum bits. *Nature* **453,** 1031 (2008).
15. Bardeen, J., Cooper, L. N. & Schrieffer, J. R. Theory of superconductivity. *Physical review* **108,** 1175 (1957).
16. Lloyd, S. Universal quantum simulators. *Science,* 1073–1078 (1996).
17. Houck, A. A., Türeci, H. E. & Koch, J. On-chip quantum simulation with superconducting circuits. *Nature Physics* **8,** 292 (2012).

18. Koch, J., Houck, A. A., Le Hur, K. & Girvin, S. Time-reversal-symmetry breaking in circuit-QED-based photon lattices. *Physical Review A* **82,** 043811 (2010).

19. Garcıa-Ripoll, J. J., Solano, E. & Martin-Delgado, M. A. Quantum simulation of Anderson and Kondo lattices with superconducting qubits. *Physical Review B* **77,** 024522 (2008).

20. Yang, X.-C., Zhang, D.-W., Xu, P., Yu, Y. & Zhu, S.-L. Simulating the dynamical quantum Hall effect with superconducting qubits. *Physical Review A* **91,** 022303 (2015).

21. Buluta, I., Ashhab, S. & Nori, F. Natural and artificial atoms for quantum computation. *Reports on Progress in Physics* **74,** 104401 (2011).

22. Ladd, T. D. *et al.* Quantum computers. *Nature* **464,** 45 (2010).

23. Zoubi, H. & Ritsch, H. Hybrid quantum system of a nanofiber mode coupled to two chains of optically trapped atoms. *New Journal of Physics* **12,** 103014 (2010).

24. Walls, D. F. Squeezed states of light. *nature* **306,** 141 (1983).

25. Kennard, E. H. Zur quantenmechanik einfacher bewegungstypen. *Zeitschrift für Physik* **44,** 326–352 (1927).

26. Shore, B. W. & Knight, P. L. The jaynes-cummings model. *Journal of Modern Optics* **40,** 1195–1238 (1993).

27. Dicke, R. H. Coherence in spontaneous radiation processes. *Physical review* **93,** 99 (1954).

28. Zou, H.-M. & Fang, M.-F. Squeezing of light field in a dissipative Jaynes–Cummings model. *Journal of Modern Optics* **63,** 2279–2284 (2016).

29. Joshi, C., Irish, E. K. & Spiller, T. P. Qubit-flip-induced cavity mode squeezing in the strong dispersive regime of the quantum Rabi model. *Scientific reports* **7,** 45587 (2017).

30. Wallraff, A. *et al.* Approaching unit visibility for control of a superconducting qubit with dispersive readout. *Physical review letters* **95,** 060501 (2005).

31. Liao, Q., Chen, L., Liu, X. & Zhou, N. Properties of hybrid entanglement among two flux qubits and a nitrogen-vacancy-center ensemble. *Laser Physics* **28,** 085204 (2018).

32. Jaynes, E. T. & Cummings, F. W. Comparison of quantum and semiclassical radiation theories with application to the beam maser. *Proceedings of the IEEE* **51,** 89–109 (1963).

33. Rempe, G., Walther, H. & Klein, N. Observation of quantum collapse and revival in a one-atom maser. *Physical review letters* **58,** 353 (1987).

34. Xie, Q., Zhong, H., Batchelor, M. T. & Lee, C. The quantum Rabi model: solution and dynamics. *Journal of Physics A: Mathematical and Theoretical* **50,** 113001 (2017).

35. Gerry, C., Knight, P. & Knight, P. L. *Introductory quantum optics* (Cambridge university press, 2005).

36. Kossakowski, A. On quantum statistical mechanics of non-Hamiltonian systems. *Reports on Mathematical Physics* **3,** 247–274 (1972).

37. Krämer, S., Plankensteiner, D., Ostermann, L. & Ritsch, H. QuantumOptics. jl: A Julia framework for simulating open quantum systems. *Computer Physics Communications* **227,** 109–116 (2018).

38. Nazir, A. *Lecture notes on open quantum systems* 2013.

39. Breuer, H.-P., Petruccione, F., *et al. The theory of open quantum systems* (Oxford University Press on Demand, 2002).

40. Slusher, R., Hollberg, L., Yurke, B., Mertz, J. & Valley, J. Observation of squeezed states generated by four-wave mixing in an optical cavity. *Physical Review Letters* **55,** 2409 (1985).

41. Loudon, R. & Knight, P. L. Squeezed light. *Journal of modern optics* **34,** 709–759 (1987).

42. Kurochkin, Y., Prasad, A. S. & Lvovsky, A. Distillation of the two-mode squeezed state. *Physical review letters* **112,** 070402 (2014).

43. Andersen, U. L., Gehring, T., Marquardt, C. & Leuchs, G. 30 years of squeezed light generation. *Physica Scripta* **91,** 053001 (2016).

44. Braunstein, S. L. & Van Loock, P. Quantum information with continuous variables. *Reviews of Modern Physics* **77,** 513 (2005).

45. Gu, M., Weedbrook, C., Menicucci, N. C., Ralph, T. C. & van Loock, P. Quantum computing with continuous-variable clusters. *Physical Review A* **79,** 062318 (2009).

46. Zhang, Z. & Duan, L. Quantum metrology with Dicke squeezed states. *New Journal of Physics* **16,** 103037 (2014).

47. Mehmet, M., Vahlbruch, H., Lastzka, N., Danzmann, K. & Schnabel, R. Observation of squeezed states with strong photon-number oscillations. *Physical Review A* **81,** 013814 (2010).

48. Didier, N., Kamal, A., Oliver, W. D., Blais, A. & Clerk, A. A. Heisenberg-limited qubit read-out with two-mode squeezed light. *Physical review letters* **115,** 093604 (2015).

49. Hong-Mei, Z. & Mao-Fa, F. Population dynamics of excited atoms in non-Markovian environments at zero and finite temperature. *Chinese Physics B* **24,** 080304 (2015).

50. Peng, J.-S. & Li, G.-X. *Introduction to modern quantum optics* (World Scientific, 1998).

51. Blais, A., Huang, R.-S., Wallraff, A., Girvin, S. M. & Schoelkopf, R. J. Cavity quantum electrodynamics for superconducting electrical circuits: An architecture for quantum computation. *Physical Review A* **69,** 062320 (2004).

52. Liu, Y.-x., Wei, L. & Nori, F. Measuring the quality factor of a microwave cavity using superconducting qubit devices. *Physical Review A* **72,** 033818 (2005).

53. Bianchetti, R. *et al.* Dynamics of dispersive single-qubit readout in circuit quantum electrodynamics. *Physical Review A* **80,** 043840 (2009).

54. Wallraff, A. *et al.* Strong coupling of a single photon to a superconducting qubit using circuit quantum electrodynamics. *Nature* **431,** 162 (2004).

55. Walls, D. F. & Milburn, G. J. *Quantum optics* (Springer Science & Business Media, 2007).

56. Janszky, J. & Adam, P. Strong squeezing by repeated frequency jumps. *Physical Review A* **46,** 6091 (1992).

57. Rigetti, C. *et al.* Superconducting qubit in a waveguide cavity with a coherence time approaching 0.1 ms. *Physical Review B* **86,** 100506 (2012).

58. Barends, R. *et al.* Coherent Josephson qubit suitable for scalable quantum integrated circuits. *Physical review letters* **111,** 080502 (2013).

59. Braumüller, J. *et al.* Concentric transmon qubit featuring fast tunability and an anisotropic magnetic dipole moment. *Applied Physics Letters* **108,** 032601 (2016).

60. Yan, F. *et al.* The flux qubit revisited. *arXiv* **1508** (2015).

61. Wilson, C. M. *et al.* Observation of the dynamical Casimir effect in a superconducting circuit. *Nature* **479,** 376 (2011).

62. Matsuo, S., Fujii, T. & Hatakenaka, N. Nonadiabatic squeezed-photon generation by a Fourier-modified Janszky-Adam scheme. *Physica B: Condensed Matter* **468-469,** 57 (2015).

63. Eberle, T. *et al.* Quantum enhancement of the zero-area Sagnac interferometer topology for gravitational wave detection. *Physical review letters* **104,** 251102 (2010).

64. Castellanos-Beltran, M., Irwin, K., Hilton, G., Vale, L. & Lehnert, K. Amplification and squeezing of quantum noise with a tunable Josephson metamaterial. *Nature Physics* **4,** 929 (2008).

65. Taylor, M. A. *et al.* Biological measurement beyond the quantum limit. *Nature Photonics* **7,** 229 (2013).

66. Purdy, T. P., Yu, P.-L., Peterson, R., Kampel, N. & Regal, C. Strong optomechanical squeezing of light. *Physical Review X* **3,** 031012 (2013).

67. Berkley, A. *et al.* Entangled macroscopic quantum states in two superconducting qubits. *Science* **300,** 1548–1550 (2003).

68. Andersen, U. L., Neergaard-Nielsen, J. S., Van Loock, P. & Furusawa, A. Hybrid discrete-and continuous-variable quantum information. *Nature Physics* **11,** 713 (2015).

69. Braunstein, S. L. & Pati, A. K. *Quantum information with continuous variables* (Springer Science & Business Media, 2012).

70. Li, M., Fei, S.-M. & Li-Jost, X. Quantum entanglement: separability, measure, fidelity of teleportation, and distillation. *Advances in Mathematical Physics* **2010** (2010).

71. Nielsen, M. A. & Chuang, I. *Quantum computation and quantum information* (AAPT, 2002).

72. Bennett, C. H., Bernstein, H. J., Popescu, S. & Schumacher, B. Concentrating partial entanglement by local operations. *Physical Review A* **53,** 2046 (1996).

73. Maleki, Y. & Zheltikov, A. M. Generating maximally-path-entangled number states in two spin ensembles coupled to a superconducting flux qubit. *Physical Review A* **97,** 012312 (2018).

74. Xiang, Z.-L., Ashhab, S., You, J. & Nori, F. Hybrid quantum circuits: Superconducting circuits interacting with other quantum systems. *Reviews of Modern Physics* **85,** 623 (2013).

75. Kubo, Y. *et al.* Hybrid quantum circuit with a superconducting qubit coupled to a spin ensemble. *Physical review letters* **107,** 220501 (2011).

76. Yang, W., Yin, Z., Hu, Y., Feng, M. & Du, J. High-fidelity quantum memory using nitrogen-vacancy center ensemble for hybrid quantum computation. *Physical Review A* **84,** 010301 (2011).

77. Bar-Gill, N., Pham, L. M., Jarmola, A., Budker, D. & Walsworth, R. L. Solid-state electronic spin coherence time approaching one second. *Nature communications* **4,** 1743 (2013).

78. Wootters, W. K. Entanglement of formation of an arbitrary state of two qubits. *Physical Review Letters* **80,** 2245 (1998).

79. Wootters, W. K. Quantum entanglement as a quantifiable resource. *Philosophical Transactions of the Royal Society of London. Series A: Mathematical, Physical and Engineering Sciences* **356,** 1717–1731 (1998).

80. Egger, D. J. *et al.* Entanglement generation in superconducting qubits using holonomic operations. *Physical Review Applied* **11,** 014017 (2019).

81. Su, W.-J., Yang, Z.-B. & Zhong, Z.-R. Arbitrary control of entanglement between two nitrogen-vacancy-center ensembles coupling to a superconducting-circuit qubit. *Physical Review A* **97,** 012329 (2018).

82. Wootters, W. K. The rebit three-tangle and its relation to two-qubit entanglement. *Journal of Physics A: Mathematical and Theoretical* **47,** 424037 (2014).

83. Yang, W., Yin, Z., Chen, Q., Chen, C. & Feng, M. Two-mode squeezing of distant nitrogen-vacancy-center ensembles by manipulating the reservoir. *Physical Review A* **85,** 022324 (2012).

84. Holstein, T. & Primakoff, H. Field dependence of the intrinsic domain magnetization of a ferromagnet. *Physical Review* **58,** 1098 (1940).

85. Hammerer, K., Sørensen, A. S. & Polzik, E. S. Quantum interface between light and atomic ensembles. *Reviews of Modern Physics* **82,** 1041 (2010).

86. Chen, G. *et al.* Qubit-induced high-order nonlinear interaction of the polar molecules in a stripline cavity. *Physical Review A* **82,** 013601 (2010).

87. Hillery, M. & Zubairy, M. S. Entanglement conditions for two-mode states. *Physical review letters* **96,** 050503 (2006).

88. Chase, B. A. & Geremia, J. Collective processes of an ensemble of spin-1/ 2 particles. *Physical Review A* **78,** 052101 (2008).

89. Sousa, E. H. & Roversi, J. Selective Engineering for Preparing Entangled Steady States in Cavity QED Setup. *Quantum Reports* **1,** 63–70 (2019).

90. Plenio, M. B. Logarithmic negativity: a full entanglement monotone that is not convex. *Physical review letters* **95,** 090503 (2005).

91. Ma, S.-l., Li, X.-k., Xie, J.-k. & Li, F.-l. Two-mode squeezed states of two separated nitrogen-vacancy-center ensembles coupled via dissipative photons of superconducting resonators. *Physical Review A* **99,** 012325 (2019).

92. Nation, P. D. & Johansson, J. *Qutip: Quantum toolbox in python* (2011).

93. Hur, K. L. Quantum phase transitions in spin-boson systems: Dissipation and light phenomena. *arXiv preprint arXiv:0909.4822* (2009).

94. Le Hur, K. *et al.* Many-body quantum electrodynamics networks: Non-equilibrium condensed matter physics with light. *Comptes Rendus Physique* **17,** 808–835 (2016).

95. Scala, M., Militello, B., Messina, A., Piilo, J. & Maniscalco, S. Microscopic derivation of the Jaynes-Cummings model with cavity losses. *Physical Review A* **75,** 013811 (2007).

96. Chen, Y. *et al.* Emulating weak localization using a solid-state quantum circuit. *Nature communications* **5,** 5184 (2014).

97. Fraleigh, J. B. *A first course in abstract algebra* (Pearson Education India, 2003).

98. Griffiths, D. J. & Schroeter, D. F. *Introduction to quantum mechanics* (Cambridge University Press, 2018).

99. Lavrov, P. M., Radchenko, O. V. & Tyutin, I. V. Jacobi-type identities in algebras and superalgebras. *Theoretical and Mathematical Physics* **179,** 550–558 (2014).

100. McMahon, D. Quantum field theory demystified: A self-teaching guide (2009).

101. Briegel, H.-J. & Englert, B.-G. Quantum optical master equations: The use of damping bases. *Physical Review A* **47,** 3311 (1993).

Appendix A

Commutation relations

Using the following commutation relations [97–100],

$$[AB, CD] = A[B, C]D + [A, C]BD + CA[B, D] + C[A, D]B,$$

we find that

$$\begin{aligned}[\sigma^+\sigma^-, a\sigma^+] &= \sigma^+[\sigma^-, a]\sigma^+ + [\sigma^+, a]\sigma^-\sigma^+ - a\sigma^+[\sigma^-, \sigma^+] + a[\sigma^+, \sigma^+]\sigma^- \\ &= -a\sigma^+[\sigma^-, \sigma^+] \\ &= -a\sigma^+.\end{aligned} \tag{A.1}$$

$$\begin{aligned}[a^\dagger a, a^\dagger\sigma^-] &= a^\dagger[a, a^\dagger]\sigma^- + [a^\dagger, a^\dagger]a\sigma^- + a^\dagger a^\dagger[a, \sigma^-] + a^\dagger[a^\dagger, \sigma^-]a \\ &= a^\dagger[a, a^\dagger]\sigma^- + [a^\dagger, a]a\sigma^- + a^\dagger a^\dagger[a, \sigma^-] + a^\dagger[a^\dagger, \sigma^-]a \\ &= a^\dagger\sigma^-.\end{aligned} \tag{A.2}$$

$$\begin{aligned}[a^\dagger a, a\sigma^+] &= a^\dagger[a, a]\sigma^+ + [a^\dagger, a]a\sigma^+ + aa^\dagger[a, \sigma^+] + a[a^\dagger, \sigma^+]a \\ &= a\sigma^+.\end{aligned} \tag{A.3}$$

$$\begin{aligned}[\sigma^+\sigma^-, a^\dagger\sigma^+] &= \sigma^+[\sigma^-, a^\dagger]\sigma^- + [\sigma^+, a^\dagger]\sigma^-\sigma^- + a^\dagger\sigma^+[\sigma^-, \sigma^-] + a^\dagger[\sigma^+, \sigma^-]\sigma^- \\ &= -a^\dagger\sigma^-.\end{aligned} \tag{A.4}$$

Appendix B

Damping Basis Method

To solve the master equation, Eq. (3.46) we apply the damping basis method [101].

For a master equation

$$\dot{\rho} = \mathcal{L}\rho, \tag{B.1}$$

the corresponding eigenvalue problem

$$\mathcal{L}\rho_\lambda = \lambda\rho_\lambda, \tag{B.2}$$

where $\mathcal{L}$ is the superoperator, ρ is the right eigenoperator with eigenvalue λ. The right eigenoperator ρ_λ constitute a basis set of linear operator that act on the Hilbert space of vectors. So, any state (density operator ρ) can be expanded in terms of this basis

$$\rho(0) = \sum_\lambda c_\lambda \rho_\lambda. \tag{B.3}$$

At time t the initial state $\rho(0)$ will be given by the state

$$\rho(t) = \sum_\lambda c_\lambda e^{\lambda t} \rho_\lambda, \tag{B.4}$$

with the coefficients of expansion given by

$$c_\lambda = Tr\{\check{\rho}_\lambda \rho(0)\}, \tag{B.5}$$

where $\check{\rho}_\lambda$ is the left eigenoperator with eigenvalue equation

$$\check{\rho}_\lambda \mathcal{L} = \lambda \check{\rho}_\lambda. \tag{B.6}$$

For a finite n dimensional Hilbert space $\mathcal{L}$ is represented by an $n^2 \times n^2$ matrix of the right and left eigenoperators. For Eq. (3.46) these left and right eigenoperators are given by the off-diagonal elements of the density matrix ρ in Eq. (3.46) also known as coherences $|E_0\rangle\langle E_{1,+}|, |E_0\rangle\langle E_{1,-}|, |E_{1,-}\rangle\langle E_{1,+}|$ with eigenvalues $i(\omega_0 - \Omega) - \gamma_a/2, i(\omega_0 + \Omega) - \gamma_b/2, i(2\Omega) - (\gamma_a + \gamma_b)/4$. The remaining three right

eigenoperators are given by $|E_0\rangle\langle E_0|, (|E_{1,-}\rangle\langle E_{1,-}| - |E_0\rangle\langle E_0|), (|E_{1,+}\rangle\langle E_{1,+}| - |E_0\rangle\langle E_0|)$ with eigenvalues of $0, -\gamma_a/2$ and $-\gamma_b/2$.

We then expand the initial state with respect to these eigenoperators. The initial state density matrix $\rho(0) = |0e\rangle\langle 0e|$ is defined as

$$\rho(0) = \frac{1}{2}\Big(|E_{1,+}\rangle\langle E_{1,+}| + |E_{1,-}\rangle\langle E_{1,-}| - |E_{1,+}\rangle\langle E_{1,-}| - |E_{1,-}\rangle\langle E_{1,+}| \Big) \tag{B.7}$$

$$= \frac{1}{2}\Big(|E_0\rangle\langle E_0| + |E_{1,+}\rangle\langle E_{1,+}| - |E_0\rangle\langle E_0| + |E_0\rangle\langle E_0| \tag{B.8}$$

$$+ |E_{1,-}\rangle\langle E_{1,-}| - |E_0\rangle\langle E_0| - |E_{1,+}\rangle\langle E_{1,-}| - |E_{1,-}\rangle\langle E_{1,+}| \Big), \tag{B.9}$$

where $|0e\rangle = \frac{1}{\sqrt{2}}\Big(|E_{1,+}\rangle - |E_{1,-}\rangle \Big)$.
At a later time t, using Eq. (B.4), we have that

$$\rho(t) = \Big(1 - \frac{1}{2}e^{\frac{-\gamma_a}{2}t} - \frac{1}{2}e^{\frac{-\gamma_b}{2}t}\Big)|E_0\rangle\langle E_0| \tag{B.10}$$

$$+ \frac{1}{2}e^{\frac{-\gamma_a}{2}t}|E_{1,-}\rangle\langle E_{1,-}| + \frac{1}{2}e^{\frac{-\gamma_b}{2}t}|E_{1,+}\rangle\langle E_{1,+}| \tag{B.11}$$

$$- \frac{1}{2}e^{\frac{-\gamma_a+\gamma_b}{4}t}\Big(e^{2igt}|E_{1,-}\rangle\langle E_{1,+}| + H.c\Big). \tag{B.12}$$

The population of the ground states given in Eq. (3.49) can now be determined where,

$$\langle 0g|\rho(t)|0g\rangle = 1 - \frac{1}{2}e^{\frac{-\gamma_a}{2}t} - \frac{1}{2}e^{\frac{-\gamma_b}{2}t}, \tag{B.13}$$

and

$$\langle 1g|\rho(t)|1g\rangle = \frac{1}{4}\Big[e^{\frac{-\gamma_a}{2}t} + e^{\frac{-\gamma_b}{2}t} - e^{(2ig - \frac{-\gamma_a+\gamma_b}{4})t} \tag{B.14}$$

$$- e^{(-2ig - \frac{-\gamma_a+\gamma_b}{4})t}\Big]. \tag{B.15}$$

Adding Eq. (B.13) and Eq. (B.14) we get Eq. (3.49).

Appendix C

Partial Trace

Given two systems A and B with density matrix ρ_A and ρ_B and composite space $\rho_A \otimes \rho_B$.

Partial trace over A

$$tr_A \begin{pmatrix} \rho_{11} & \rho_{12} & \rho_{13} & \rho_{14} \\ \rho_{21} & \rho_{22} & \rho 23 & \rho_{24} \\ \rho_{31} & \rho_{32} & \rho_{33} & \rho_{34} \\ \rho_{41} & \rho_{42} & \rho_{43} & \rho_{44} \end{pmatrix} = \begin{pmatrix} tr \begin{pmatrix} \rho_{11} & \rho_{13} \\ \rho_{31} & \rho_{33} \end{pmatrix} & tr \begin{pmatrix} \rho_{12} & \rho_{14} \\ \rho_{32} & \rho_{34} \end{pmatrix} \\ tr \begin{pmatrix} \rho_{21} & \rho_{23} \\ \rho_{41} & \rho_{43} \end{pmatrix} & tr \begin{pmatrix} \rho_{22} & \rho_{24} \\ \rho_{42} & \rho_{44} \end{pmatrix} \end{pmatrix} = \begin{pmatrix} \rho_{11} + \rho_{33} & \rho_{12} + \rho_{34} \\ \rho_{21} + \rho_{43} & \rho_{22} + \rho_{44} \end{pmatrix} \tag{C.1}$$

Partial trace over B

$$tr_B \begin{pmatrix} \rho_{11} & \rho_{12} & \rho_{13} & \rho_{14} \\ \rho_{21} & \rho_{22} & \rho 23 & \rho_{24} \\ \rho_{31} & \rho_{32} & \rho_{33} & \rho_{34} \\ \rho_{41} & \rho_{42} & \rho_{43} & \rho_{44} \end{pmatrix} = \begin{pmatrix} tr \begin{pmatrix} \rho_{11} & \rho_{12} \\ \rho_{21} & \rho_{22} \end{pmatrix} & tr \begin{pmatrix} \rho_{13} & \rho_{14} \\ \rho_{23} & \rho_{24} \end{pmatrix} \\ tr \begin{pmatrix} \rho_{31} & \rho_{32} \\ \rho_{41} & \rho_{42} \end{pmatrix} & tr \begin{pmatrix} \rho_{33} & \rho_{34} \\ \rho_{43} & \rho_{44} \end{pmatrix} \end{pmatrix} = \begin{pmatrix} \rho_{11} + \rho_{22} & \rho_{13} + \rho_{24} \\ \rho_{31} + \rho_{42} & \rho_{33} + \rho_{44} \end{pmatrix} \tag{C.2}$$